# Development and Testing of Fuel Cell Membranes from Reinforced Poly(Phenylene Sulfonic Acid)

By

Zhihao Shang

Dissertation

Submitted to the Faculty of the

Graduate School of Vanderbilt University

in partial fulfillment of the requirements

for the degree of

DOCTOR OF PHILOSOPHY

in

Chemical Engineering

August 12, 2022

Nashville, Tennessee

Approved:

Peter N. Pintauro, Ph.D.

Kane Jennings, Ph.D.

Piran Kidambi, Ph.D.

Shihong Lin, Ph.D.

I dedicate this writing to my family and friends for their support and encouragement.

## ACKNOWLEDGMENTS

First, I would like to thank the United States Department of Energy (DOE) Fuel Cell Technologies Office for funding my work presented in this dissertation (Grant DE-EE0008435). I would also like to thank the Department of Chemical and Biomolecular Engineering at Vanderbilt University for financial support during my time as a Teaching Assistant for the Modeling and Simulation in Chemical Engineering class.

I am very grateful for the support provided by my advisor, Dr. Peter N. Pintauro, for all of the help and guidance he has given me during my time at Vanderbilt. I very much appreciate his mentorship and encouragement. The guidance and expertise from Dr. Ryszard Wycisk, who served as a secondary mentor, helped me to become a more competent electrochemist. Additionally, I thank Drs. Kane Jennings, Piran Kidambi, and Shihong Lin for serving on my dissertation committee and for giving me invaluable advices throughout my PhD work. I also thank Dr. Paul Laibinis for helping me improve my dissertation.

Dr. Md Masem Hossain contributed his professional knowledge of polymer synthesis to cPPSA projects. Dr. Narae Kang helped me familiarize with fuel cell testing. The other members of Pintauro's group, in particular, Zezhou Yang, Xiaomin Xu, and Xiaozong Fan, also helped me in enriching my knowledge in electrochemistry.

Dr. Darrell H. Reneker, the other mentor of my life, has helped me to discover the beauty of electrospinning. I will always remember his kind smile and unconditional help.

Finally, I want to thank all of the members of my family, who have been amazingly supportive through my entire graduate career. My parents, Xiaoling Liu and Wei Shang, have been the best parents I could ever ask for. My grandmother, Shuqin Wang, has been one of my life-biggest cheerleaders, and I am so fortunate to be her grandson.

Finally, I would like to express my thanks to Di Bo, my girlfriend, for all the support she has been giving me. You are the love of my life.

## TABLE OF CONTENTS

Page

## LIST OF TABLES

## LIST OF FIGURES

# CHAPTER 1 - INTRODUCTION

With the inevitable depletion of fossil fuels such as coal and oil and the increasingly stringent requirements for reduction of greenhouse gas emissions, it is urgent to seek environmentally friendly, renewable energy sources that can replace conventional carbon-based systems. Green energy such as solar, tidal, wind, biomass, geothermal, hydro, nuclear, and hydrogen ($H_2$) have the potential to satisfy future needs, while addressing climate change and mitigating global warming. However, most green energy sources such as tidal, wind, and solar fluctuate over time resulting in intermittent power generation. Electrochemical batteries can be coupled to green energy sources to minimize this problem [1]. Additionally, batteries are slowly becoming the desired power source for the automotive industry. Fuel cells are another option.

Fuel cells can have an important role in the automotive and heavy-duty vehicle transportation sector, as an environmentally clean alternative to the internal combustion engine and a long drive-distance alternative to Li-ion batteries. Fuel cells convert the chemical energy of a fuel and oxidant into electrical energy at efficiencies that are typically higher than those achieved in an internal combustion engine. The most promising type of fuel cell uses $H_2$ as the fuel, with only water as the reaction product. Such a carbon-free and potentially reversible energy system (where hydrogen is regenerated by water electrolysis) is highly desirable. Hydrogen fuel cells are being considered for a variety of different applications, including power plants in passenger and heavy-duty vehicles and for distributed electricity generators [2].

In recent years, various experimental cars utilizing fuel cells have emerged on the market, such as the Toyota Mirai, the Honda Clarity, and the Mercedes Benz F-Cell. However, various factors remain that limit the widespread use of these cars, such as lack of infrastructure for hydrogen supply, reliable and cost-effective sources for hydrogen, and the unsatisfactory durability and high cost of components.

The membrane-electrode assembly (MEA) is an important part of automotive fuel cells as it contains the materials necessary for conversion of hydrogen and oxygen (from air) to electricity and water. The MEA consists of two electrochemically active electrodes and a proton-exchange membrane (PEM). This membrane must separate the electrodes, prevent fuel crossover, and allow proton conduction (which is highly dependent on the presence of water) under the operating conditions of the fuel cell. The membrane must also be resistant to mechanical failure (such as tears or holes) and chemical degradation (polymer degradation by peroxide radicals).

PEMs are made of ionomers, i.e. ion-containing polymers. Ionomers are typically highly conductive when fully hydrated at mild temperatures, but under hot (90-120 °C) and dry (below 50% RH) conditions, their ionic conductivity drops significantly [3–6]. This shortcoming creates the need for humidification subsystems

in fuel cell units (to keep the ionomer hydrated), which can complicate fuel cell system design. In addition, many ionomers undergo undesirable swelling and shrinkage as the fuel cell is turned on/off (going from hot and wet when on, to cold and dry when off). Such dimensional changes can lead to the mechanical degradation of the PEM (the generation of cracks or pinholes, or delamination between the membrane and electrode) [7–9], thus shortening the lifetime of the MEA [10–13].

This dissertation focuses on the fabrication of a series of composite membranes with properties suitable for $H_2$/air fuel cell applications. In particular, mechanically strong membranes with an area-specific resistance (ASR) and swelling properties that approach the targets defined by the U.S. Department of Energy (an ASR of 0.02 Ω-cm$^2$ or less at 80 °C and 40-100 % relative humidity, and an in-plane swelling of 10% or less after equilibration in water) are desired. While chemical durability is important, the focus of this dissertation is to improve the mechanical durability of the membranes while maintaining an acceptable ASR at operational conditions.

The structure of the thesis is as follows. Chapter 2 provides background information on fuel cells and fuel cell membranes, followed by three chapters on the fabrication, characterization, and improvements in the characteristics of various composite PEMs. Chapter 3 discusses cPPSA-based membranes where electrospun nanofiber scaffolds are used as the reinforcement. In Chapter 4, work on cPPSA-ePTFE membranes is described where a commercially available, porous, expanded PTFE is used as the membrane reinforcement. Lastly, in Chapter 5, cPPSA is used as a conductivity enhancement for a commercial PFSA ionomer.

In fuel cell membrane electrode assemblies (MEAs) ionomers not only serves as the membrane materials, they are also used serve as catalyst binders. In Chapter 6, the final chapter of this dissertation, preliminary attempts to fabricate MEAs with cPPSA binder are described.

### 1.1 References


[1] Zhang, Huan, and Chuanyu Sun. "Cost-effective iron-based aqueous redox flow batteries for large-scale energy storage application: A review." *Journal of Power Sources* 493 (2021): 229445.

[2] Staffell, Iain, et al. "The role of hydrogen and fuel cells in the global energy system." *Energy & Environmental Science* 12.2 (2019): 463-491.

[3] Ballengee, J. B., et al. "Properties and fuel cell performance of a nanofiber composite membrane with 660 equivalent weight perfluorosulfonic acid." *Journal of The Electrochemical Society* 160.4 (2013): F429.

[4] Yang, C., et al. "Approaches and technical challenges to high temperature operation of proton exchange membrane fuel cells." *Journal of Power Sources* 103.1 (2001): 1-9.

[5] Maalouf, Manale, et al. "Proton exchange membranes for high temperature fuel cells: Equivalent weight and end group effects on conductivity." *ECS Transactions* 25.1 (2009): 1473.

[6] Wang, Feng, et al. "Direct polymerization of sulfonated poly (arylene ether sulfone) random (statistical) copolymers: candidates for new proton exchange membranes." *Journal of Membrane Science* 197.1-2 (2002): 231-242.

[7] Wu, Jinfeng, et al. "A review of PEM fuel cell durability: Degradation mechanisms and mitigation strategies." *Journal of Power Sources* 184.1 (2008): 104-119.

[8] De Bruijn, F. A., V. A. T. Dam, and G. J. M. Janssen. "Durability and degradation issues of PEM fuel cell components." *Fuel cells* 8.1 (2008): 3-22.

[9] Banan, R., J. Zu, and A. Bazylak. "Humidity and temperature cycling effects on cracks and delaminations in PEMFCs." *Fuel Cells* 15.2 (2015): 327-336.

[10] Ous, T., and C. Arcoumanis. "Degradation aspects of water formation and transport in proton exchange membrane fuel cell: a review." *Journal of Power Sources* 240 (2013): 558-582.

[11] Borup, Rod, et al. "Scientific aspects of polymer electrolyte fuel cell durability and degradation." *Chemical Reviews* 107.10 (2007): 3904-3951.

[12] Kusoglu, Ahmet, et al. "Mechanical behavior of fuel cell membranes under humidity cycles and effect of swelling anisotropy on the fatigue stresses." *Journal of Power Sources* 170.2 (2007): 345-358.

[13] Rodgers, Marianne P., et al. "Fuel cell perfluorinated sulfonic acid membrane degradation correlating accelerated stress testing and lifetime." *Chemical Reviews* 112.11 (2012): 6075-6103.

# CHAPTER 2 - BACKGROUND

## 2.1 Background on Fuel Cells

Fuel cells provides energy through electrochemical reactions between fuels (such as hydrogen, methanol) and oxidants (such as oxygen, bromine). They are different from batteries which are just energy storage devices, as once the reactants stored in them are exhausted, they need to be either disposed of/recycled (primary batteries) or recharged (secondary batteries). For fuel cells, as long as fuel is supplied, they can continue to generate electricity. Further, their high energy conversion efficiencies, less harmful emissions, and ease of use in large-scale applications make them increasingly attractive.

Fuel cells can be classified by their operating temperature, electrolyte type, or fuel type. For example, low temperature fuel cells operate generally over 25-100 ℃, such as for solid polymer electrolyte fuel cells, medium temperature fuel cells operate generally over 100-500 ℃, such as for phosphoric acid fuel cells, and high temperature type fuel cells operate generally over 500-1000 ℃ as for molten carbonate and solid oxide fuel cells. Classifying by their fuel used, they can be divided into hydrogen fuel cells, methanol fuel cells, ethanol fuel cells, etc. Depending on the type of electrolyte used, fuel cells can be classified into alkaline fuel cells (AFCs), solid oxide fuel cells (SOFCs), phosphoric acid fuel cells (PAFCs), molten carbon salt fuel cells (MCFCs), and proton exchange membrane fuel cells (PEMFCs) [1]. A summary of these fuel cells is provided below.

Alkaline fuel cells (AFCs) appeared very early, and have been used in the aerospace field. They mainly use a highly corrosive liquid KOH as electrolyte, hydrogen as the fuel, and working temperature of usually 20-80 °C. Because its electrolyte is extremely sensitive to carbon dioxide, they cannot be widely used on the ground [2].

Solid oxide fuel cells (SOFCs) mainly use a solid oxide as the electrolyte. Their operating temperature is usually 800-1000 °C, and the higher operating temperature enables the use of catalysts free of precious metals. Since the fuel cell system uses an all-solid structure, their stability is good but their assembly is difficult. Also, due to their high operating temperature, the heat resistance of the fuel cell materials needs to be extremely high, making their use rare [3]. To decrease their operating temperature below 800 °C, some researchers have introduced alternative oxide ion conductors, such as Scandia stabilized zirconia (ScSZ), having excellent conductivity at lower temperature (750 °C) and reliable to operate in the SOFC system [4].

Phosphoric acid fuel cells (PAFCs) use highly corrosive liquid phosphoric acid as electrolyte. Their working temperature is usually 100-200 °C. Catalysts containing costly precious metals are generally required for catalysis. At present, most of them are used in large independent power stations and in specialized

applications. PAFs have been practically applied since 1993 [5].

Molten carbonate fuel cells (MCFCs) mainly use molten alkali metal carbonate as the electrolyte. Their working temperature is usually 600-700 °C. Catalysts free of precious metals can be used which reduce their cost. Their high operating temperature and highly corrosive conditions lead to short lifespans for these fuel cells [6].

Polymer exchange membrane fuel cells (PEMFCs) have been aggressively developed during the last several decades. This type of fuel cell uses a polymer membrane as the electrolyte material to separate two electrodes. The introduction of polymer membrane shortens the distance between electrodes, reduces internal energy consumption, and improves the overall performance of fuel cell. The size and weight of fuel cell are also reduced. At present, proton exchange membrane fuel cells are the most widely used fuel cell worldwide [7]. PEMFCs first became popular for aerospace use during the 1960s [8] and continue to be attractive due to their high-power density capability, fast start-up times, and easily adjustable stack size to meet a variety of different power needs. The most common PEMFCs utilize $H_2$ as the fuel and Pt-containing catalyst powder electrodes. $H_2$ gas is oxidized to $H^+$ at the anode and $O_2$ from air is reduced to form water at the cathode [9], as shown in Figure 2.1. A thin proton-exchange membrane (polymer electrolyte membrane) physically separates the anode and cathode to prevent both electrical shorting and mixing of the reactant gases. The membrane also provides pathways for proton conduction between the anode and the cathode. Many fuel cell proton-exchange membranes (henceforth denoted as PEMs) are used in redox flow batteries, water electrolyzers for $H_2$ gas production, electrodialysis separations, and industrial processes such as the chlor-alkali membrane process for producing $Cl_2$ and concentrated NaOH [10].

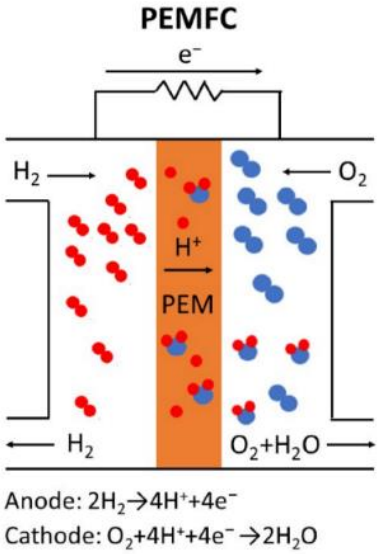


Figure 2.1: Schematic diagram of a PEMFC with the relevant electrode reactions [11].

The membrane (PEM) is an important part of the PEMFC. Desired PEMs are those with high proton conductivity and low fuel permeation. Currently, the most widely used PEM material is perfluorosulfonic acid (PFSA) polymer (ionomer). The polarity difference between the perfluorinated backbone and the sulfonic acid-containing side chains induces internal phase separation which along with chemical robustness of perfluorosulfonic acid make these ionomers particularly suitable for FC applications Unfortunately, PFSA polymers are very costly and additionally, PFSA PEMs suffer from dramatic loss of proton conductivity at reduced cell humidification. As a result, new proton conducting membrane polymers with improved low RH performance are urgently needed.

### 2.2 Requirements of FC PEMs

For PEM fuel cells, it is generally necessary to assemble the electrolyte membrane into a membrane electrode assembly (MEA). To ensure excellent fuel cell performance, the proton exchange membrane needs to meet the following conditions: i) Excellent proton conductivity. Only membranes with proton conductivity ≥ 100 mS/cm at operational temperature have practical value. ii) Good chemical and thermal stability, which affect the lifetime of fuel cells. Free radicals generated during fuel cell operation can degrade the ionomer. iii) Small lateral swelling. The proton exchange membrane tends to deform during the processes of hydration and dehydration. If the deformation is large, pinholes and cracks may form which degrade FC performance. iv) Low gas permeation. The proton exchange membrane separates fuel and oxidant, preventing the two from reacting directly on the electrodes and reducing the power output and the lifetime of fuel cell. v) Cost-effective. Lower manufacturing costs are required for the widespread adoption of PEM fuel cells.

### 2.3 Prior Research on Proton Exchange Membrane

After several decades of worldwide research, improved PFSAs and new hydrocarbon-based ionomers have been developed. Generally, these membrane materials can be classified into the following categories—perfluorosulfonic acid polymers, partial fluoropolymers, non-fluorine polymers and composites. Below there is a brief description of membranes from these materials.

#### 2.3.1 Perfluorosulfonic Acid Membrane

Ideally, a fuel cell PEM should have a high $H^+$ conductivity at both low and high relative humidity (RH) at temperatures near 80 °C. The PEM must also exhibit good chemical and mechanical stability, with minimal water swelling variations during fuel cell operation. As described earlier, the most common membranes in PEMFCs are based on a perfluorosulfonic acid (PFSA) ionomer [12]. PFSA ionomers and membranes are manufactured by a number of companies. Figure 2.2 shows the chemical structure of perfluorosulfonic acid polymer. The most well-known PFSA membrane has the trade name Nafion™. It was first manufactured in the 1970s by DuPont (now The Chemours Company, Wilmington, DE, USA) for chlor-alkali cells. Other companies that make PFSA fuel cell ionomers and membranes include Asahi Glass Company (Flemion® products, Chiyoda, Japan), 3M Company (Saint Paul, MN, USA), W. L Gore (GORE-SELECT® membranes,

Newark, DE, USA), and Solvay S.A. (Aquivion® products, Brussels, Belgium). Nafion has a very high proton conductivity of ~0.1 S/cm at fuel cell operating conditions of 80 °C and 100% RH and good mechanical properties. The high proton conductivity of Nafion is attributed to the combined superacidity of the sulfonic groups and the phase-separated morphology where sulfonic groups are aggregated into hydrophilic domains that are dispersed within its hydrophobic PTFE backbone matrix [13]. The process of synthesizing PFSA is complicated and costly, and the mechanical properties of neat ionomer films still need to be improved for a better control of water uptake and minimization of creep, and to make the membrane resistant to repeated water swelling/dehydration cycles [14]. PFSA degradation by peroxide and/or hydroxide radicals in an operating PEMFC and the associated release of fluorides represent a serious durability issue as well as an environmental pollution concern [15].

In addition to Nafion PFSA membranes, a number of other PFSA-based PEMs have been developed, including those with short side-chain, low EW (<1100) PFSA ionomers from Solvay (Aquivion) and 3M Company [16]. They have shorter lengths of side-chains compared with Nafion. Examples of the chemical structures of Nafion, 3M, and Aquivion ionomers are given in Figure 2.2.

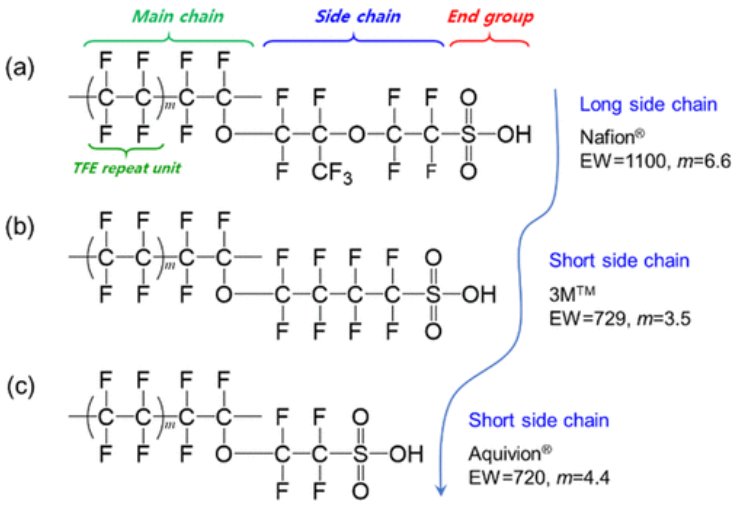


Figure 2.2: Chemical structures of (a) Nafion, (b) 3M, and (c) Aquivion ionomers [17].

Proton exchange membranes are normally fabricated by either melt extrusion or solution casting. Originally, Nafion membranes were made by melt extruding the sulfonyl fluoride precursor of PFSA, followed by a hydrolysis step to create sulfonic acid fixed charges [18]. With this technique, the fabrication of thin membranes was a challenge. A solution casting method is used today to make most fuel cell PEMs. While the method requires the identification of a suitable solvent for ionomer dissolution/dispersion, which may be problematic, it allows for the fabrication of ultrathin films (<20 μm for PEMs) from pristine ionomers and of composites via impregnation of an ionomer solution into a pre-formed porous polymer scaffold.

### 2.3.2 Partially Fluorinated Membrane

Membranes based on sulfonated α, β, β-trifluorostyrene-based polymers have been developed for use in proton exchange membrane fuel cells. The mechanical strength and chemical stability of membrane electrode assembly prepared with such membranes were initially poor and could not meet the needs of long-term applications. Through improvements, the Canadian Ballard company developed a membrane, BMA3G, with a lower content of sulfonic acid groups (Figure 2.3) that worked well and had relatively long lifetime [19]. The partially fluorinated material had lower cost compared to Nafion.

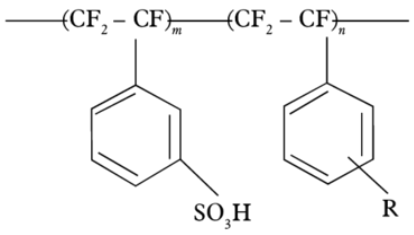


Figure 2.3: Chemical structure of BAM3G membrane.

### 2.3.3 Non-fluorinated Membrane

Fluorinated polymers have the advantages of good chemical stability, but their high cost and complex monomer synthesis are limitations for fuel cell applications. To address those limitations, researchers have developed many non-fluorinated polymers as alternatives to perfluorosulfonic acid polymer [20]. Non-fluorinated polymers are typically hydrocarbon polymers, which are offer lower cost and less impact on the environment. Initially, it was hoped to use sulfonated phenolic resin membranes, sulfonated vinyl materials, and sulfonated polyimide as proton exchange membrane materials in fuel cells [21]. Through testing, these materials all exhibited important shortcomings. The best results were obtained with various polyarylene-based ionomers, such as sulfonated polyetheretherketone (SPEEK) [22] shown in Figure 2.4. Due to its inability to micro-phase separate, as observed for PFSAs, the same level of proton conductivity as Nafion can only be achieved at a higher ion exchange capacity. However, high IECs are often accompanied by poor dimensional stability, so balancing the relationship between proton conductivity and dimensional stability of such materials is key to improving the overall performance of membranes based on these materials.

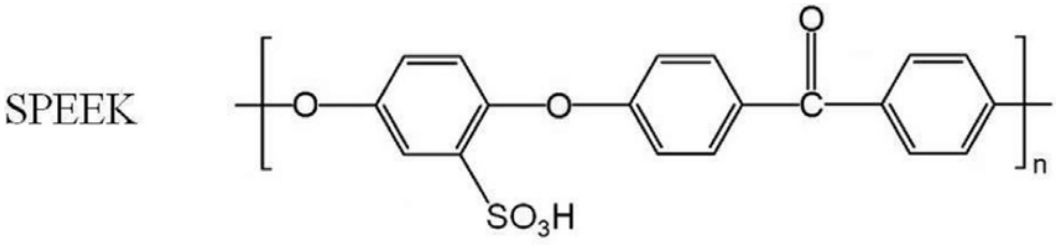


Figure 2.4: Chemical structure of SPEEK.

## 2.4 Polymer Nanofiber Electrospinning

Since 1995, electrospinning has received increased attention as a viable commercial manufacturing technology [23,24]. It is by far the easiest and fastest way to produce nonwoven polymer fiber mats, when the fiber diameter must be <500 nm [25]. The main components of a fiber electrospinning apparatus are a high-voltage power supply, a pump, one or more spinnerets, and a fiber collector (see Figure 2.5). Typically, a polymer solution is pumped through the spinneret or spinneret array, which is connected to a high voltage power supply. When the generated surface charge on the solution at the spinneret tip overcomes surface tension, a Taylor cone forms from which a liquid jet is ejected. The jet travels toward the collector and undergoes stretching and bending instabilities while solvent evaporates. The deposited dry polymer form randomly distributed fibers of submicrometer diameters.

Electrospinning is affected by polymer molecular weight and molecular weight distribution, the polymer solution properties, the applied voltage, the spinneret to collector distance, the external environment (air temperature and humidity), the collector movement, and the spinneret type/shape. Polymer molecular weight and molecular weight distribution have a significant impact on the rheological behavior and electrical properties of the electrospinning solution. Generally, due to limited chain entanglement, polymers with a low molecular weight or an excessively broad molecular weight distribution tend to form beads during electrospinning rather than fibers [26]. Similarly, if the polymer concentration in solution is too low, the electrospinning jet will break up into droplets without forming fibers. High polymer concentrations may also present problems when electrospinning, where viscous forces inhibit Taylor cone formation or fiber jet stretching. The solvent in the electrospinning solution should not evaporate too quickly in order to avoid solution clogging, or too slowly to prevent fusion of fibers on the collector. When the applied voltage is low, a Taylor cone will not form because the surface charge on the solution at the spinneret tip cannot overcome surface tension forces. As the electric field strength increases, it is easier to form, stretch, and bend the polymer solution jet, resulting in nanofibers of smaller diameters [27]. In a typical electrospinning process, the spinneret-to-collector distance is 10–20 cm, which usually gives the polymer solution jet a sufficient time-of-flight for solvent evaporation (where the actual time-of-flight distance of a jet is extended beyond the spinneret-to-collector distance by bending instabilities). The effect of humidity on fiber diameter depends on the interaction between the spinning solution and surrounding water vapor. For some polymers, a high relative humidity may result in a decrease in fiber diameter, whereas water-soluble fibers are best prepared at low humidity to prevent fiber melting or beaded fibers. Small inner diameter spinnerets can reduce clogging (by reducing exposure of the electrospinning solution to air) and create smaller diameter fibers (less surface tension for smaller droplets at the spinneret tip) with fewer bead-on-fiber defects. Spinnerets with special shapes can also be used to make electrospun fibers with special structures such as hollow or core-

shell fibers. Electrospinning can produce high specific surface area and high porosity fiber mats with an average fiber diameter often approaching 200 nm or less [28].

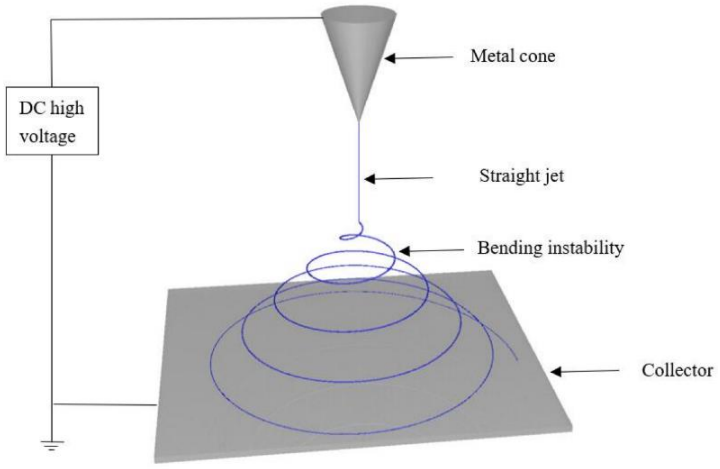


Figure 2.5: A simplified schematic of an electrospinning system [11].

Nanofiber electrospinning is cost-effective for a number of commercial products and has been employed in the fabrication of composites [29], filtration media [30], biomedical and pharmaceutical products [31], textiles [32], and sensors [33]. It has recently been used to prepare fuel cell and battery electrodes, as either particle/polymer fiber mats or carbon fiber mats (from pyrolyzed polymer fibers) [34,35].

## 2.5 Nanofiber-Reinforced Composite Proton-Exchange Membranes

There are two major benefits of using electrospinning for the fabrication of PEMs for fuel cells. First, electrospinning allows the easy fabrication of high-quality reinforcing nanofiber scaffolds of controlled porosity from various mechanically and chemically robust polymers. Second, by using multiple spinnerets fed with different polymer solutions, electrospinning enables one to obtain multicomponent, macroscopically homogeneous polymer blends or composites that cannot be made using other methods, e.g., direct solution casting or melt extrusion.

Three kinds of electrospun nanofiber composite PEMs have been reported in the literature. The first was made by pore-filling of electrospun nanofiber mats composed of ionomer or uncharged polymer with either uncharged polymer or ionomer [36]. Frequently, an additional carrier polymer was added to the ionomer solution to enable its electrospinning. Typically, poly(ethylene oxide) (PEO), poly(acrylic acid) (PAA), poly(vinyl alcohol), or polyvinylpyrrolidone carriers have been employed [37,38]. The second kind of membrane was fabricated through dual fiber electrospinning, where the ionomer and reinforcing (uncharged) polymer solutions were concurrently electrospun onto a common collector as a mixed fiber mat. After mat densification, which lead to interfiber pore closure, a dense two-component membrane was obtained, where

either ionomer fibers or the reinforcing polymer fibers were retained [39]. Membranes of the third kind were fabricated using single-fiber electrospinning, where a mixed solution of ionomer and uncharged polymer was electrospun to form a mat of blended polymer nanofibers, which upon mechanical densification led to a dense membrane [40]. Table 2.1 list the composition, thickness, and properties of these fuel cell membranes. In some cases, the electrospun fibers are the ionomer component of the membrane while in other cases, nanofibers are used to reinforce an ionomer matrix.

Table 2.1: Summary of electrospun PEMs and their properties.

| Nanofiber | Matrix | Membrane Thickness (μm) | Ionomer Fraction (%) | Effective IEC (mmol/g) | $H^+$ Conductivity (mS/cm) | $H_2$ Crossover (mA/cm$^2$) | Reference |
|---|---|---|---|---|---|---|---|
| - | Nafion [1] | 25 | 100 | 0.91 | 100 (at 80 °C, 90% RH) | 4.1 (at 80 °C, 200 kPa backpressure, 100% RH) | [41] |
| sPAES | NOA 63 | 39 | 70 | 1.65 | 86 (at 25 °C, liq. water) | - | [42] |
| 733 EW PFSA | NOA 63 | 75 | 70 | 1.36 | 160 (at 80 °C, 80% RH) | - | [43] |
| Nafion [1] | PPSU | 31 | 70 | 0.63 | 70 (at 25 °C, liq. water) | 1.3 (at 80 °C, ambient pressure, 100% RH) | [44] |
| 660 EW PFSA | PPSU | 51 | 72 | 1.23 | 166 (at 80 °C, 80% RH) | - | [45] |
| PSUT | Aquivion [2] | 30 | 70 | 0.98 | 180 (at 80 °C, 95% RH) | - | [46] |
| PVDF | Nafion [1] | 48 | 60 | 0.54 | 55 (at 25 °C, liq. water) | - | [47] |
| PAI | 825 EW PFSA | 20 | 80 | 0.97 | 91 (at 25 °C, liq. water) | 4.9 (at 80 °C, 200 kPa backpressure, 100% RH) | [41] |
| PPSU | cPPSA | 100 | 75 | 4.70 | 429 (at 80 °C, 90% RH) | - | [48] |
| sPAES/sPOSS | NOA 63 | 70 | 70 | 2.24 | 94 (at 30 °C, 80% RH) | - | [49] |
| 825 EW PFSA /sPOSS | NOA 63 | - | 74 | 2.41 | 357 (at 80 °C, 90% RH) | - | [50] |
| NU6@PPNF | SPEEK | 96 | 97 | - | 133 (at 60 °C, 100% RH) | - | [51] |
| Sulfated $SnO_2$ | SPPESK | 80 | 93 | 1.72 | 227 (at 80 °C, 80% RH) | 1.7 (at 80 °C, ambient pressure, 100% RH) | [52] |
| PVDF | 825 EW PFSA /S-$SiO_2$ | 40 | 80 | 1.46 | 89 (at 20 °C, liq. water) | - | [53] |
| P(VDF-TrFE)/S-$SiO_2$ | Nafion [1] | 108 | - | - | 102 (at 70 °C, 100%RH) | - | [54] |

[1] 1100 EW PFSA (0.91 mmol/g IEC). [2] 830 EW PFSA (1.20 mmol/g IEC).

### 2.6 ePTFE-Reinforced Composite Proton-Exchange Membranes

The material most widely used for reinforcing proton exchange membranes is porous ePTFE due to its high porosity, good mechanical strength, and excellent chemical stability. The basic technique for preparing an ePTFE composite proton exchange membrane is pouring ionomer solution onto a pre-cleaned ePTFE film, followed by drying and annealing. Huang et al. [55] prepared an ultra-thin reinforced membrane using hexagonal boron nitride nanosheets (h-BN), high sulfonated poly (ether-ether-ketone) (sPEEK, DS = 81.4%), and expanded polytetrafluoroethylene (ePTFE) to form a low-humidification proton exchange membrane fuel cell (PEMFC), without requiring special treatment for the ePTFE. The BN@sPEEK/ePTFE-reinforced membrane showed good proton conductivity, low hydrogen permeation current, and high cell performance. A 0.5%-BN@sPEEK/PTFE-reinforced membrane exhibited the highest proton conductivity with 283 mS/cm at 60 °C. Its peak power density was 567.7 mW/cm$^2$, which was 16.6% higher than that of Nafion 212 (486.7

mW/cm$^2$) under the same testing condition. These results indicate that the BN@sPEEK/PTFE composite membrane prepared with ultra-high sulfonation degree sPEEK has broad application potential in a low-humidity PEMFC.

Huang et al. [56] designed and fabricated a novel PEM containing expanded polytetrafluoroethylene (ePTFE) functionalized with amino and hydroxyl groups to enhance the PEM's proton conductivity and electrochemical performance at low RH, and to improve its mechanical stability. The introduction of the hydrophilic groups and the generation of stable acid–base pairs yield a PFSA ionomer that has better compatibility with and adhesion to the hydrophilic functionalized ePTFE membrane. These attributes significantly lowered the membranes' $H_2$ crossover current density, improved their proton conductivity and single-cell performance. In addition, generated water was retained inside the PEM, keeping the cell performance high at low RH. The PEM's mechanical durability also improved by the increased dimensional stability and compatibility of the ionomer and reinforcement layer. These factors provide a promising way for improving the proton conductivity and cell performance of PEMs at low RH and for creating PEM fuel cells with high mechanical durability.

### 2.7 PFSA-hydrocarbon Ionomer Blend Membranes

Many different kinds of additives had been combined with PFSA ionomer to enhance its proton conductivity, chemical stability, and fuel cell performance. For example, hydrocarbon ionomers have been successfully blended with PFSA ionomers. Guimet et al. [57] designed and fabricated a series of blends of perfluorosulfonated acid ionomer (Aquivion®) and disulfonated poly(aryl ether ketone) (DS-PAEK) with compositions ranging between 10 and 90 wt.%. For blends with 10–20 wt.% of sulfonated hydrocarbon polyelectrolyte, the main mechanical relaxation temperature of the side chains of Aquivion increased 10–20 °C as compared to pure Aquivion. This shift demonstrated the presence of interactions between Aquivion and DS-PAEK that occurred with little change in the ion exchange capacity, the capacity to absorb water, and the proton conductivity of blends from that of pure Aquivion. In addition, these new materials showed improved robustness and better performance in fuel cell operation at 105 °C as compared to Aquivion. These results proved that PFSA materials could be upgraded by adding a suitable sulfonated hydrocarbon ionomer.

Wang et al. [58] prepared Nafion/SNPAEK-x composite membranes by blending raw Nafion and custom-synthesized side-chain-type naphthalene-based sulfonated poly(arylene ether ketone) with a sulfonation degree of 1.35 (SNPAEK-1.35). The incorporation of SNPAEK-1.35 polymer with ion exchange capacity (IEC) of 2.01 mmol/g into a Nafion matrix yielded property enhancements, such as increasing IEC and proton conductivity, enhancing mechanical properties, reducing methanol crossover, and improving single cell performance of Nafion. Morphology studies showed that Nafion/SNPAEK-x composite membranes form a

well-defined microphase separated structure depending on the contents of SNPAEK-1.35 polymer. Nafion/SNPAEK-7.5% with a bicontinuous morphology exhibited the best overall properties. For example, it showed the highest proton conductivities in liquid water of 92 mS/cm at 25 °C and 163 S/cm at 80 °C, which are higher than those of recast Nafion with 73 mS/cm at 25 °C and 133 mS/cm at 80 °C, respectively. Nafion/SNPAEK-5.0% membrane also had comparable tensile strength (12.7 MPa) to recast Nafion (13.7 MPa), and a higher Young's modulus (330 MPa) to recast Nafion (240 MPa). By combining their high proton conductivities, comparable mechanical properties, and good single cell performance, Nafion/SNPAEK-x composite membranes show potential as a polymer electrolyte material for fuel cell applications.

### 2.8 2020 DOE Technical Targets

The US Department of Energy (DOE) has been strongly supporting membrane R&D "to increase the operating temperature and humidity ranges of fuel cells while improving conductivity, to increase membrane mechanical, chemical, and thermal stability with diminished fuel crossover, particularly for automotive applications" [59]. The Fuel Cell sub-program in the Fuel Cell Technologies Office has been addressing key challenges to accelerate deployment of fuel cell vehicles. With input from the US DRIVE Partnership, the DOE's Fuel Cell Technical Team has developed a set of performance targets to assist developers in evaluating their R&D progress on proton conducting membranes. The 2020 targets are listed in Table 2.2 [60].

Table 2.2: 2020 DOE technical targets for developers of PEMs for transportation application.

| Characteristic | Units | 2020 Targets |
|---|---|---|
| Maximum oxygen crossover[a] | $mA/cm^2$ | 2 |
| Maximum hydrogen crossover[a] | $mA/cm^2$ | 2 |
| Area specific proton resistance at: | | |
| Maximum operating temperature and water partial pressure 40–80 kPa | $ohm\text{-}cm^2$ | 0.02 |
| 80 °C and water partial pressure 25–45 kPa | $ohm\text{-}cm^2$ | 0.02 |
| 30 °C and water partial pressure up to 4 kPa | $ohm\text{-}cm^2$ | 0.03 |
| −20 °C | $ohm\text{-}cm^2$ | 0.2 |
| Maximum operating temperature | °C | 120 |
| Minimum electrical resistance | $ohm\text{-}cm^2$ | 1000 |
| Cost[b] | $\$/m^2$ | 20 |
| Durability | | |
| Mechanical | Cycles until >15 $mA/cm^2$ $H_2$ crossover | 20,000 |
| Chemical | Hours until >15 $mA/cm^2$ crossover or >20% loss in OCV | >500 |
| Combined chemical/mechanical | Cycles until >15 $mA/cm^2$ crossover or >20% loss in OCV | 20,000 |

[a] Tested in MEA on $O_2$ or $H_2$, 80 °C, fully humidified gasses, 1 atm total pressure.
[b] Cost projected to high-volume production (500,000 80 kW systems per year).

## 2.9 References


[1] Steele B.C.H., Heinzel A. "Materials for fuel-cell technologies. " *Nature* 414, (2001): 345-352.

[2] McLean, G. F., et al. "An assessment of alkaline fuel cell technology." *International Journal of Hydrogen Energy* 27.5 (2002): 507-526.

[3] Gupta, Nidhi, and Gagan Deep Yadav. "Solid oxide fuel cell: A review." *International Research Journal of Engineering and Technology* 3.6 (2016): 1006-1011.

[4] Zhang, Qi, et al. "Effect of Nb2O5 doping on improving the thermo-mechanical stability of sealing interfaces for solid oxide fuel cells." *Scientific Reports* 7.1 (2017): 1-8.

[5] Sammes, Nigel, Roberto Bove, and Knut Stahl. "Phosphoric acid fuel cells: Fundamentals and applications." *Current Opinion in Solid State and Materials Science* 8.5 (2004): 372-378.

[6] Dicks, Andrew L. "Molten carbonate fuel cells." *Current Opinion in Solid State and Materials Science* 8.5 (2004): 379-383.

[7] Wee, Jung-Ho. "Applications of proton exchange membrane fuel cell systems." *Renewable and sustainable energy reviews* 11.8 (2007): 1720-1738.

[8] Burstein, G. T., et al. "ELECTROCHEMICAL SOCIETY LETTERS." *J. Electrochem. Soc* 143.7 (1996).

[9] Wycisk, Ryszard, Peter N. Pintauro, and Jun Woo Park. "New developments in proton conducting membranes for fuel cells." *Current Opinion in Chemical Engineering* 4 (2014): 71-78.

[10] Zhang, Huan, and Chuanyu Sun. "Cost-effective iron-based aqueous redox flow batteries for large-scale energy storage application: A review." *Journal of Power Sources* 493 (2021): 229445.

[11] Shang, Zhihao, Ryszard Wycisk, and Peter Pintauro. "Electrospun composite proton-exchange and anion-exchange membranes for fuel cells." *Energies* 14.20 (2021): 6709.

[12] Gloukhovski, Robert, Viatcheslav Freger, and Yoed Tsur. "Understanding methods of preparation and characterization of pore-filling polymer composites for proton exchange membranes: a beginner's guide." *Reviews in Chemical Engineering* 34.4 (2018): 455-479.

[13] Kusoglu, Ahmet, and Adam Z. Weber. "New insights into perfluorinated sulfonic-acid ionomers." *Chemical reviews* 117.3 (2017): 987-1104.

[14] Itoh, T. "Hyperbranched polymer electrolytes for high temperature fuel cells." *Polymer Electrolytes*. Woodhead Publishing, 2010. 524-549.

[15] Feng, Mingbao, et al. "Characterization of the thermolysis products of Nafion membrane: A potential source of perfluorinated compounds in the environment." *Scientific Reports* 5.1 (2015): 1-8.

[16] Li, Junrui, Mu Pan, and Haolin Tang. "Understanding short-side-chain perfluorinated sulfonic acid and its application for high temperature polymer electrolyte membrane fuel cells." *RSC Advances* 4.8 (2014): 3944-3965.

[17] Shin, Sung-Hee, et al. "Improving the mechanical durability of short-side-chain perfluorinated polymer electrolyte membranes by annealing and physical reinforcement." *ACS Omega* 4.21 (2019): 19153-19163.

[18] Smith, Roger A., and Michael S. Withers. "Coextruded multilayer cation exchange membranes." U.S. Patent No. 4,437,952. 20 Mar. 1984.

[19] Souzy, Renaud, and Bruno Ameduri. "Functional fluoropolymers for fuel cell membranes." *Progress in Polymer Science* 30.6 (2005): 644-687.

[20] Roziere, Jacques, and Deborah J. Jones. "Non-fluorinated polymer materials for proton exchange membrane fuel cells." *Annual Review of Materials Research* 33.1 (2003): 503-555.

[21] Miyatake, Kenji, et al. "Highly proton conductive polyimide electrolytes containing fluorenyl groups." *Chemical Communications* 3 (2003): 368-369.

[22] Kaliaguine, S., et al. "Properties of SPEEK based PEMs for fuel cell application." *Catalysis Today* 82.1-4 (2003): 213-222.

[23] Zheng, Gaofeng, et al. "Nanofiber membranes by multi-jet electrospinning arranged as arc-array with sheath gas for electrodialysis applications." *Materials & Design* 189 (2020): 108504.

[24] Doshi, Jayesh, and Darrell H. Reneker. "Electrospinning process and applications of electrospun fibers." *Journal of electrostatics* 35.2-3 (1995): 151-160.

[25] Niu, Haitao, Hua Zhou, and Hongxia Wang. "Electrospinning: an advanced nanofiber production technology." *Energy Harvesting Properties of Electrospun Nanofibers*; IOP Publishing: Bristol, UK (2019): 1-1.

[26] Hu, Juanping, et al. "One-step electro-spinning/netting technique for controllably preparing polyurethane nano-fiber/net." *Macromolecular Rapid Communications* 32.21 (2011): 1729-1734.

[27] Higashi, Shougo, et al. "Dynamic viscosity recovery of electrospinning solution for stabilizing elongated ultrafine polymer nanofiber by TEMPO-CNF." *Scientific reports* 10.1 (2020): 1-8.

[28] Ramakrishna, Seeram, et al. "Electrospun nanofibers: solving global issues." *Materials today* 9.3 (2006): 40-50.

[29] Cheng, Geng, et al. "A robust composite proton exchange membrane of sulfonated poly (fluorenyl ether ketone) with an electrospun polyimide mat for direct methanol fuel cells application." *Polymers* 13.4 (2021): 523.

[30] Cui, Jiaxin, et al. "Flexible and transparent composite nanofibre membrane that was fabricated via a “green” electrospinning method for efficient particulate matter 2.5 capture." *Journal of Colloid and Interface Science* 582 (2021): 506-514.

[31] Zadeh, Zahra Eivazi, et al. "Electrospun polyurethane/carbon nanotube composites with different amounts of carbon nanotubes and almost the same fiber diameter for biomedical applications." *Materials Science and Engineering: C* 118 (2021): 111403.

[32] Zhou, Wen, et al. "Environmentally friendly waterborne polyurethane nanofibrous membranes by emulsion electrospinning for waterproof and breathable textiles." *Chemical Engineering Journal* 427 (2022): 130925.

[33] Huang, Jieyu, et al. "All-fiber-structured triboelectric nanogenerator via one-pot electrospinning for self-powered wearable sensors." *ACS Applied Materials & Interfaces* 13.21 (2021): 24774-24784.

[34] Slack, John J., et al. "Impact of polyvinylidene fluoride on nanofiber cathode structure and durability in proton exchange membrane fuel cells." *Journal of The Electrochemical Society* 167.5 (2020): 054517.

[35] Desai, Fenil, et al. "Preparation and characterization of KOH-treated electrospun nanofiber mats as electrodes for iron-based redox-flow batteries." *Journal of Energy Storage* 27 (2020): 101053.

[36] Baghali, Mitra, W. A. D. M. Jayathilaka, and Seeram Ramakrishna. "The role of electrospun nanomaterials in the future of energy and environment." *Materials* 14.3 (2021): 558.

[37] Chen, Hong, Joshua D. Snyder, and Yossef A. Elabd. "Electrospinning and solution properties of Nafion and poly (acrylic acid)." *Macromolecules* 41.1 (2008): 128-135.

[38] Bajon, R., S. Balaji, and S. M. Guo. "Electrospun Nafion nanofiber for proton exchange membrane fuel cell application." *Journal of fuel cell science and technology* 6.3 (2009).

[39] Ballengee, Jason B., and Peter N. Pintauro. "Composite fuel cell membranes from dual-nanofiber electrospun mats." *Macromolecules* 44.18 (2011): 7307-7314.

[40] Park, Jun Woo, et al. "Electrospun Nafion/PVDF single-fiber blended membranes for regenerative H2/Br2 fuel cells." *Journal of Membrane Science* 541 (2017): 85-92.

[41] Powers, Devon, Ryszard Wycisk, and Peter N. Pintauro. "Electrospun tri-layer membranes for H2/Air fuel cells." *Journal of Membrane Science* 573 (2019): 107-116.

[42] Choi, Jonghyun, et al. "Nanofiber network ion-exchange membranes." *Macromolecules* 41.13 (2008): 4569-4572.

[43] Choi, Jonghyun, et al. "Nanofiber composite membranes with low equivalent weight perfluorosulfonic acid polymers." *Journal of Materials Chemistry* 20.30 (2010): 6282-6290.

[44] Ballengee, Jason B., and Peter N. Pintauro. "Preparation of nanofiber composite proton-exchange membranes from dual fiber electrospun mats." *Journal of membrane science* 442 (2013): 187-195.

[45] Ballengee, J. B., et al. "Properties and fuel cell performance of a nanofiber composite membrane with 660 equivalent weight perfluorosulfonic acid." *Journal of The Electrochemical Society* 160.4 (2013): F429.

[46] Sood, Rakhi, et al. "Active electrospun nanofibers as an effective reinforcement for highly conducting and durable proton exchange membranes." *Journal of Membrane Science* 622 (2021): 119037.

[47] Park, Jun Woo, Ryszard Wycisk, and Peter N. Pintauro. "Nafion/PVDF nanofiber composite membranes for regenerative hydrogen/bromine fuel cells." *Journal of Membrane Scienc*e 490 (2015): 103-112.

[48] Hossain, M., et al. "Pore-Filled PEMs from Poly (Phenylene Sulfonic Acid) S and Electrospun Poly (Phenylene Sulfone) Fiber Mats." *ECS Transactions* 98.9 (2020): 367.

[49] Choi, Jonghyun, et al. "Sulfonated polysulfone/POSS nanofiber composite membranes for PEM fuel cells." *Journal of The Electrochemical Society* 157.6 (2010): B914.

[50] Choi, Jonghyun, et al. "High conductivity perfluorosulfonic acid nanofiber composite fuel-cell membranes." *ChemSusChem* 3.11 (2010): 1245-1248.

[51] Zhu, Bensheng, et al. "NH2-UiO-66 coated fibers to balance the excellent proton conduction efficiency and significant dimensional stability of proton exchange membrane." *Journal of Membrane Science* 628 (2021): 119214.

[52] Chen, Wanting, et al. "SO42–/SnO2 solid superacid granular stacked one-dimensional hollow nanofiber for a highly conductive proton-exchange membrane." *ACS Applied Materials & Interfaces* 12.36 (2020): 40740-40748.

[53] Santos, Leslie Dos, et al. "Electrospun hybrid perfluorosulfonic acid/sulfonated silica composite membranes." *Membranes* 10.10 (2020): 250.

[54] Mojarrad, Naeimeh Rajabalizadeh, et al. "Nanofiber based hybrid sulfonated silica/P (VDF-TrFE) membranes for PEM fuel cells." *International Journal of Hydrogen Energy* 46.25 (2021): 13583-13593.

[55] Huang, Ziyi, et al. "Ultra-thin h-BN doped high sulfonation sulfonated poly (ether-ether-ketone) of PTFE-reinforced proton exchange membrane." *Journal of Membrane Science* 644 (2022): 120099.

[56] Huang, Henghui, et al. "Microporous expanded polytetrafluoroethylene layer functionalized hydrophilic groups for excellent mechanical durability and superior performance in proton exchange membrane fuel cell." *Journal of Power Sources* 526 (2022): 231130.

[57] Guimet, Adrien, et al. "Strengthening of perfluorosulfonic acid ionomer with sulfonated hydrocarbon polyelectrolyte for application in medium-temperature fuel cell." *Journal of Membrane Science* 514 (2016): 358-365.

[58] Wang, Baolong, et al. "Property enhancement effects of side-chain-type naphthalene-based sulfonated poly (arylene ether ketone) on Nafion composite membranes for direct methanol fuel cells." *ACS applied materials & interfaces* 9.37 (2017): 32227-32236.

[59] US DOE funding opportunity announcement (FOA) number: DE-FOA-0001874, https://eere-exchange.energy.gov/Default.aspx?foaId=79690f66-6dc9-47e9-ac9f-86057538ae44 (2018).

[60] US DOE fuel cell Technologies Office, multi-year research, development & demonstration plan: fuel cells, https://www.energy.gov/sites/prod/files/2017/05/f34/fcto_myrdd_fuel_cells.pdf (2017).

# CHAPTER 3 - ELECTROSPUN FIBER REINFORCED POLY(PHENYLENE SULFONIC ACID)-BASED COMPOSITE MEMBRANES

## 3.1 Background on Crosslinkable Poly(Phenylene Sulfonic Acid)s

Water management during fuel cell operation becomes simpler at high temperature and low RH. Litt's research group demonstrated the successful synthesis of a number of thermally stable, poly(aromatic sulfonic acid)s with excellent proton conductivity, even at low RH [1-3]. High water retention was associated with what Prof. Litt called a "frozen-in free volume", i.e., an excess microporosity resulting from sulfonic acid group crowding and/or incorporation of bulky co-monomers, which forces the chains apart. Initial work was on poly(naphthalene bisimides), which were hydrolytically unstable, before shifting to chemically stable poly(phenylene sulfonic acid)s and as copolymers, grafts, and crosslinked derivatives. The latest materials, based on crosslinked poly(phenylene sulfonic acid) (cPPSA) (Figure 3.1), showed good proton conductivity (>0.1 S/cm down to 20 %RH), between room temperature and 80 °C [4]. Unfortunately, the unusually high proton conductivity of cPPSA films was offset by their significant brittleness in dry state, which made their handling and processing difficult. In the present project, all membranes contain cPPSA ionomers synthesized by Dr. Hossain, a postdoc in Prof. Pintauro's lab.

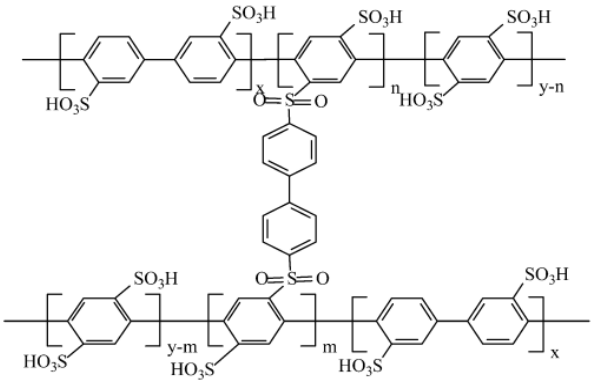


Figure 3.1: Chemical structure of crosslinked poly(phenylene sulfonic acid).

## 3.2 Experimental

### 3.2.1 Reagents Used

4,4′-Dibromobiphenyl, 1,4-dibromobenzene, biphenyl, copper powder, phosphoric acid (85%), and lithium hydroxide were purchased from Acros Organics (USA). Oleum (fuming sulfuric acid with 15% $SO_3$), 1-methyl-2-pyrrolidinone, anhydrous, 2.2′-bipyridine and iodine were purchased from Alfa Aesar (USA). Poly(ethylene oxide) (PEO, with a MW of 1 MDa), polyacrylic acid (PAA, with a MW of 400 kDa), N,N-dimethylacetamide 99.8% (DMAc), dimethyl sulfoxide (DMSO), 1-methyl-2-pyrrolidone (NMP), and phosphorous pentoxide were purchased from Sigma-Aldrich (USA). Radel® 5500 polyphenylsulfone (PPSU) particles were supplied by Solvay Specialty Polymers (Alpharetta, GA, USA). 26 wt.% PBI in DMAc stock solution was supplied by PBI Performance Products, Inc. (Charlotte, NC, USA).

### 3.2.2 Polyphenylene Ionomer Synthesis

4,4'-Dibromobiphenyl-3,3'-disulfonic acid (DBBPDSA), 1,4-dibromobenzene 2,5-disulfonic acid (DBPDSA) were synthesized from 4,4'-dibromobiphenyl-1,4-dibromobenzene and 1,4-dibromobenzene, respectively, using fuming sulfuric acid as the sulfonating agent [3]. The proton form of both dibromodisulfonic acid monomers was converted to the respective Li-salt form using LiOH. The copolymer was synthesized by Ullmann coupling polymerizations of DBPDSA-Li with DBBPDSA-Li ($P_xB_y$), at 170 ℃ in dry NMP, employing activated copper powder with 2,2'-bipyridine as the catalyst, according to the protocols developed by Litt and coworkers [3]. The ratio of the two comonomers was adjusted to obtain a phenylene disulfonic acid content of 25 mol%. Figure 3.2 shows the reaction scheme of copolymerization [5].

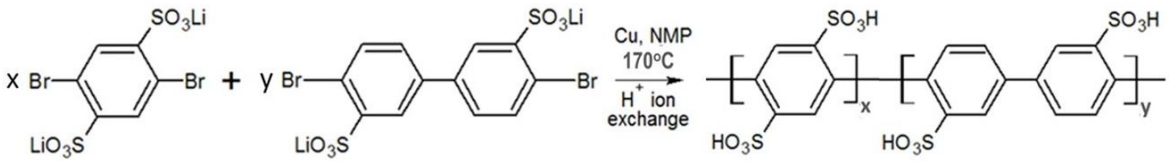


Figure 3.2: Copolymerization of DBPDSA-Li and DBBPDSA-Li salts to form the precursor ionomer $P_xB_y$ (x = 0.75, y = 0.25).

Grafting of biphenyl (BP) linkers was performed as proposed by Graybill [6] and involved reaction between the sulfonic acid group and biphenyl in polyphosphoric acid (generated in-situ from $P_2O_5$ and $H_3PO_4$) which served as both the solvent and the dehydrating agent. The grafting was done at 125 ℃ for 8-16 hours, which led to cPPSA with 9 - 18% of BP grafts. Figure 3.3 shows the reaction scheme of BP grafting [5].

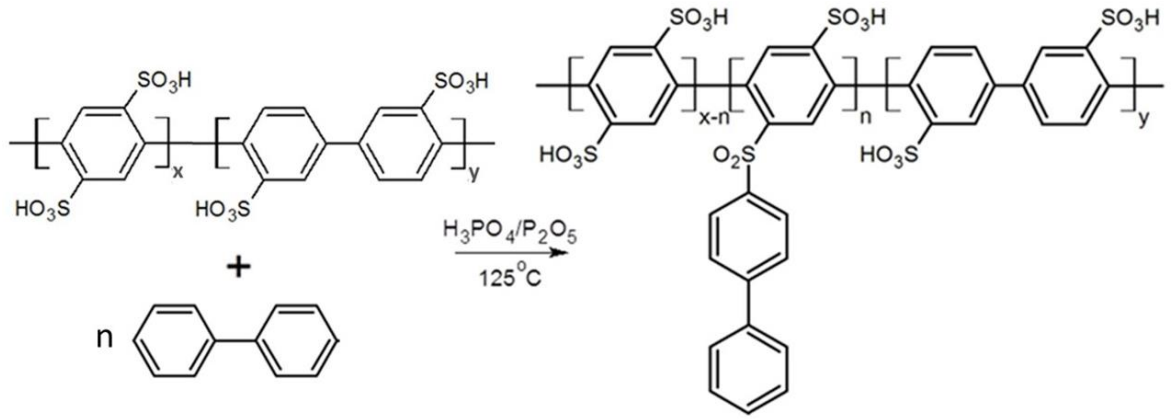


Figure 3.3: BP grafting onto $P_xB_y$ in polyphosphoric acid generated in situ from $H_3PO_4$ and $P_2O_5$. The resultant graft copolymer is described as crosslinkable poly(phenylenesulfonic acid), cPPSA.

Proton NMR spectrum was collected on a Bruker 400 MHz instrument equipped with a 9.4 Tesla Oxford magnet, controlled by a Bruker AV-400 console.

### 3.2.3 Nanofiber Electrospinning

#### 3.2.3.1 Reinforcing Polymer Electrospinning

To make nanofiber-reinforced proton exchange membranes, the first step is electrospinning reinforcing polymer nanofiber mats. In this case, high-performance polymer PPSU and PBI were used for fiber electrospinning. Electrospun PPSU fibers were previously made in Prof. Pintauro's lab to reinforce PFSA proton exchange membranes [7]. PPSU particles were dissolved in NMP-acetone (9:1) to prepare a 30 wt.% solution used to produce electrospun fibers. A 26 wt.% PBI in DMAc stock solution was diluted to 20 wt.% for electrospinning. Previous experiments showed that PBI solution can be electrospun to yield nanofibers [8]. Table 3.1 shows the best electrospinning conditions for PPSU and PBI fibers, respectively.

Table 3.1: Summary of electrospinning conditions for reinforcing polymer fibers.

| Reinforcing Polymer | Spinneret to collector distance (cm) | Relative humidity | Voltage (kV) | Flow rate (mL/h) |
|---|---|---|---|---|
| 30 wt.% PPSU | 12 | 30 % | 10 | 0.08 |
| 20 wt.% PBI | 10 | 35 % | 15 | 0.1 |

#### 3.2.3.2 cPPSA Electrospinning

To prepare dual fiber membranes, conditions were examined to identify the best for electrospinning cPPSA. Since the cPPSA has a short molecular chain length and a stiff aromatic backbone, it's hard for cPPSA to form necessary molecular chain entanglements for electrospinning. Thus, an electrospinning polymer carrier which is miscible with cPPSA is required. Two water-soluble carriers were tested for electrospinning cPPSA: polyethylene oxide (PEO, 1 MDa) and polyacrylic acid (PAA, 450 kDa). PEO and PAA have previously been used as carriers in electrospinning PFSA fibers to make composite proton exchange membranes [8,9].

While PEO with 1 MDa molecular weight can be used in electrospinning cPPSA, a high molecular weight PAA (such as 1.25 MDa) will form a gel with water as solvent limiting its use as a carrier for electrospinning cPPSA. In preliminary experiments, two other water soluble carriers were also tested: poly(vinyl alcohol), (PVA, 85 k -124 kDa and 146 k -186 kDa) and poly(vinyl pyrrolidone), (PVP, 1.3 MDa). While PVP has been used as carrier to electrospin PFSA fiber [10], both PVA and PVP unfortunately caused cPPSA precipitation or gelation preventing their use as carriers.

The following electrospinning conditions were employed for making cPPSA-PEO fiber mats: ~50 % relative humidity, 10 kV accelerating voltage, 10 cm spinneret to collector distance, and 0.1 mL/h flow rate. The carrier content was defined as the ratio of carrier weight to cPPSA weight. The fiber radius distribution was measured from SEM images of a fiber mat surface using ImageJ software. Example images and the associated frequency plots are shown later in the chapter as Figures 3.9 to 3.11, for the PEO contents of 5, 4, and 3 wt.%,

respectively, relative to cPPSA weight in the electrospinning solutions.

Based on preliminary electrospinning experiments of cPPSA-PAA fibers, the following parameters were identified as optimal: 450 kDa PAA at 6 wt.% content relative to cPPSA weight, accelerating voltage of 10 kV, and a needle to collector distance of 9 cm. The experimental variables were relative humidity (RH, %) and solution flow rate (in mL/h). Solvent composition was also important. After testing different solvent combinations, those yielding the best electrospun cPPSA fibers morphology were 1:1 $H_2O$-isopropanol (IPA) for cPPSA-PEO and 3:1 $H_2O$-DMSO for cPPSA-PAA. The cPPSA-PEO and cPPSA-PAA electrospinning solutions were prepared by adding a specific amount of PEO or PAA stock solution to cPPSA solution to achieve 30 and 25 wt.% concentrations, respectively. Table 3.2 summarizes the best electrospinning conditions. The carrier content was defined as the percentage of carrier polymer weight to cPPSA weight. 6 wt.% 450 kDa PAA is the minimum amount required to obtain electrospun cPPSA-PAA fibers.

Table 3.2: Summary of cPPSA electrospinning conditions using PEO and PAA as carrier.

| Carrier | Carrier content | Spinneret to collector distance (cm) | Relative humidity | Voltage (kV) | Flow rate (mL/h) |
|---|---|---|---|---|---|
| PEO | 3 % | 10 | 50 % | 10 | 0.1 |
| PAA | 6 % | 9 | 40 % | 10 | 0.25 |

### 3.2.4 Fabrication of Dual-fiber Composite Membrane

The fabrication of a dual-fiber composite membrane required simultaneous electrospinning of cPPSA fibers and reinforcing polymer fibers. The dual-fiber electrospinning conditions were the same as those found for individual cPPSA and reinforcing (PPSU or PBI) polymer fibers. Since cPPSA is hydrophilic, a thin layer of reinforcing polymer fibers was first deposited on the collector first during dual-electrospinning experiments. Usually, 0.03 mL of reinforcing polymer solution was electrospun first to prevent the cPPSA fibers from adhering strongly to the aluminum foil on the collector.

When electrospinning was finished, the fiber mat was peeled from the aluminum foil and placed into a vacuum oven overnight to fully evaporate solvent. Then, the fiber mat was cut into 5 cm x 5 cm size pieces, clamped by two square Teflon frames, and exposed to methanol vapor by suspending the mat in a closed chamber above a methanol surface. cPPSA fibers selectively melted in the methanol atmosphere and filled the voids between reinforcing polymer fibers. During solvent exposure procedure, the reinforcing polymer maintained the fiber structure, as it was unaffected by methanol vapor.

The resultant dual-fiber composite membranes had a cPPSA matrix with embedded electrospun reinforcing polymer fibers. Such a membrane morphology (an uncharged reinforcing polymer fiber network embedded in an ionomer matrix) have been shown to exhibit low in-plane swelling [11], which was identified as a critical

feature for long-term membrane durability in a fuel cell. After solvent exposure, the dual-fiber composite membrane sample was compressed to densify the membrane, and the cPPSA component of dual-fiber membranes was then crosslinked at a temperature > 200 ℃ under vacuum. After crosslinking, the membrane was equilibrated under ambient condition. Figure 3.4 summarizes the overall process for fabricating the dual fiber membrane.

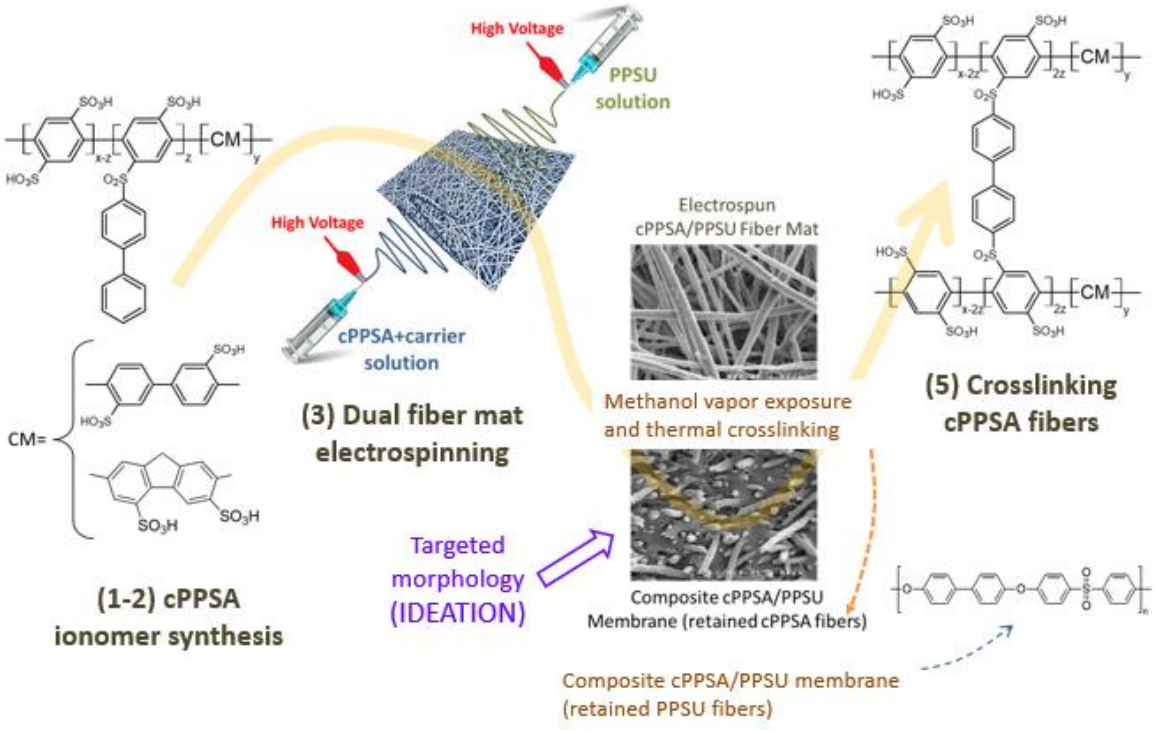


Figure 3.4: Overview of cPPSA/PPSU dual-fiber composite membrane fabrication.

### 3.2.5 Fabrication of Pore-filled Composite Membrane

The usual method of creating a pore-filled composite membrane (i.e., immersion of a reinforcing polymer fiber mat into an ionomer solution [12]) could not be used because of the low viscosity of cPPSA MeOH solution and the limited amount of cPPSA ionomers synthesized at Vanderbilt University. Initially when fabricating pore-filled composite membranes, cPPSA solution was dropped onto the surface of an electrospun reinforcing polymer fiber mat and a casting knife was used to coat ionomer into the fiber mat. Since the short chain length of the PPSA limited entanglements, the viscosity of the cPPSA methanol solution was very low. This solution caused the reinforcing polymer fiber mat to wrinkle and left solution residue on the casting knife. Uniform pore-filled membrane can't be obtained by solution casting method. To avoid the disadvantages of solution casting, a new method to fabricate pore-filled membrane was examined.

First, casted cPPSA films were prepared with dimensions of 5 cm x 5 cm. Usually, cPPSA was dissolved in MeOH to prepare a 2 wt.% solution and then the solution was spread onto a flat Teflon-FEP sheet in a fume

hood, where the solvent was allowed to evaporate. Then the casted cPPSA film was heated to 30 ℃ and peeled off from the Teflon-FEP sheet. To increase interface compatibility, a reinforcing polymer fiber mat was soaked in a Poloxamer 407 (surfactant) solution in 1:1 ethanol (EtOH): $H_2O$ and then put in fume hood to evaporate solvent.

After this treatment, surfactant remained on the reinforcing polymer fibers, making the reinforcing polymer fiber mat hydrophilic. The casted cPPSA film was placed on the top of the surfactant-treated reinforcing polymer fiber mat, and the two layers were exposed to MeOH vapor to soften/melt the cPPSA film. The cPPSA impregnated the reinforcing fiber mat, filling the void space between fibers. A dense, uniform pore-filled membrane was obtained. Figure 3.5 shows the procedure for fabricating the pore-filled composite membrane.

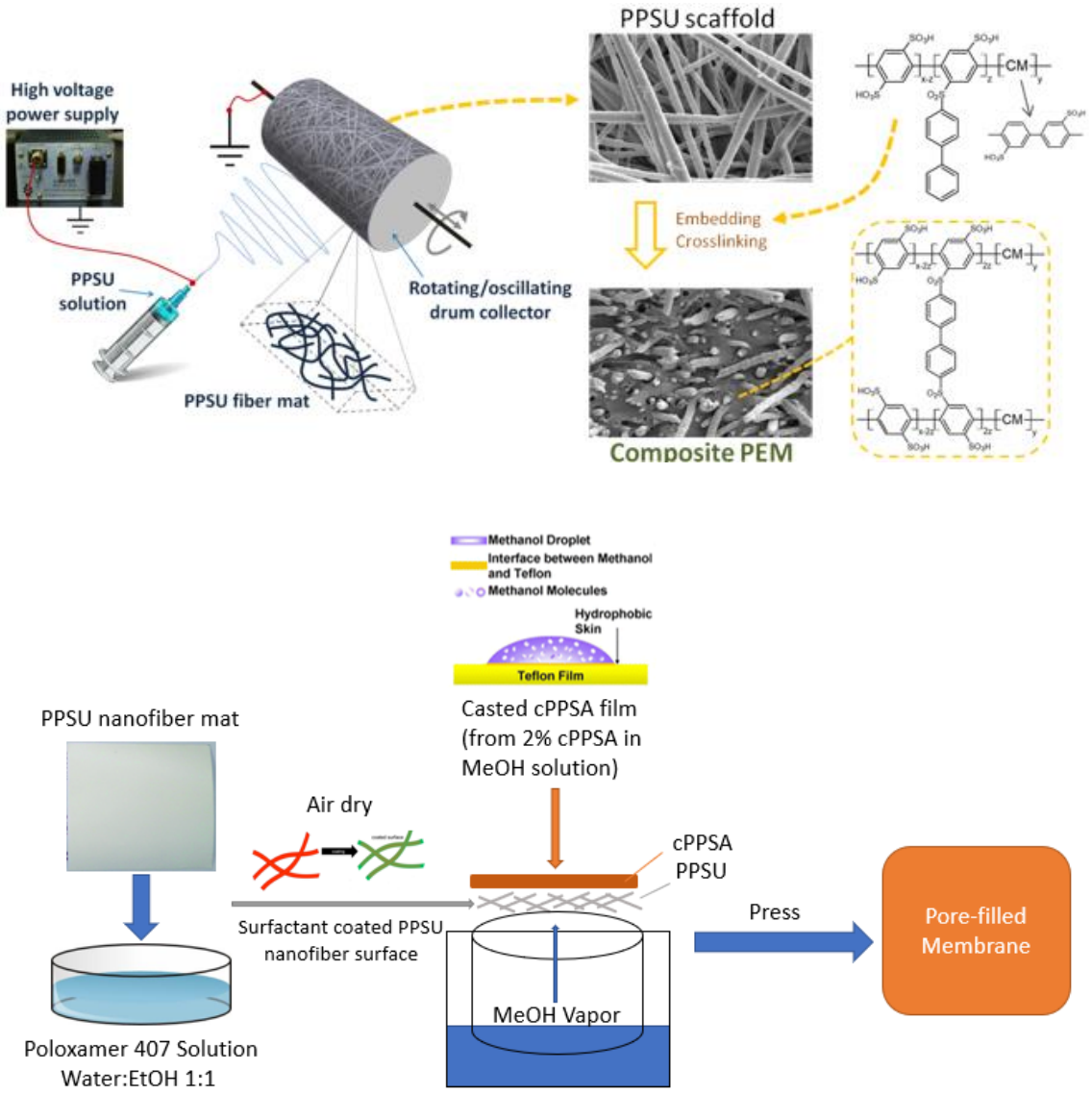


Figure 3.5: Overview of cPPSA/PPSU pore-filled membrane fabrication.

### 3.2.6 Fabrication of Cast cPPSA Film

Pristine cPPSA was cast into a film to check its proton conductivity after different crosslinking conditions. cPPSA was dissolved in MeOH and cast on a flat Teflon-FEP sheet in a fume hood. After the solvent was evaporated, the cast cPPSA film was peeled off the Teflon-FEP sheet and thermally crosslinked at different temperature/time combinations to make it insoluble in water.

### 3.2.7 Characterization of Proton-Exchange Membranes

#### 3.2.7.1 Proton Conductivity

In-plane proton conductivity was determined by AC impedance measurements, using a BekkTech four-electrode test cell [13]. Although through-plane conductivity is more relevant to fuel cell PEM characterization, its measurement is difficult and prone to errors caused by the impedance at the membrane/electrode interfaces [14]. For this reason, the in-plane testing was employed in the present work. The BekkTech cell was placed in an ESPEC Corp. temperature/humidity controlled environmental chamber (Model: SH-241) for testing at 80 °C and 40 - 90 %RH. In-plane conductivity was calculated using Equation 3.1

$$\sigma = \frac{1000L}{wtR} \qquad \text{(Equation 3.1)}$$

where σ (mS/cm) is in-plane proton conductivity, R (Ω) is the resistance (real axis intercept on Nyquist plot), L (cm) is the distance between the inner electrodes, w (cm) is the width of a membrane sample (typically 0.4 cm), and t (cm) is the thickness of the membrane sample.

#### 3.2.7.2 Morphology

Surface and cross-section morphology of electrospun nanofiber mats surface and composite membranes were imaged with a Hitachi S-4200 scanning electron microscope. Samples were sputter-coated with a gold layer to prevent charging of the specimen and reduce thermal damage while improving secondary electron emission. The distribution of electrospun nanofiber mats was analyzed using SEM images and DiameterJ (plugin of ImageJ) [15].

#### 3.2.7.3 Mechanical Properties

Stress and strain of composite membrane samples were measured with a TA Instruments Q800 dynamic mechanical analyzer (DMA, TA Instruments, New Castle, NY, USA). Stress-strain curves were obtained for membranes equilibrated in air at 25 °C. The DMA was operated in tension using the controlled strain mode, where the sample was strained at 10%/min until failure.

#### 3.2.7.4 MEA Fabrication and Fuel Cell Testing

Membrane-electrode assemblies (MEAs) were prepared with cPPSA/PPSU pore-filled membrane and with Nafion XL, using commercial Pt/C gas diffusion electrodes (GDEs) with 5 $cm^2$ catalyzed area, purchased from

the Fuel Cell Store. The anode and cathode Pt loading was 0.12 mg/cm$^2$. MEAs with cPPSA/PPSU pore-filled membranes were not hot-pressed; the membrane was just sandwiched between the electrodes and PTFE gaskets, and then directly installed into a test cell (single serpentine $H_2$ and air flow channels, Fuel Cell Technologies Inc.). MEAs with Nafion XL were hot-pressed in a heated hydraulic press at 140 °C and 690 kPa, for 10 min before use.

MEAs were evaluated using a Scribner 850e hydrogen/air fuel cell test station. Data were collected at 80 °C, 100 %RH and 50 %RH without backpressure, the same for the both feed streams. The $H_2$ and oxidant (air) flow rates were 0.125 L/min and 0.5 L/min, respectively. All experimental runs were repeated at least two times. Typically, the current density variability was within 5% for a given cell voltage.

### 3.3 Results and Discussion

Three types of fiber mats were electrospun (reinforcing polymer fiber mats, from PPSU and PBI, ionomer fiber mats, from cPPSA, and dual fiber mats, from cPPSA co-spun with PPSU), and three types of membranes were fabricated from these fibers: (1) Cast membranes (2) Dual-fiber membranes and (3) Pore-filled membranes.

#### 3.3.1 NMR Spectrum

Figure 3.6 shows the $^1$H NMR spectrum for P75B25-g-BP15%. For comparison, $^1$H NMR spectrum of the P75B25 copolymer (un-grafted) is also shown in the same figure. The fraction of phenylenedisulfonic acid units in the copolymer (75%) was calculated from the integrals of protons (a) and (b) of the un-grafted copolymer. The fraction of sulfonic acid groups grafted with biphenyl (BP, 15%) was calculated using the integral of protons c+c'.

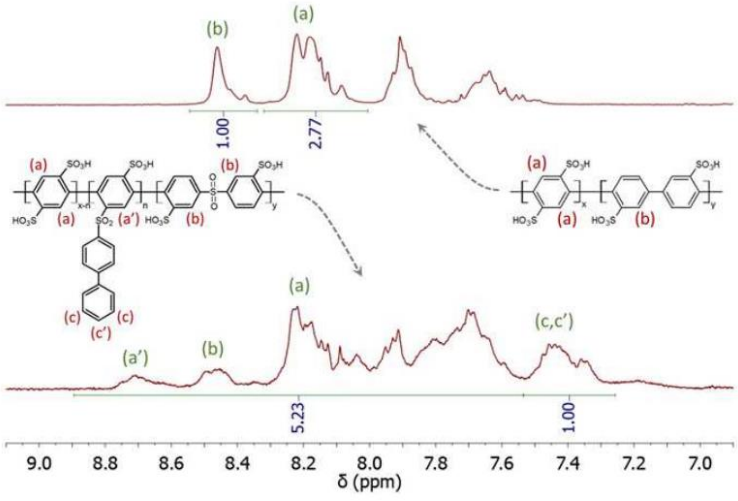


Figure 3.6: $^1$H NMR spectra (400 MHz) of P75B25 (upper), and P75B25-g-BP15% (lower) copolymers in $CD_3OD$.

### 3.3.2 Morphology

#### 3.3.2.1 Morphology of Reinforcing Polymer Fibers

Electrospun PPSU and PBI fiber mats were imaged (top-down) using scanning electron microscopy (SEM); Figure 3.7 and 3.8 show SEM images of these fiber mats along with plots of their fiber diameter distribution. The fiber diameters were relatively uniform for both polymers. The average diameter for PPSU fibers was 1.22 μm and for PBI fibers was 462 nm.

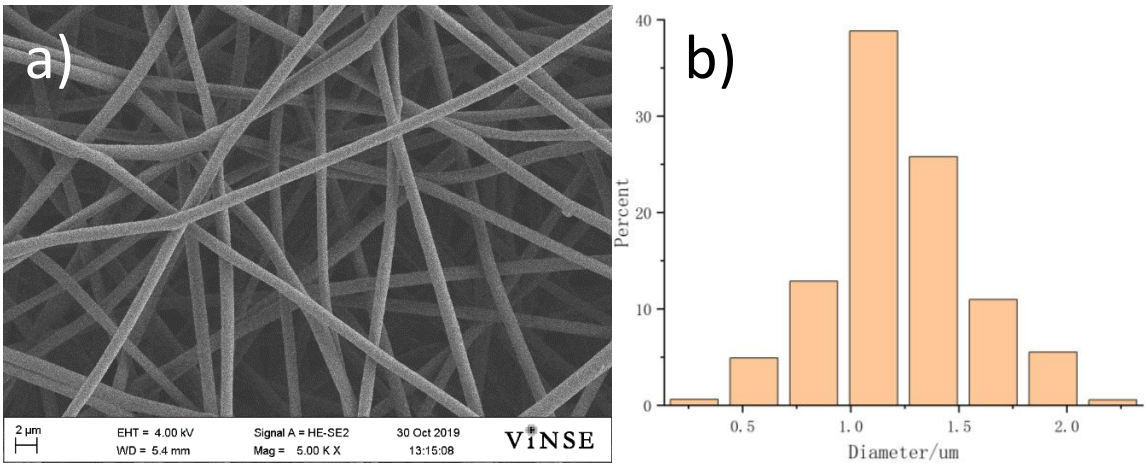


Figure 3.7: a) Top-down SEM image of as-spun PPSU fibers. b) Diameter distribution of PPSU fibers.

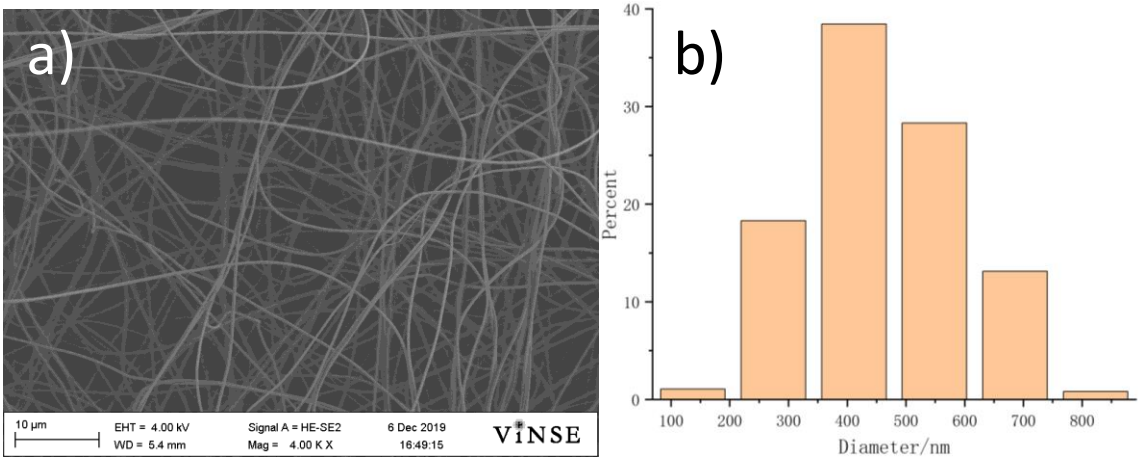


Figure 3.8: a) Top-down SEM image of as-spun PBI fibers. b) Diameter distribution of PBI fibers.

#### 3.3.2.2 Morphology of cPPSA-PEO Fibers

The main objective of the electrospinning activity was to optimize the cPPSA electrospinning conditions to obtain ionomer fiber mats with relatively uniform fibers defined as "*less than 10% beads and droplets, fiber diameter variability < 50% by ImageJ*." As evidenced in Figures 3.9 to 3.11, the obtained cPPSA fibers were relatively uniform, with no beads or droplets.

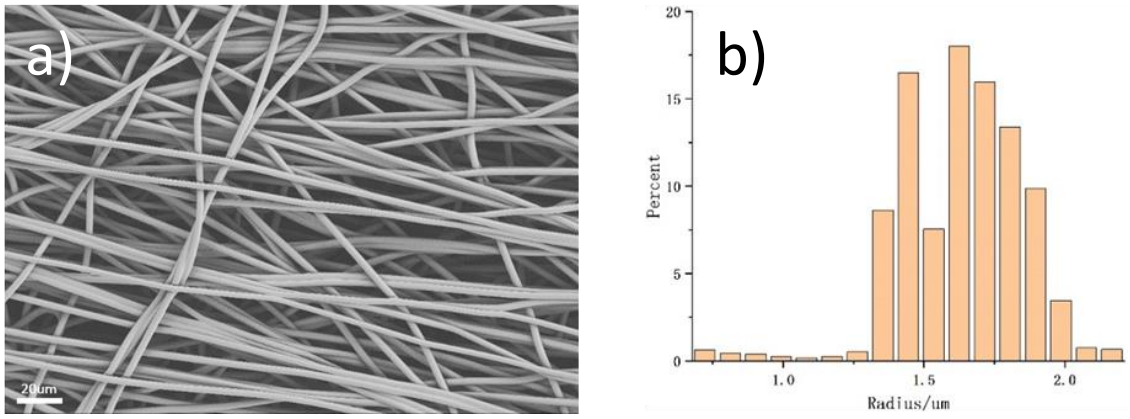


Figure 3.9: a) Top-down SEM image of as-spun fibers of cPPSA-PEO with 5 wt.% of PEO, b) Fiber radius distribution.

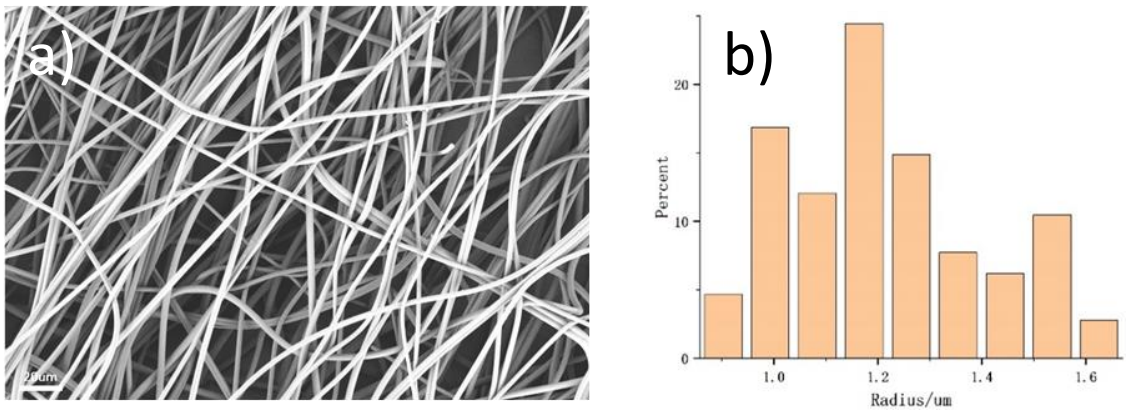


Figure 3.10: a) Top-down SEM image of as-spun fibers of cPPSA-PEO with 4 wt.% of PEO, b) Fiber radius distribution.

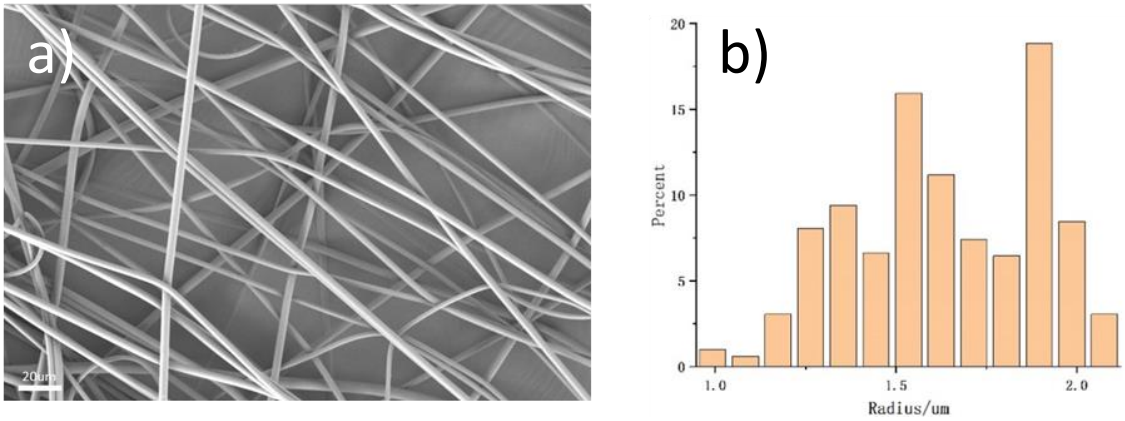


Figure 3.11: a) Top-down SEM image of as-spun fibers of cPPSA-PEO with 3 wt.% of PEO, b) Fiber radius distribution.

A summary of the fiber radius distribution for the electrospun cPPSA-PEO fiber mats with three PEO (carrier)

contents is shown in Table 3.3. The criterion of electrospun fiber uniformity was 90% of the fibers with radii within ± 25% of the mean fiber radius. As shown in the table, the left and right tails of the three radius distributions constituted less than 10% of fibers, which indicated meeting the milestone criterion.

Table 3.3: Fiber radius results of cPPSA-PEO mats with different PEO carrier content.

| PEO Content | Average Radius/µm | 50% Variability Range/µm | Left Tail/% | Right Tail/% | Fiber Uniformity |
|---|---|---|---|---|---|
| 3% | 1.62 | 1.23-2.04 | 4.6 | 3.0 | Yes |
| 4% | 1.22 | 0.91-1.52 | 4.7 | 2.7 | Yes |
| 5% | 1.64 | 1.22-2.04 | 2.2 | 1.4 | Yes |

#### 3.3.2.3 Morphology of cPPSA-PAA Fibers

Figures 3.12 to 3.17 show SEM images and the associated plots of fiber radii distributions obtained for cPPSA-PAA fibers at various RH and flowrate values.

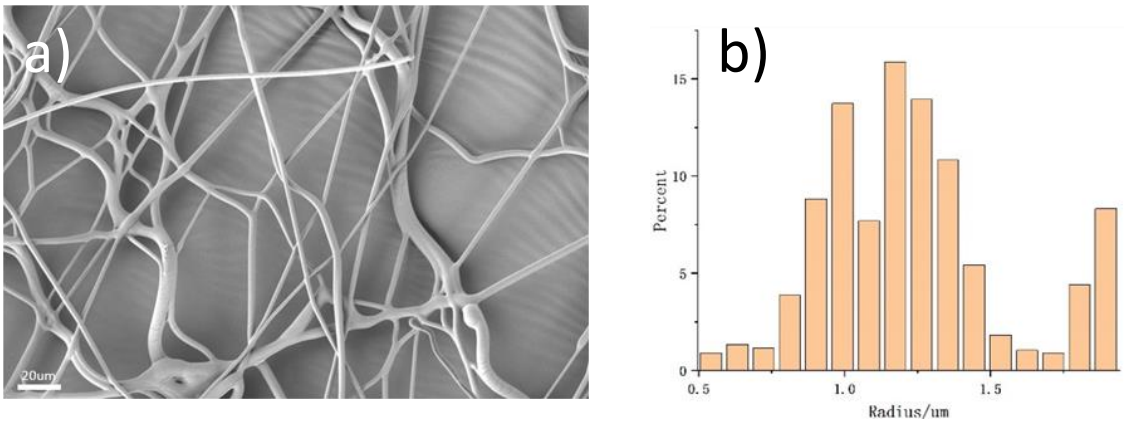


Figure 3.12: a) Top-down SEM image of as-spun fibers of cPPSA-PAA b) Fiber radius distribution for RH/flowrate: 45%/0.10 mL/h.

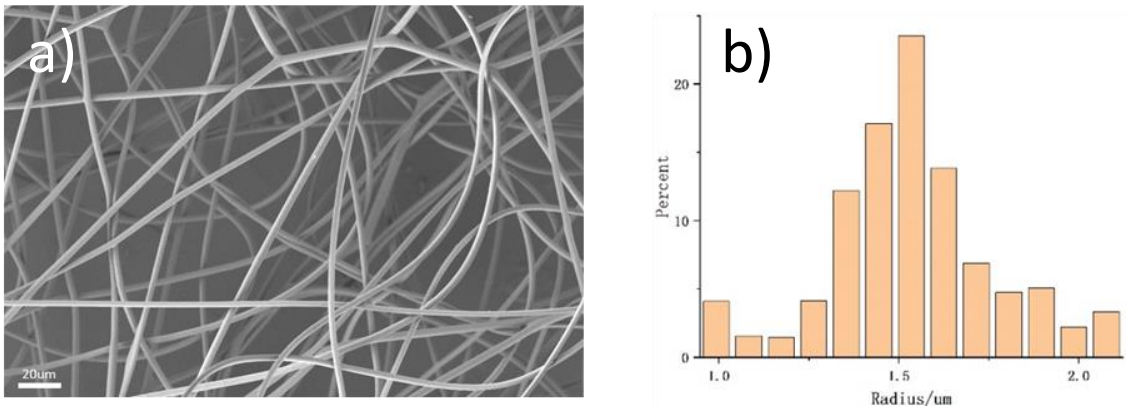


Figure 3.13: a) Top-down SEM image of as-spun fibers of cPPSA-PAA b) Fiber radius distribution for RH/flowrate: 35%/0.15 mL/h.

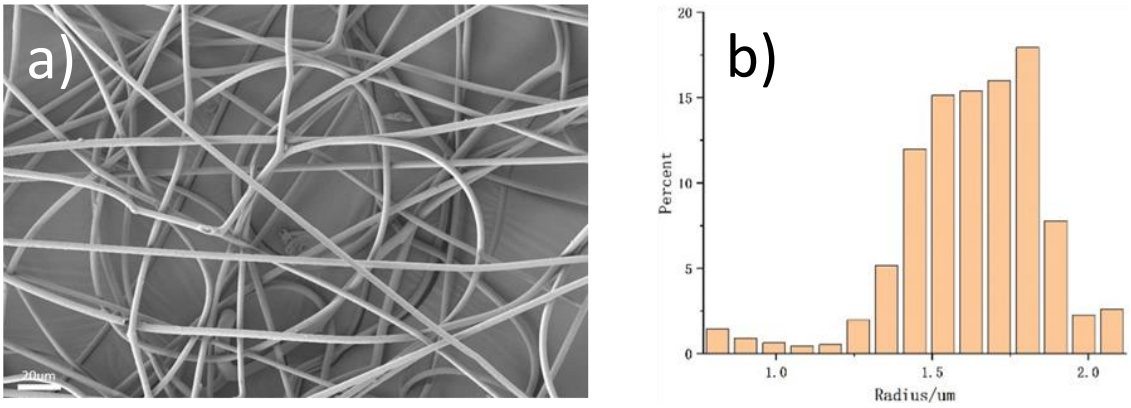


Figure 3.14: a) Top-down SEM image of as-spun fibers of cPPSA-PAA b) Fiber radius distribution for RH/flowrate: 40%/0.15 mL/h.

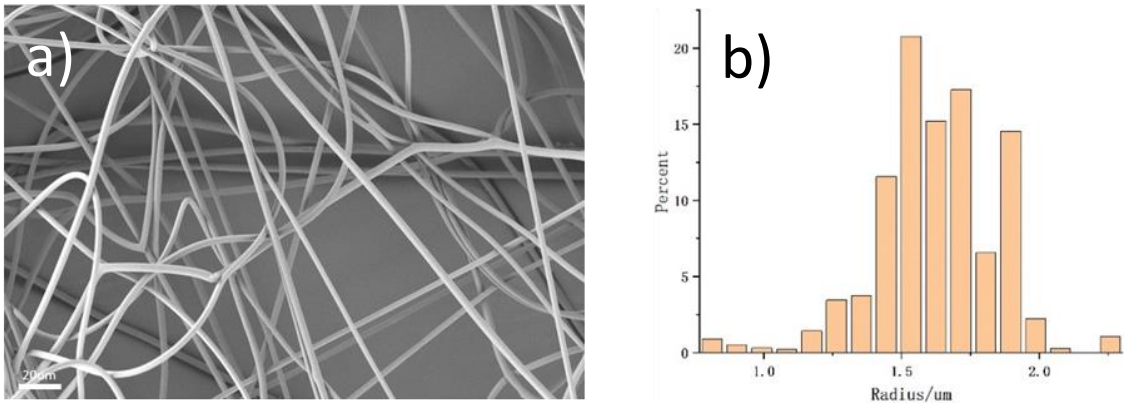


Figure 3.15: a) Top-down SEM image of as-spun fibers of cPPSA-PAA b) Fiber radius distribution for RH/flowrate: 40%/0.15 mL/h.

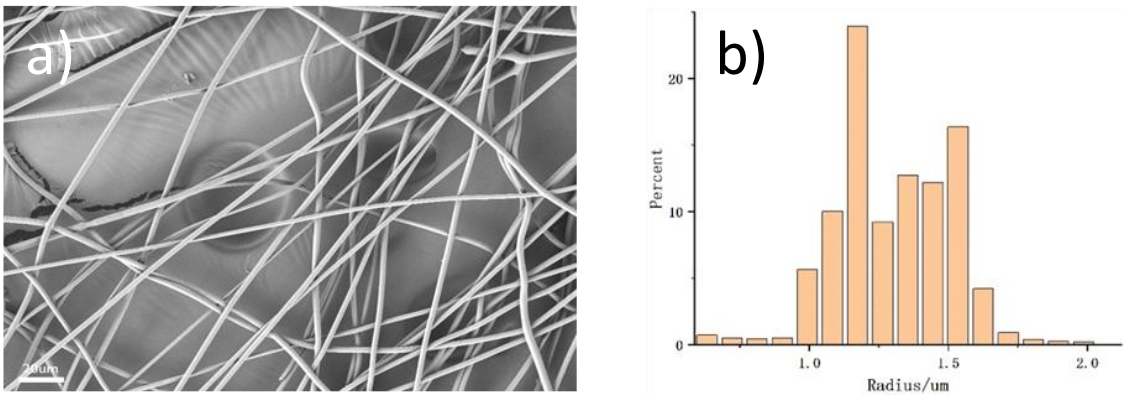


Figure 3.16: a) Top-down SEM images of as-spun fibers of cPPSA-PAA b) Fiber radius distribution for RH/flowrate: 40%/0.25 mL/h.

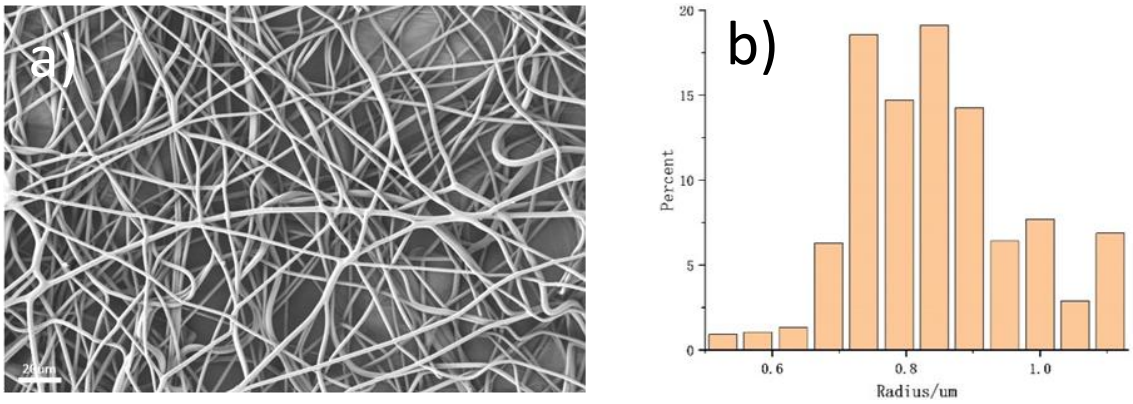


Figure 3.17: a) Top-down SEM image of as-spun fibers of cPPSA-PAA b) Fiber radius distribution for RH/flowrate: 40%/0.30 mL/h.

As seen in Figures 3.12 to 3.17, the obtained cPPSA-PAA fibers, except those shown in Figure 3.12a, were relatively uniform, with no beads or droplets. Most of the fibers had radii in the 1 - 2 μm range. A summary of the fiber radius distribution for the cPPSA-PAA mats is shown in Table 3.4.

Table 3.4: Fiber radius results for cPPSA-PAA mats prepared under various conditions.

| RH (%) | Flow Rate (mL/h) | Average Radius (μm) | 50% Variability Range (μm) | Left Tail (%) | Right Tail/ (%) | Fiber Uniformity |
|---|---|---|---|---|---|---|
| 45 | 0.10 | 1.24 | 0.92-1.55 | 16.1 | 14.6 | No |
| 35 | 0.15 | 1.54 | 1.15-1.92 | 5.6 | 5.5 | No |
| 40 | 0.15 | 1.63 | 1.22-2.04 | 3.9 | 2.6 | Yes |
| 40 | 0.20 | 1.63 | 1.22-2.03 | 3.4 | 1.3 | Yes |
| 40 | 0.25 | 1.30 | 0.98-1.63 | 2.2 | 1.8 | Yes |
| 40 | 0.30 | 0.85 | 0.64-1.06 | 3.3 | 6.9 | No |

As seen in the table, the left and right tails for three of the six radii distributions constituted less than 10% of the electrospun fibers, which indicated meeting the milestone criterion. The fiber mat electrospun at 45 %RH/0.10 mL/h, failed to meet the 50% fiber radius variability criterion the most, while the mats spun at 35 %RH/0.15 ml/h and 40 %RH/0.30 ml/h failed the criterion by a small margin.

Figure 3.18 shows photographs of an electrospun dual-fiber composite membrane and a pore-filled composite membrane (cPPSA-PPSU). Both of these composite membranes were translucent with no evidence of macroscopic non-homogeneity, suggesting the cPPSA and reinforcing polymer components are dispersed on the nano/micro level.


Figure 3.18: Photographs of a composite a) cPPSA-PPSU dual-fiber membrane and b) cPPSA-PPSU pore-filled membrane.

Figure 3.19 shows SEM images of a cross-section and a surface of the dual-fiber composite membrane. Figure 3.20 and 3.21 show SEM images of the pore-filled membranes with PPSU and PBI as reinforcing fibers. The membranes show no evidence of leftover voids or defects, suggesting a uniform distribution of reinforcing fibers throughout the cross-sections. What appear to be small pores in the membrane are actually artifacts of the freeze-fracturing procedure, where reinforcing polymer fibers were pulled from the freeze-fractured surfaces. An important observation is the lack of cPPSA overlayers, which is a much-desired feature. The membrane surface is also uniform with no holes or other defects.

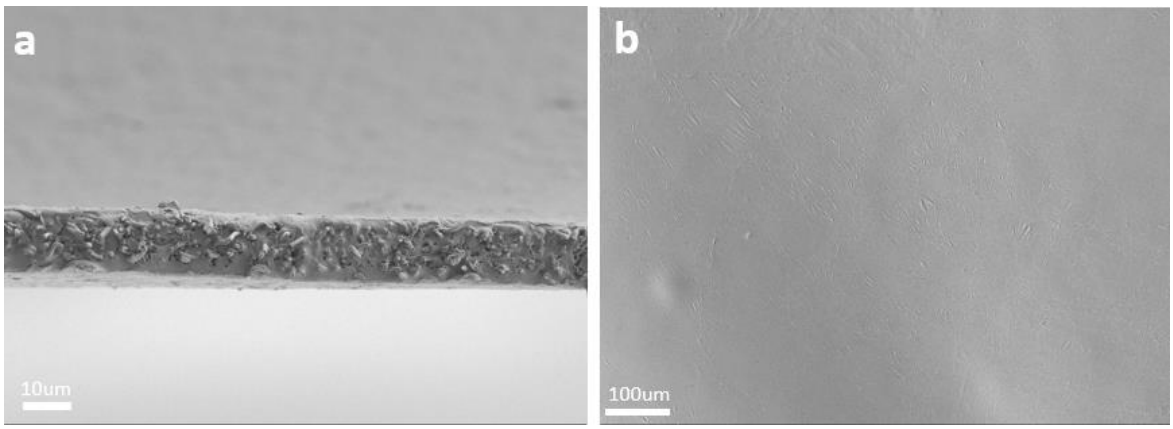


Figure 3.19: a) SEM image of the dual-fiber membrane freeze-fractured cross-section, b) Top-down SEM image of dual-fiber membrane surface.

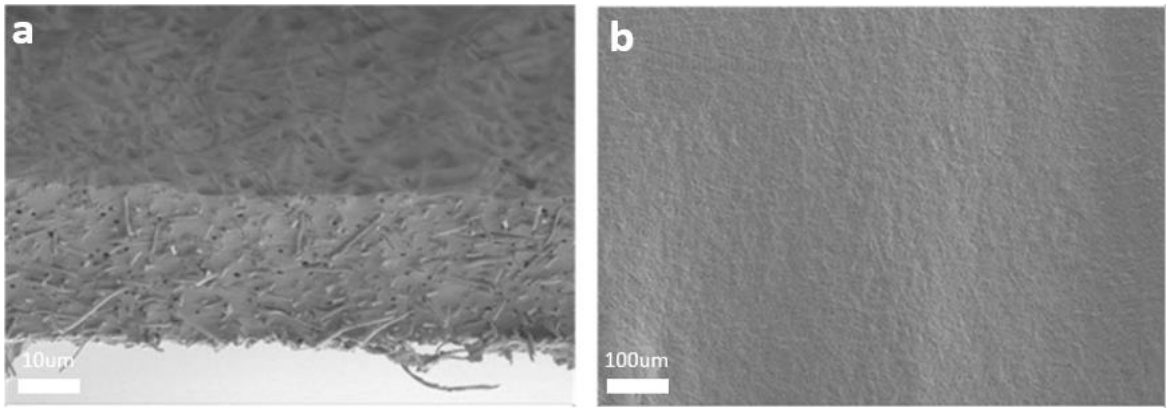


Figure 3.20: a) SEM image of the freeze-fractured cross-section of pore-filled membrane with PPSU reinforcing fibers, b) Top-down SEM image of pore-filled membrane with PPSU reinforcing fibers.

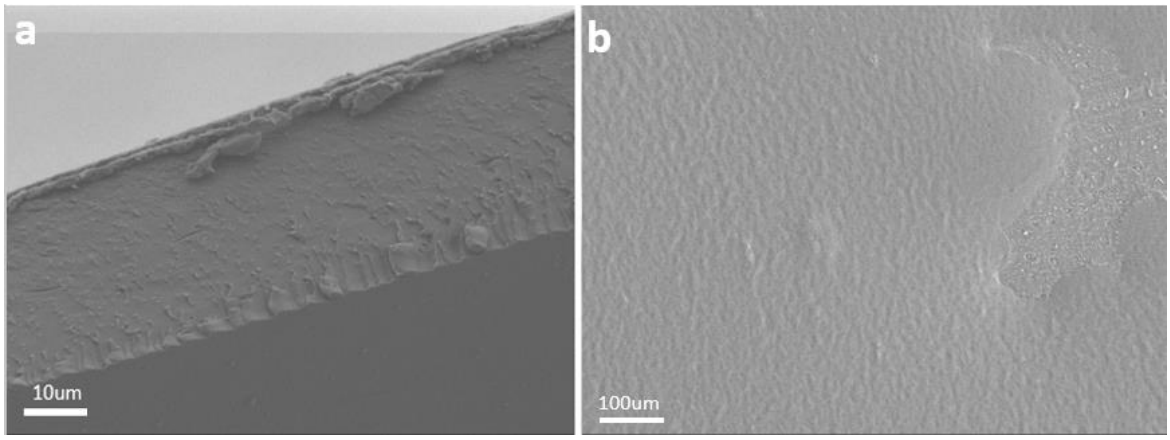


Figure 3.21: a) SEM image of the pore-filled membrane with PBI as reinforcing fibers freeze-fractured cross-section, b) Top-down SEM image of pore-filled membrane PBI as reinforcing fibers surface.

### 3.3.3 Proton Conductivity

Figure 3.22 shows the dependence of proton conductivity on relative humidity at 80 °C for the cast pristine cPPSA films with different crosslinking conditions and for Nafion 211 (equivalent weight: 1100). The data show that crosslinking time and temperature influence the proton conductivity of pristine cPPSA, where proton conductivity decreased with longer crosslinking time. This decrease may result from possible condensation of sulfonic acid group [16]. The crosslinking condition of 1 h at 210 ℃ was sufficient to make pristine cPPSA water-insoluble and yielded materials with the highest proton conductivities: 63 mS/cm at 40 %RH and 336 mS/cm at 90 %RH, which are more than 3 times that for Nafion 211 at these RH values (18 mS/cm at 40 %RH, and 94 mS/cm at 90 %RH). Even cPPSA crosslinked at 210 ℃ for 5 h showed conductivity values greater than that of Nafion 211. The results demonstrate that cPPSA is a much better proton conductor than Nafion 211.

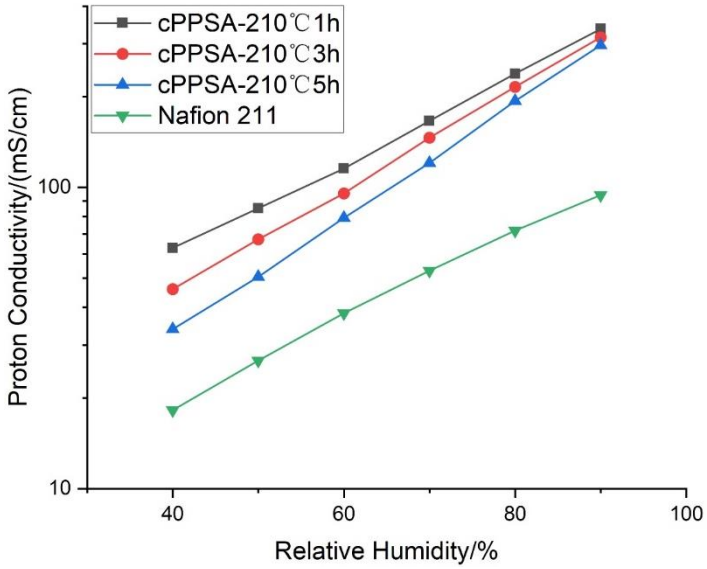


Figure 3.22: Proton conductivity of crosslinked pristine cPPSA and Nafion 211.

Figure 3.23a shows the proton conductivity of dual-fiber membranes (DFMs) fabricated from electrospun cPPSA (1 MDa PEO carrier) and PPSU mats after various times for crosslinking where the ratio of cPPSA to PPSU was 4:1 and the PEO carrier content was 3 wt.%. cPPSA was selectively melted to form the membrane matrix with embedded PPSU reinforcing fiber. In the figure, adding carrier to cPPSA fibers dramatically reduced the proton conductivity, which may reflect reaction between cPPSA sulfonic acid groups and PEO to form sulfonate esters [17]. Even crosslinking at 210 ℃ for only 1 h lowered the proton conductivity of dual-fiber membrane at 40 %RH to lower than that of Nafion XL. At 90 %RH, the conductivity remained high at 252 mS/cm.

To examine whether the PEO carrier reacted with the cPPSA ionomer and to exclude a significant influence of the reinforcing polymer fibers on proton conductivity, cPPSA was mixed with various amounts of 1 MDa PEO, casted into films, and crosslinked at 210 ℃ for 1 h under vacuum. Figure 3.23b shows that as little as 0.25 wt.% PEO decreased the proton conductivity of cPPSA by 26% at 40 %RH. The data suggest that higher PEO content, such as 3 wt.% as used in electrospinning, will decrease cPPSA conductivity even more significantly.

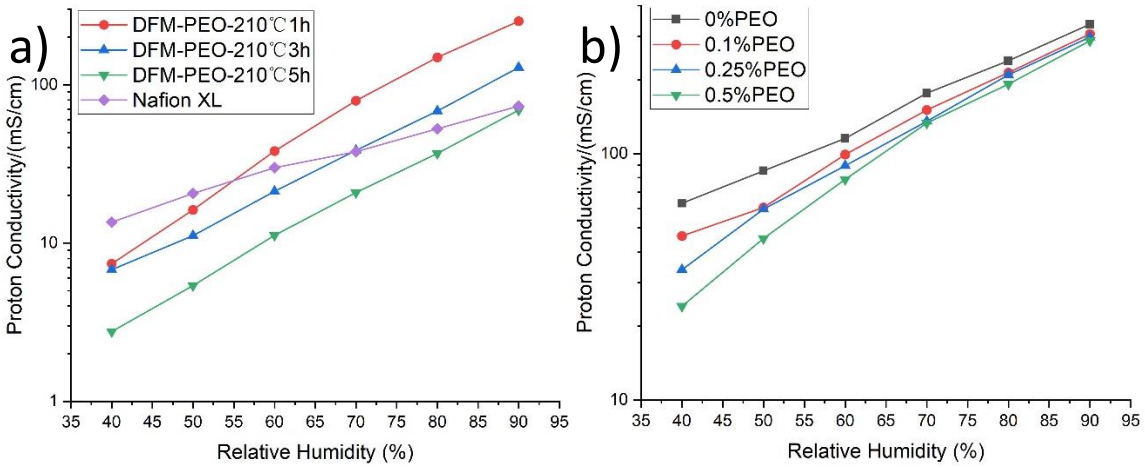


Figure 3.23: a) Proton conductivity of crosslinked dual-fiber membranes with PEO as carrier and of Nafion XL. b) Proton conductivity of crosslinked cast cPPSA-PEO films with different PEO content.

PAA was selected as an alternative carrier for cPPSA electrospinning as the interaction of cPPSA with PAA was expected to impact the proton conductivity to a lesser extent than for PEO. Figure 3.24 shows the proton conductivity of dual-fiber membranes with 450 kDa PAA as carrier, crosslinked at different conditions. The ratio of cPPSA to PPSU was 4:1 and the PAA carrier content is 6 wt.%. With PAA as the carrier, there is greater proton conductivity compared to PEO. The membrane crosslinked at 210 ℃ for 1 h showed 34 mS/cm at 40 %RH and 266 mS/cm at 90 %RH. However, the both values were still > 40% lower than those of the crosslinked pristine cPPSA. In particular, crosslinking at 210 ℃ for 5 h has the lowest the proton conductivity of membrane at 40 %RH, indicating the need to reduce crosslinking time.

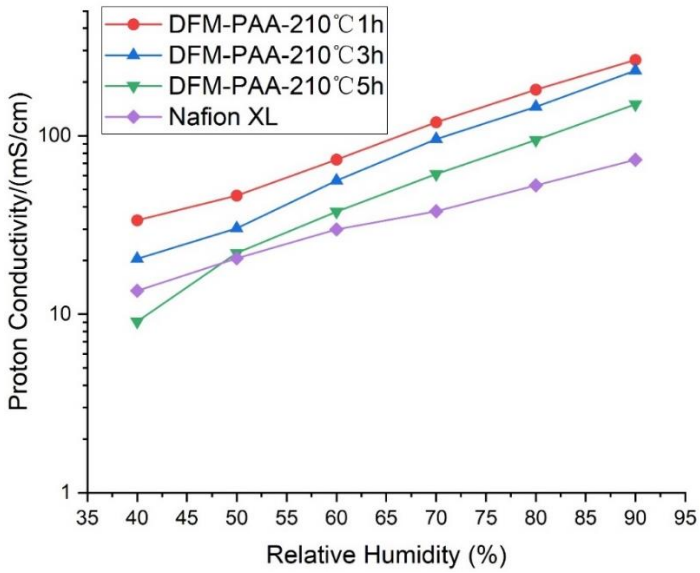


Figure 3.24: Proton conductivity of crosslinked dual-fiber membranes with PAA as electrospinning carrier and of Nafion XL.

Since both PEO and PAA carriers reduced the conductivity of dual-fiber membranes, I examined another membrane fabrication strategy, which did not require electrospinning of cPPSA, namely, pore-filling [17]. Here, cPPSA was just added to the electrospun reinforcing mat (scaffold) to fill the interfiber pores. The weight ratio of cPPSA to the reinforcing polymer was 85:15. Figure 3.25a and 3.25b show the proton conductivities for pore-filled membranes with PPSU and PBI as reinforcements for different crosslinking conditions.

From the figure, the pore-filled composite membranes can show higher proton conductivities than the dual-fiber composite membranes. Electrospun PPSU and PBI fibers reinforced composite membranes can retain more than 70-80% proton conductivity as compared to that of the pristine cPPSA film crosslinked at the same conditions. The data also show that the proton conductivity of fiber-reinforced composite membranes is proportional to their ionomer content. The proton conductivity of the PBI-reinforced membranes was slightly lower than that of PPSU-reinforced membranes over all examined relative humidities. Crosslinking at 210 ℃ for 1 h resulted in the highest proton conductivity with PPSU and PBI reinforced membranes showing ~50 mS/cm at 40 %RH and ~285 mS/cm at 90 %RH. The proton conductivities of pore-filled membranes crosslinked at 210 ℃ for 5h were still higher than for Nafion XL.

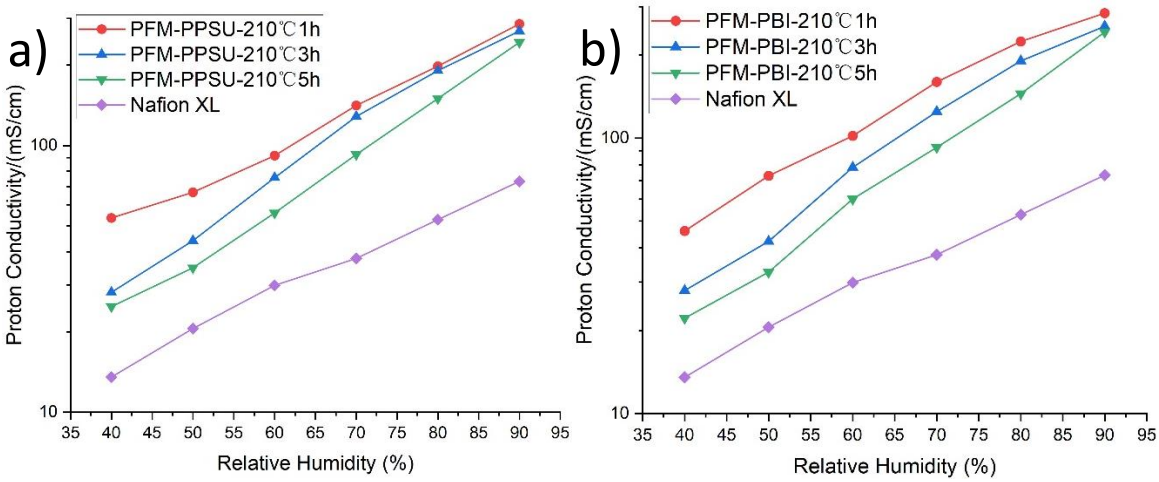


Figure 3.25: Proton conductivities of crosslinked pore-filled membrane with a) PPSU-reinforcing fibers and b) PBI-reinforcing fibers vs. Nafion XL.

### 3.3.4 Mechanical Property

Tensile strength is an important mechanical characteristic of proton conducting membranes [18]. Figure 3.26 shows the mechanical properties of pristine cPPSA films crosslinked at different conditions. For all crosslinked pristine cPPSA films, their tensile strengths were much lower than the project target of 20 MPa. The stress-strain curves of the crosslinked pristine cPPSA films varied greatly with crosslinking conditions. The highest stress, 11 MPa, was obtained when the pristine cPPSA film was crosslinked at 210 ℃ for 3 h. Longer crosslinking led to increase in brittleness, where the ultimate strain was only 1.73% for crosslinking for 5 h.

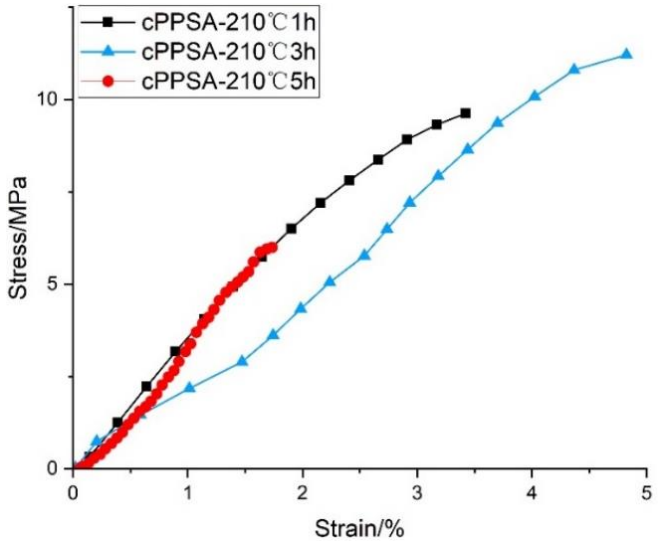


Figure 3.26: Stress-strain curves of crosslinked pristine cPPSA.

Since results in Figure 3.23 showed that adding PEO as carrier would dramatically decrease proton conductivity of dual-fiber membrane, I focused making tensile strength measurements only on dual-fiber membranes with PAA carrier and PPSU reinforcing fibers. Figure 3.27 shows the stress-strain curves obtained for the dual-fiber membranes crosslinked at different conditions. The data show that adding reinforcing fiber into cPPSA significantly enhanced the mechanical properties, similarly as in the case of PFSA dual-fiber membranes obtained in our lab previously [11]. Crosslinking at 210 ℃ for 3 h gave the highest tensile strength of 18 MPa, which was still below the target of 20 MPa. The measured ultimate strains were ~5%. Unquestionably, the presence of reinforcing fiber modified the mechanical properties of cPPSA.

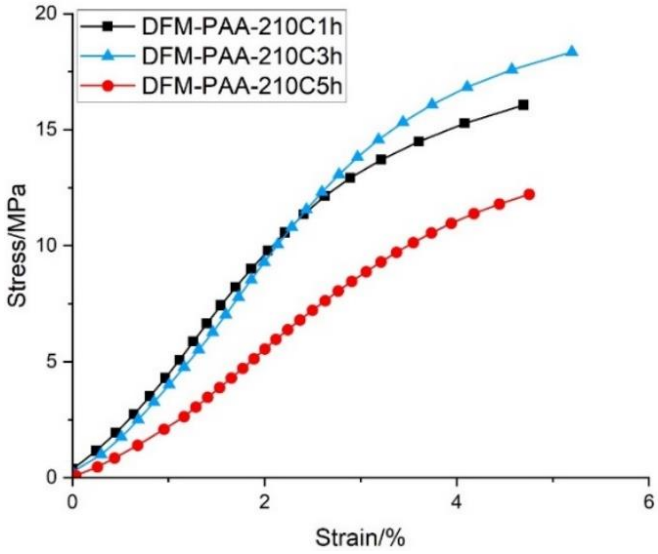


Figure 3.27: Mechanical characteristics of crosslinked dual-fiber membranes with PAA carrier and PPSU reinforcing fibers.

Figure 3.28 shows stress-strain curves of pore-filled composite membranes with PPSU and PBI fibers crosslinked at different conditions. Here, the mechanical characteristics of these membranes are better than those of the dual-fiber membranes. Interestingly, even though the tensile strength of bulk PBI is higher than that of bulk PPSU, PPSU-reinforced membranes had better mechanical characteristics compared to those of membranes with PBI fibers. This difference may be the result of a nearly 3 times greater diameter of the PPSU fibers. The ultimate stress of PPSU and PBI reinforced membranes reached 23 and 19 MPa, respectively.

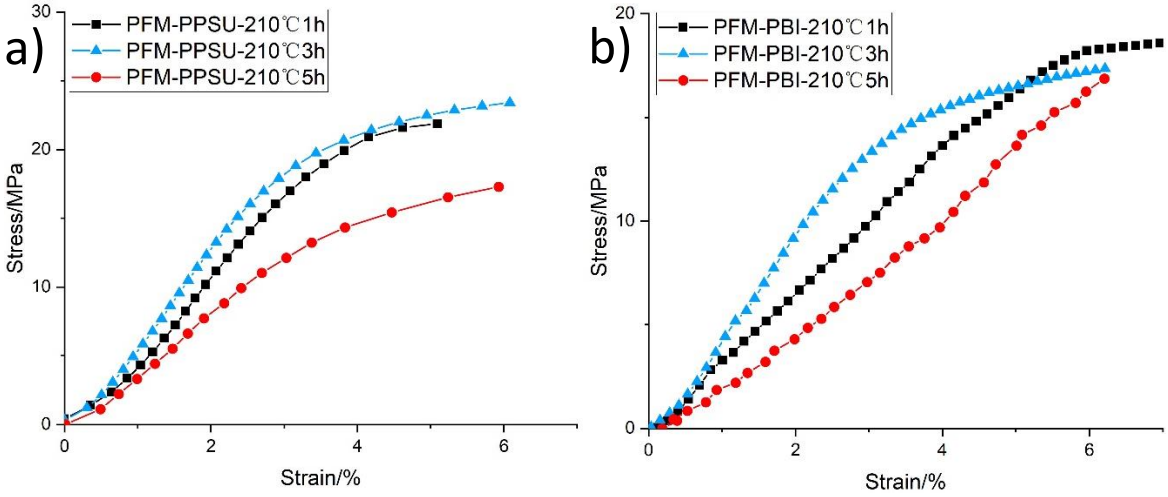


Figure 3.28: Mechanical characteristics of crosslinked pore-filled membranes with a) PPSU and b) PBI as reinforcing polymer fibers.

### 3.3.5 Fuel Cell Performance

Figure 3.29 compares the $H_2$/Air fuel cell performance (power density and I-V curves) of Nafion XL MEA and MEA-containing pore-filled composite membrane at 100 and 50% RH. At both values, Nafion XL MEA showed better power output. The low fuel cell performance was caused by poor adhesion between the pore-filled membrane and the electrodes and additionally, the pore-filled membrane was damaged during fuel cell test, where typically cracks developed along the edge of the carbon paper electrode. It was reflected by open circuit voltage, which was lower than 0.8 V for PFM-PPSU.

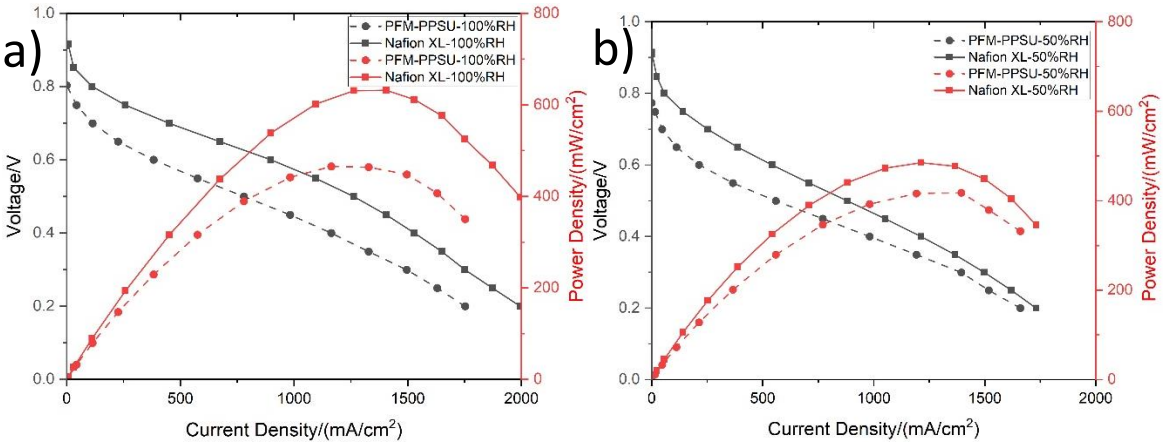


Figure 3.29: Fuel cell performance comparison of the MEAs with PFM-PPSU (not hot-pressed) and Nafion XL membranes (hot-pressed) at 80 ℃ and (a) 100 %RH and (b) 50 %RH with no backpressure.

Figure 3.30 compares the area specific high frequency resistance (HFR) for the two MEAs. HFR can reflect the properties of composite membranes in the through-plane direction. At 100 %RH, the PFM-based MEA had a HFR of 30 - 34 mΩ $cm^2$, as compared to 70 - 72 mΩ $cm^2$ for the Nafon XL-based MEA. Similarly, at 50 %RH, the resistance of the PFM-based MEAs was signifcantly lower (80 -113 mΩ $cm^2$) as compared to the Nafion XL-based MEA (180 – 189 mΩ $cm^2$). The results showed the excellent water retention ability of cPPSA compared with Nafion XL.

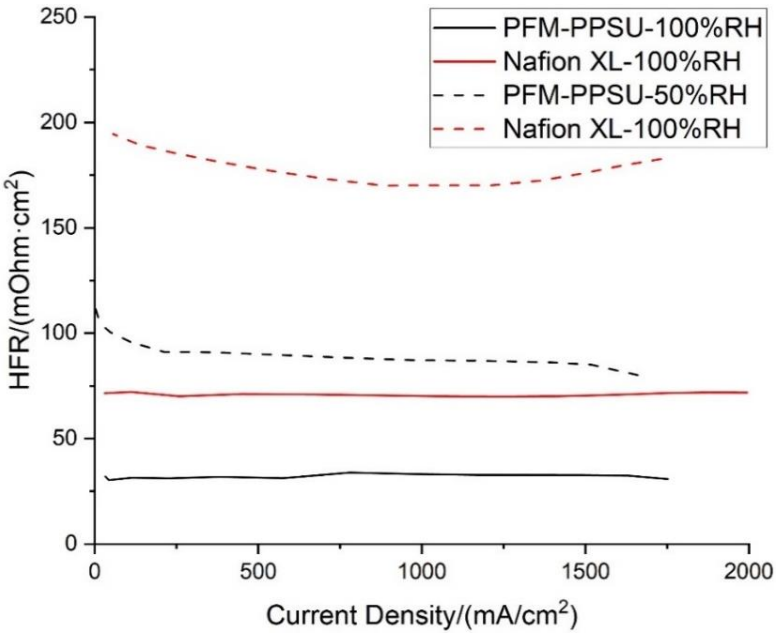


Figure 3.30: HFR dependence on current density for PFM-PPSU MEA (black lines) and Nafion XL MEA (red lines) at 80 ℃ at 100 %RH (solid lines) and 50 %RH (dashed lines).

### 3.4 Conclusions

PPSU and PBI fiber reinforced composite proton exchange membranes containing cPPSA ionomer were fabricated via dual-fiber electrospinning and via pore-filling, for the application in $H_2$/air fuel cells. The objective was to maximize the proton conductivity and mechanical strength of these membranes, to meet the DOE EERE 2020 targets. Electrospun dual fiber cPPSA/PPSU mats were densified by solvent exposure to melt cPPSA, which filled the void volume between reinforcing PPSU fibers. This treatment led to composite membranes with PPSU fibers embedded in cPPSA matrix. Solution cast cPPSA films were also prepared and evaluated as a reference. The best electrospun fiber reinforced membrane, in terms of highest proton conductivity, was made by the pore-filling technique and crosslinking at 210 ℃ for 1 h, while the lowest conductivity was observed for dual-fiber membrane fabricated with PEO as the cPPSA electrospinning carrier. All pore-filled membranes containing 85 wt.% cPPSA and 15 wt.% reinforcing fibers were superior to Nafion XL PFSA membrane in terms of the proton conductivity across 40–90 %RH at 80 °C. Unfortunately, fuel cell performance of PFM-PPSU was lower than Nafion XL due to the poor adhesion between the membranes and the electrodes. Additionally, the PFM-PPSU membranes degraded during a fuel cell test, where cracks developed along the edge of the carbon paper electrode. Positively, there was only small difference in fuel cell power output when the relative humidity changed from 100 to 50%, indicating the good water retention ability of cPPSA. Also, HFR at different RH conditions also reflected the good proton conductivity for PFM-PPSU. To address the cracking issue with the cPPSA-based membrane, a better reinforcing scaffold needs to be used.

### 3.5 References


[1] Litt, Morton, et al. "Rigid Rod Poly (p-Phenylene Sulfonic Acid) PEMs: High Conductivity at Low Relative Humidity Due to" Frozen-In-Free Volume"." *ECS Transactions* 33.1 (2010): 695.

[2] Si, Kun, et al. "Synthesis and characterization of poly (para-phenylene disulfonic acid), its copolymers and their n-alkylbenzene grafts as proton exchange membranes: high conductivity at low relative humidity." *Journal of Materials Chemistry* 22.39 (2012): 20907-20917.

[3] Si, Kun, et al. "Rigid-rod poly (phenylenesulfonic acid) proton exchange membranes with cross-linkable biphenyl groups for fuel cell applications." *Macromolecules* 46.2 (2013): 422-433.

[4] Litt, Morton, and Ryszard Wycisk. "Poly (arylenesulfonic acids) with frozen-in free volume as hydrogen fuel cell membrane materials." *Polymer Reviews* 55.2 (2015): 307-329.

[5] Hossain, M., et al. "Pore-Filled PEMs from Poly (Phenylene Sulfonic Acid) S and Electrospun Poly (Phenylene Sulfone) Fiber Mats." *ECS transactions* 98.9 (2020): 367.

[6] Graybill, Bruce M. "Synthesis of aryl sulfones." *The Journal of Organic Chemistry* 32.9 (1967): 2931-2933.

[7] Park, Jun Woo, et al. "Electrospun Nafion®/Polyphenylsulfone composite membranes for regenerative Hydrogen bromine fuel cells." *Materials* 9.3 (2016): 143.

[8] Li, Hsieh-Yu, and Ying-Ling Liu. "Polyelectrolyte composite membranes of polybenzimidazole and crosslinked polybenzimidazole-polybenzoxazine electrospun nanofibers for proton exchange membrane fuel cells." *Journal of Materials Chemistry A* 1.4 (2013): 1171-1178.

[9] Powers, Devon, Ryszard Wycisk, and Peter N. Pintauro. "Electrospun tri-layer membranes for H2/Air fuel cells." *Journal of Membrane Science* 573 (2019): 107-116.

[10] Choi, Jonghyun, et al. "High conductivity perfluorosulfonic acid nanofiber composite fuel-cell membranes." *ChemSusChem* 3.11 (2010): 1245-1248.

[11] Ballengee, Jason B., and Peter N. Pintauro. "Composite fuel cell membranes from dual-nanofiber electrospun mats." *Macromolecules* 44.18 (2011): 7307-7314.

[12] Zhao, Junhong, et al. "Evaluation of electrospun nanofiber formation of perfluorosulfonic acid and poly (N-vinylpyrrolidone) through solution rheology." *Journal of materials science* 46.23 (2011): 7501-7510.

[13] Germer, Wiebke, et al. "Comparison of conductivity measurement systems using the example of nafion and anion exchange membrane." *Solid State Ionics* 275 (2015): 71-74.

[14] Lee, Chang Hyun, et al. "Importance of proton conductivity measurement in polymer electrolyte membrane for fuel cell application." *Industrial & engineering chemistry research* 44.20 (2005): 7617-7626.

[15] Hotaling, Nathan A., et al. "DiameterJ: A validated open source nanofiber diameter measurement tool." *Biomaterials* 61 (2015): 327-338.

[16] Choi, Jiyeon, et al. "Fabrication of an anion-exchange membrane by pore-filling using catechol–1, 4-diazabicyclo-[2, 2, 2] octane coating and its application to reverse electrodialysis." *Langmuir* 34.37 (2018): 10837-10846.

[17] Huang, Tsang-Min, et al. "Chemical cross-linking of conducting poly (3, 4-ethylenedioxythiophene): poly (styrenesulfonate)(PEDOT: PSS) using poly (ethylene oxide)(PEO)." *Polymer* 54.23 (2013): 6455-6462.

[18] Gloukhovski, Robert, Viatcheslav Freger, and Yoed Tsur. "Understanding methods of preparation and characterization of pore-filling polymer composites for proton exchange membranes: a beginner's guide." *Reviews in Chemical Engineering* 34.4 (2018): 455-479.

# CHAPTER 4 - EXPANDED PTFE REINFORCED POLY(PHENYLENE SULFONIC ACID)S-BASED COMPOSITE MEMBRANES

## 4.1 Introduction

In the previously reported work [1], which I co-authored, the fabrication and characterization of cPPSA-based membrane was described, where mechanical stabilization was provided by electrospun fiber mat [2], and the cPPSA ionomer embedded in the pores imparted proton conductivity. The membrane had good tensile strength and its conductivity was greater than that of Nafion® in the 40–90 %RH range at 80 °C. The shear strength of electrospun fiber reinforced membrane was not good. When membranes were combined with carbon paper electrodes, they often broke at transition region between the carbon paper electrode and PTFE gasket.

New types were then developed, where the electrospun fiber scaffold was replaced with a commercially available porous ePTFE film. The hope was that the resultant PEMs would have better mechanical characteristics which would enable fabrication of robust MEAs for further testing in a fuel cell.

## 4.2 Experimental

### 4.2.1 Polyphenylene Ionomer Synthesis for cPPSA-BDM and cPPSA-ePTFE-A

#### 4.2.1.1 Synthesis of 1,4-dibromobenzene-2,5-disulfonic Acid Dilithium Salt (DBPDSA-Li)

A 500 mL 3-necked flask equipped with a magnetic stirrer and condenser was charged with 1,4-dibromobenzene (64 g, 266 mmol), 220 mL fuming sulfuric acid (17% $SO_3$), and heated at 223 °C for 24 h after brief purging with argon. A solid precipitated from the acid solution when the flask was cooled to room temperature. This precipitate was filtered and washed with brine solution until the pH of the filtrate reached 7. Subsequently, the obtained crud mixture of DBPDSA-Na and NaCl was dissolved in DI water and passed through a proton exchange column to get DBPDSA-H and HCl solution. The solution was then dry inside a hood at 50 °C to get pure DBPDSA-H. Afterward DBPDSA-H was dissolve in DI water and titrated with LiOH. After water evaporation, DBPDSA-Li was dried under vacuum at 80 °C for 24 h; 80 g of pure DBBDSA-Li was obtained (yield 72%).

#### 4.2.1.2 Synthesis of 4,4'-dibromobiphenyl-3,3'-disulfonic Acid Dilithium Salt (DBBPDSA-Li)

4,4'-Dibromobiphenyl (30 g, 96.2 mmol) was placed in a 250 mL 3-necked flask equipped with a mechanical stirrer and 75 mL fuming sulfuric acid (15%) was added. The flask was heated to 110 °C in an oil bath with stirring for 40 min. After the mixture was cooled, it was poured into 1 L of crushed ice. The resulting white precipitate was filtered and 100 g NaCl was added to the filtrate, a solid precipitated from the solution. This precipitate was filtered and washed with 15% NaCl solution until pH of filtrate become 7. To get pure DBBPDSA-Li, the obtained crud mixture of DBBPDSA-Na and NaCl was treated as describe above section. 23 g of DBBPDSA-Li was obtained with yield of 50%.

#### 4.2.1.3 Synthesis of PxBy Copolymer

PxBy copolymers were synthesized by Ullmann coupling polymerization of DBPDSA-Li with DBBPDSA-Li at 175 °C in N-methyl-2-pyrrolidone (NMP), employing activated copper powder as the catalyst, according to the protocols developed by Litt and coworkers. Here is an example of the procedure for the synthesis of copolymer with 75% DBPDSA and 25% DBBPDSA (P75B25): DBPDSA-Li salt (3.58 g) and DBBPDSA-Li (1.42 g) were placed in a 250 mL three-neck heavy-duty flask with a magnetic stirring bar and dried at 175 °C under vacuum for 2h. Then, freshly activated and pre-dried copper powder (~8.0 g, <150 mesh) was added into the flask.

Instantly, dry NMP (100 mL) was added to the system using a double-tipped needle, under argon pressure. The mixture was degassed by bubbling with argon for 10 min. Finally, 2, 2′-bipyridine (1.4 g) was added into the flask and the degassing was repeated for another 5 minutes. The monomers were copolymerized at 175 °C for 24 h under vigorous stirring. After polymerization, the mixture was cooled down to room temperature and filtered. The solid was extracted at room temperature by stirring with 100 mL cation exchange column (IR-120) for 2 h followed by filtration. The copolymer solution was purified by ultrafiltration (cut off value 5 KDa) with deionized water (1L).

After water evaporation, the purified product was dried under vacuum at 80 °C for 24 h; 3.0 g of purified copolymer was obtained. The structure of the copolymer was confirmed by $^{1}$H NMR; the copolymer is denoted as P75B25 (yield 94%). In the previous quarterly report, we have discussed issues with new catalysts. XPS analyses showed that the only difference between the two new copper powders was the surface oxide layer thickness. However, the catalyst purchased from Alfa Aesar caused us a lot of wasted time with no specific conclusion as what made it unsuitable for the polymerization.

#### 4.2.1.4 Grafting Biphenyl Groups (BP) on Copolymer

Samples of 1.0 g of PxBy copolymer and 16.8 g of 75% $H_3PO_4$ (PA) were placed in a 100 mL round-bottom flask, heated to 80 °C, and stirred at 125 rpm (about 2h). 1.35 g (0.009 mol) of biphenyl (BP) was added to the solution. Then 23 g of $P_2O_5$ was added in batches of ~0.5 g (~14 min.) for upholding temperature of the reaction mixture bellow 100 °C. the temperature was slowly raised to 125 °C after the $P_2O_5$ addition was accomplished, and stirred at 180 rpm for 67-72 h.

The reaction mixture was then cooled down and transferred into cold water (300 mL). The solution was neutralized with 20% alkali solution (100 mL), and residual BP was discarded by filtration. By ultrafiltration with deionized water, the solution was purified. The graft polymer solution was then passed through an ion exchange column to get $H^+$ form polymer. After water evaporation, the polymer product was dried under vacuum at 80 °C for 24 h; ~0.70 g of graft copolymer was obtained. By $^{1}$H NMR, a grafting degree (GD) of

9-12% was determined; the grafted copolymer is represented as PxBy-g-BP-x% (yield 65%).

In addition to the importance of the use of proper Cu powder, for the copolymer synthesis additional critical parameter is the molecular weight (MW) of the copolymer as it determines "graftability" of the copolymer. The solubility of the copolymer in polyphosphoric acid (PPA) decreases with the increase of MW. Since MW of the copolymer depends on the ratio of the two monomers (DBPDSA and DBBPDSA), the MW of the copolymer can easily be controlled by varying the monomer ratio. It was found that, if the DBBPDSA monomer content in the copolymer is less than 19% (e.g., copolymer P82B18), it shows good biphenyl grafting ability. However, above this biphenyl monomer content (e.g., copolymer P75B25), the solubility of the copolymer in PPA is very low thus it doesn't show good biphenyl grafting ability. For example using P75B25, P78B22, P80B20 or P82B18 and the ratio copolymer:PA:$P_2O_5$:BP of 1:17:23:1.35 at 125 °C for 72 h gave grafting degree within 9-12% bracket with high reproducibility.

### 4.2.2 Polyphenylene Ionomer Synthesis for cPPSA-ePTFE-B

4,4′-Dibromobiphenyl-3,3′-disulfonic acid (DBBPDSA) and 1,4-dibromobenzene 2,5-disulfonic acid (DBPDSA) were obtained by sulfonation of 4,4′-dibromobiphenyl-1,4-dibromobenzene and 1,4-dibromobenzene, respectively, with oleum (Figure 4.1), as described in Refs. [1,3].

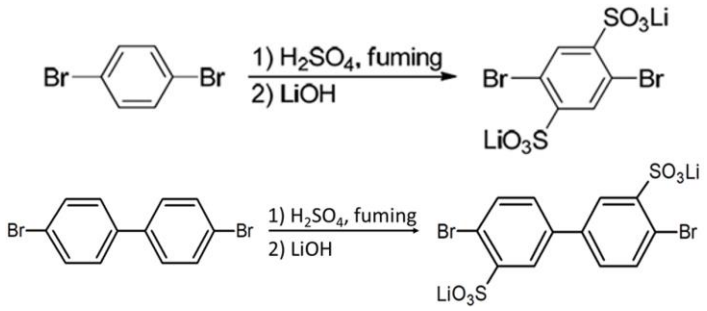


Figure 4.1: Sulfonation of dibromophenylene (DBP) and dibromobiphenylene (DBBP) with fuming sulfuric acid and conversion to the lithium salts.

Neutralization with LiOH gave the needed Li-salt forms. Copper catalyzed Ullmann coupling polymerization of DBPDSA-Li with DBBPDSA-Li in NMP at 170 °C, was used to prepare the PxBy copolymer (Figure 4.2), and 2,2′-Bipyridine was employed to increase the product yield [1,3]. Based on preliminary experiments, the ratio of the two co-monomers was set to obtain a biphenylene disulfonic acid co-monomer fraction of 0.25. Typically, from 3.58 g of DBPDSA-Li (8.8 mmol) and 1.42 g of DBBPDSA-Li (2.9 mmol), 2.9 g of the purified P75B25 copolymer was obtained in the acid form (94% yield).

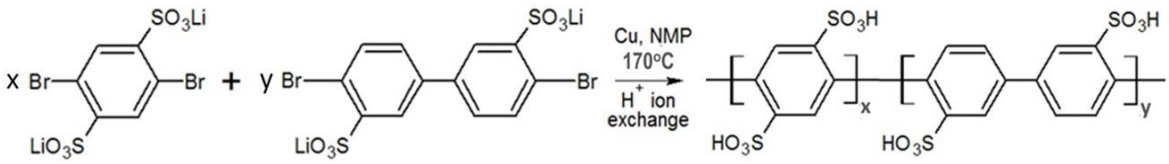


Figure 4.2: Copolymerization of DBPDSA-Li and DBBPDSA-Li salts to form the precursor ionomer PxBy (x=0.75, y=0.25).

Grafting of biphenyl (BP) was carried out with in-situ generated poly(phosphoric acid) following the method of Graybill (Figure 4.3) [4]. The reaction was carried out at 125 °C for 72 h, and the resultant crosslinkable poly(phenylenesulfonic acid) (cPPSA) containing 17% of BP grafts was separated by precipitation in water and ultrafiltration. It was then ion-exchanged to obtain the final $SO_3H$-form [1,3]. Typically, 0.7 g of purified cPPSA was obtained (65% yield) from 1.0 g of P75B25 copolymer, 16.8 g of 85% $H_3PO_4$, 23 g of $P_2O_5$ and 1.35 g of BP.

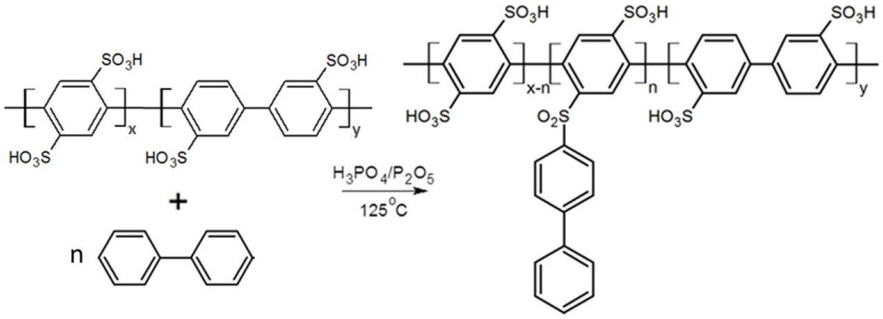


Figure 4.3: BP grafting onto PxBy in polyphosphoric acid generated in situ from $H_3PO_4$ and $P_2O_5$. The resultant graft copolymer was labelled as crosslinkable poly(phenylenesulfonic acid), cPPSA.

The ratio of DBPDSA and DBBPDSA after copolymerization, and the degree of biphenyl grafting onto P75B25 was determined by proton NMR, using a Bruker Spectrometer with a 9.4 T magnet and AV-400 console.

### 4.2.3 Membrane Fabrication

#### 4.2.3.1 cPPSA-BDM cast membranes

To improve the crosslinking ability of cPPSA ionomer and shorten the crosslinking time. A new additive (1,4-benzenedimethanol, BDM) was selected to mix with cPPSA and improve crosslinking ability. 95 wt.% cPPSA and 5 wt.% BDM was dissolved in MeOH to prepare a solution. This solution was poured on a pre-cleaned Teflon-FEP sheet and put in fume hood to evaporate solvent. After solvent evaporation, the cast cPPSA-BDM membrane was peeled off from the Teflon-FEP sheet, placed in a Teflon dish and heated in a vacuum oven for crosslinking.

#### 4.2.3.2 Development of cPPSA-ePTFE-A Pore Filled Composite Membranes

The following procedure was employed for the fabrication of cPPSA-ePTFE pore filled membrane. First, ePTFE-L film (Shanghai Lingqiao Fluorine Materials, pore size 0.4 μm, porosity 70%) was placed on top of a Teflon-FEP sheet and all the air between the two was squeezed out by brushing. Once ePTFE-L adhered well to the Teflon-FEP sheet, a 0.5 wt.% Poloxamer solution in methanol was brushed onto ePTFE-L until it became transparent. After methanol evaporation, a 2 wt.% cPPSA solution in methanol plus 5 wt.% BDM (relative to cPPSA) was spread over ePTFE-L. After solvent evaporation, the membrane was annealed at 200 °C for 20 min. to crosslink cPPSA (Figure 4.4).

#### 4.2.3.3 Development of cPPSA-ePTFE-B Pore Filled Composite Membranes

An ePTFE-Z film (pore size 5 μm) was placed on top of a Teflon-FEP sheet and the air between the two was squeezed out by pressing with a soft brush. Once the ePTFE-Z was well adhered to the Teflon-FEP sheet, a calculated volume of 2 wt.% cPPSA solution in methanol was spread over the ePTFE-Z, to uniformly cover its area. After evaporating methanol at room temperature for 30 min, the pore-filled mat was heated in a vacuum oven at 210 °C for 1 h, to crosslink cPPSA (Figure 4.4). The light brown color of the membrane slightly deepened indicating no significant desulfonation. Through the above-described sequence of processing steps, the originally opaque, white porous ePTFE-Z film was converted into a dense translucent membrane with light brown color and a thickness of 15 μm, in the dry state.

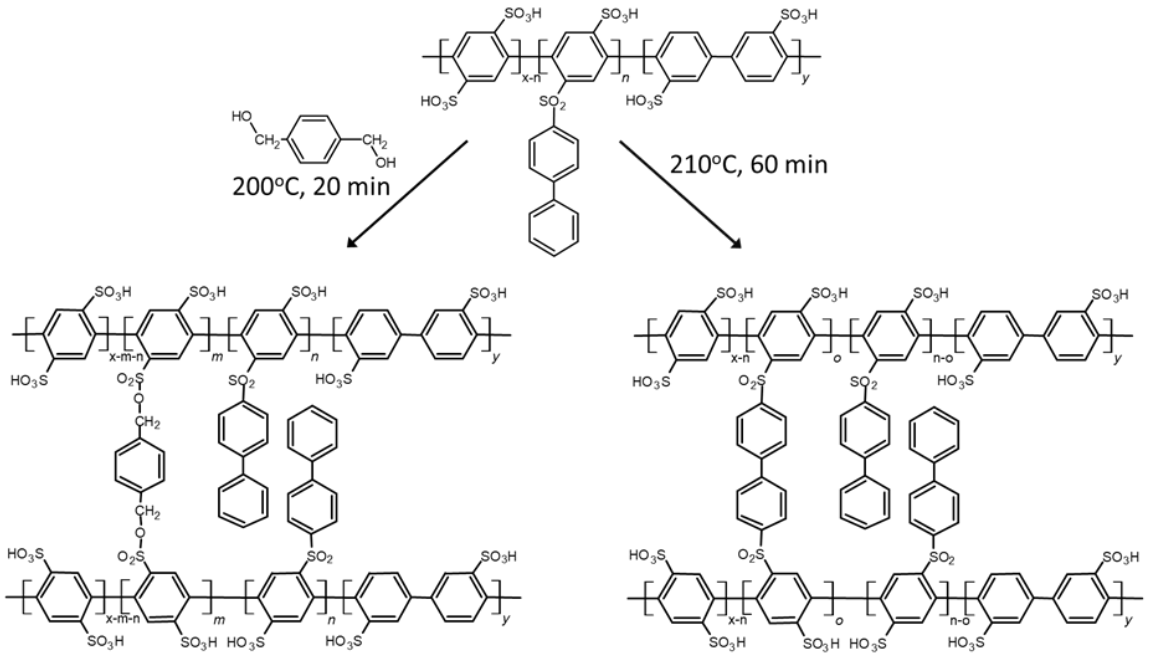


Figure 4.4: Thermal crosslinking of cPPSA with and without addition of BDM. Incomplete utilization of BP linker was assumed.

### 4.2.4 Characterization of Proton-Exchange Membranes

#### 4.2.4.1 Proton Conductivity

In-plane proton conductivity was determined by an AC impedance method, using a BekkTech four-electrode test cell. The BekkTech cell was placed in an ESPEC Corp. temperature/humidity controlled environmental chamber (Model: SH-241) for testing at 80°C and 40 %RH - 90 %RH. In-plane conductivity was calculated using the following Equation 4.1,

$$\sigma = \frac{1000L}{wtR} \quad \text{(Equation 4.1)}$$

where σ (mS/cm) is in-plane proton conductivity, R (Ω) is the resistance (real axis intercept on Nyquist plot), L (cm) is the distance between the inner electrodes, w (cm) is the width of a composite membrane sample (typically 0.4 cm), and t (cm) is the thickness of the membrane sample. For conductivity calculations of water-equilibrated samples, air-dried dimensions were used for the conductivity of vapor-equilibrated samples.

#### 4.2.4.2 Morphology

Surfaces and cross-section morphology of composite membranes and expanded PTFE scaffold were imaged with a Hitachi S-4200 scanning electron microscope. Samples were sputter-coated with a gold layer to prevent charging of the specimen and to reduce thermal damage while improving secondary electron emission.

#### 4.2.4.3 Mechanical Properties

Stress and strain of composite membrane samples were measured with a TA Instruments Q800 dynamic mechanical analyzer (DMA, TA Instruments, New Castle, NY, USA). Stress-strain curves were obtained for membranes equilibrated in air at 25 °C. The DMA was operated in tension using the controlled strain mode, where the sample was strained at 10%/min until failure.

#### 4.2.4.4 Gravimetric Water Uptake

Gravimetric water uptake of rectangular membrane samples were determined by measuring the relative change in sample weight and dimensions after equilibrating with water vapor at 40 %RH - 90 %RH and 80 °C, and then drying at 80 °C in a vacuum oven. Gravimetric water uptake were calculated using the following Equation 4.2.

$$Water\ Uptake\ (\%) = \frac{x_{wet} - x_{dry}}{x_{dry}} \quad \text{(Equation 4.2)}$$

where x is the membrane mass (for water uptake) in the wet or dry states.

#### 4.2.4.5 Ion Exchange Capacity

Ion exchange capacity (IEC) was measured in the following way. Approximately 50 mg of dry membrane sample was placed in 10 $cm^3$ of 2.0 M NaCl solution, which was stirred overnight. Then, three 2.5 $cm^3$ solution samples were removed and each was titrated with 0.01 M NaOH solution in presence of bromothymol blue indicator (two drops). The IEC of the sample was calculated by dividing the mean number of mmoles of NaOH titrant used at the equivalence point by the dry weight of the sample in the acid form (in grams), and multiplying the result by four.

#### 4.2.4.6 MEA Fabrication and Fuel Cell Testing

Membrane-electrode assemblies (MEAs) were prepared with a cPPSA-ePTFE pore-filled membrane and with Nafion XL, using commercial Pt/C gas diffusion electrodes (GDEs) with 5 $cm^2$ catalyzed area, purchased from the Fuel Cell Store. The anode and cathode Pt loading was 0.12 $mg/cm^2$. MEAs with cPPSA-ePTFE pore-filled membrane were not hot-pressed; the membrane was just sandwiched between the electrodes and PTFE gaskets, and then directly installed into a test cell (single serpentine $H_2$ and air flow channels, Fuel Cell Technologies Inc.). MEAs with Nafion XL were hot-pressed in a heated hydraulic press at 140 °C and 690 kPa, for 10 min before use.

MEAs were evaluated using a Scribner 850e test station. Data were collected at 80 °C, 100 %RH, 50 %RH and 30 %RH, with and without backpressure, the same for the both feed streams. The $H_2$ and oxidant (air or oxygen) flow rates were 0.125 L/min and 0.5 L/min, respectively. All experimental runs were repeated at least two times. Typically, the current density variability was within 5% for a given cell voltage.

$H_2$ crossover was measured via linear sweep voltammetry [5]. The humidified hydrogen gas was fed to the anode (reference electrode) while the cathode (working electrode) was purged with humidified nitrogen. The $H_2$ and $N_2$ flow rates were 0.125 L/min and 0.5 L/min, respectively. An anodic sweep was applied between 0.01 V and 0.4 V at a rate of 10 mV/s using a potentiostat (Reference 3000, Gamry Instruments), which resulted in oxidation of the $H_2$ permeating through the membrane. The cell current density at 0.4 V (plateau) represented the $H_2$ crossover rate.

## 4.3 Results and Discussion

### 4.3.1 NMR Spectrum

Figure 4.5a is the $^1H$ NMR spectrum (aromatic protons region only) of ungrafted P75B25 copolymer (PPSA) used in cPPSA-ePTFE-B and Figure 4.5b is the spectrum of the BP grafted copolymer P75B25-g-BP17% (cPPSA). Based on the integrals of proton signals (a) and (b) of the ungrafted copolymer, the fraction of phenylenedisulfonic acid mers was found equal 75%. None of the two upfield signals could be used for calculations, as they each represent more than two protons, due to the overlap with resonances of the terminal mers. From the sum of integrals of (c) and (c') in Figure 4.5b, the fraction of sulfonic acid groups that were

grafted with BP was estimated as 17%.

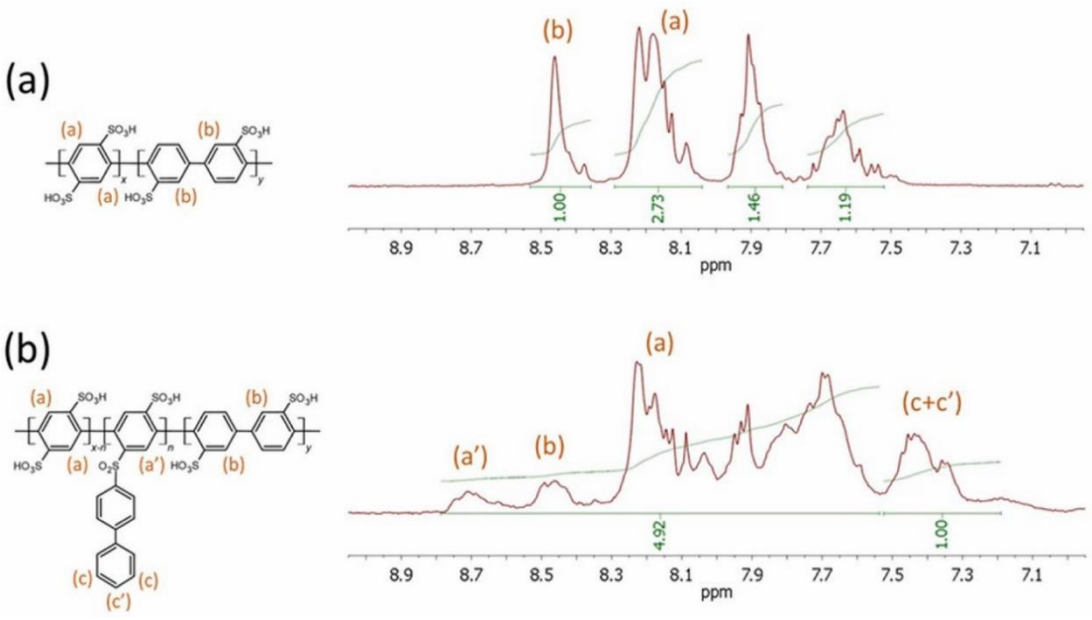


Figure 4.5: $^{1}H$ NMR spectra in $CD_3OD$ of: (a) P75B25 (PPSA), and (b) P75B25-g-BP17% (cPPSA).

The synthesized cPPSA ionomer was used to impregnate the expanded polytetrafluoroethylene (ePTFE) film. At 210 °C, biphenylene disulfone bridges formed (Figure 4.4) that made cPPSA water-insoluble, as reported by Litt et al. [3]. Our previously published work [1] showed that no desulfonation was observed during thermal crosslinking until around 300 °C, which was consistent with the findings of Litt's group [3]. Therefore, no degradation was expected during the 200 °C–210 °C crosslinking.

### 4.3.2 Ex-situ Experimental Results

#### 4.3.2.1 Improvement of Grafting with 1,4-Benzenedimethanol Additive

The use of a new additive (1,4-benzenedimethanol, BDM) enabled effective crosslinking at lower temperature and shorter time (200 °C, 15 min). Figure 4.6 shows the in-plane proton conductivity of cPPSA-BDM membranes.

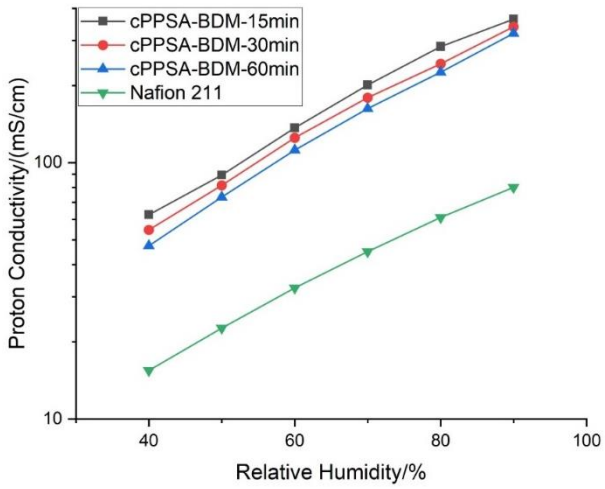


Figure 4.6: In-plane proton conductivity of the cPPSA-BDM membrane and Nafion 211 reference at 80 °C and 40 to 90 %RH.

The resultant composite cPPSA-ePTFE pore-filled membranes were soaked in water at 80 °C, and their dry weights were recorded after 12, 24, 36, and 48 h. In Figure 4.7, only a small fraction (~4-6%) of the initial membrane weight was lost (extracted) after the 48 h soak, with little change after 36 h, indicating effective crosslinking, as the un-crosslinked cPPSA is highly soluble in water.

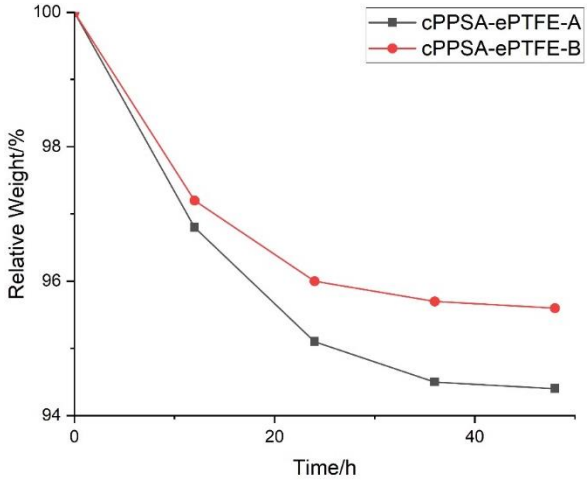


Figure 4.7: Remaining membrane weight, as percent of the initial weight, after soaking cPPSA-ePTFE pore-filled membranes in water at 80 °C for 12, 24, 36, and 48 h.

The thickness of dry composite cPPSA-ePTFE-A and cPPSA-ePTFE-B were 25 and 15 μm, respectively, with their thickness mainly determined by the thickness of ePTFE scaffolds. The membranes were light-brown in color, nearly transparent, and appeared macroscopically homogeneous (Figure 4.8). Based on the weight increase after pore-filling and crosslinking, the cPPSA-ePTFE-A and cPPSA-ePTFE-B contained around 70 and 75 wt.% of cPPSA, respectively.

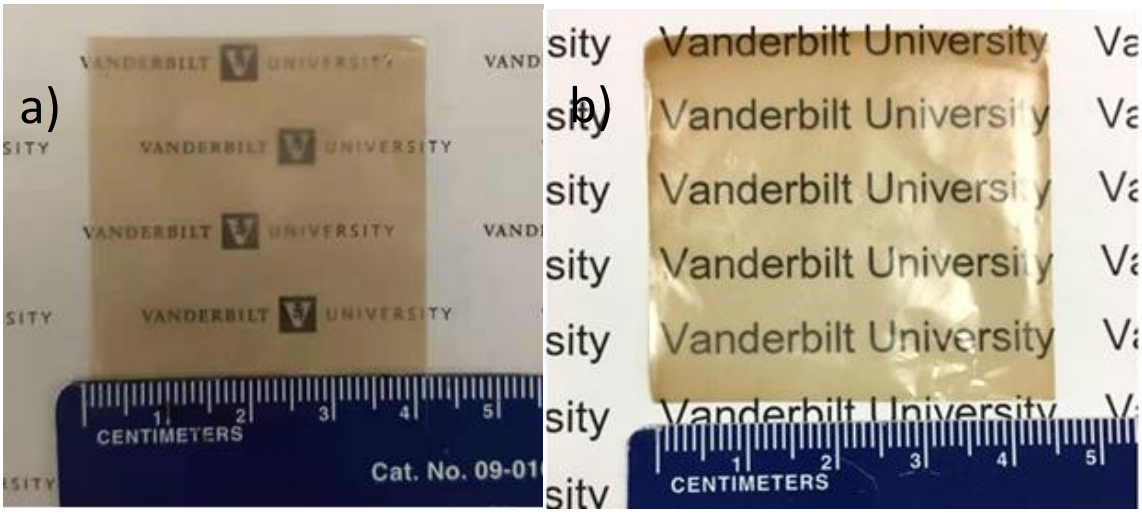


Figure 4.8. Photographs of the pore-filled a) cPPSA-ePTFE-A and b) cPPSA-ePTFE-B composite membrane samples [6].

The measured ion-exchange capacity (IEC) of the cPPSA was 5.8 mmol/g, close to the theoretical value of 6.1 mmol/g calculated for 17% grafting. The measured IEC of the cPPSA-ePTFE-B was 2.7 mmol/g, which translated into 3.6 mmol/g for the pore-filling ionomer (taking into account 75 wt.% loading of the cPPSA in the membrane). This value indicated that about 39% of the sulfonic groups were crosslinked by BP grafts (3.1 crosslinks per 8 sulfonic groups).

Figure 4.9a and 4.9d show SEM images of the reinforcing ePTFE scaffolds surface. It is evident that the porous structure is somewhat anisotropic. Figure 4.9b and 4.9e show SEM images of the top surface of cPPSA-ePTFE. No defect voids and no traces of ePTFE scaffold can be seen, indicating complete pore-filling and/or the presence of ionomer overlayers. Figure 4.9c and 4.9f show SEM images of pore-filled composite membranes cross-section. A dense, top surface overlayer (~5-10 μm in thickness) can be seen and perfect pore-filling with no detectable open pores is evident.

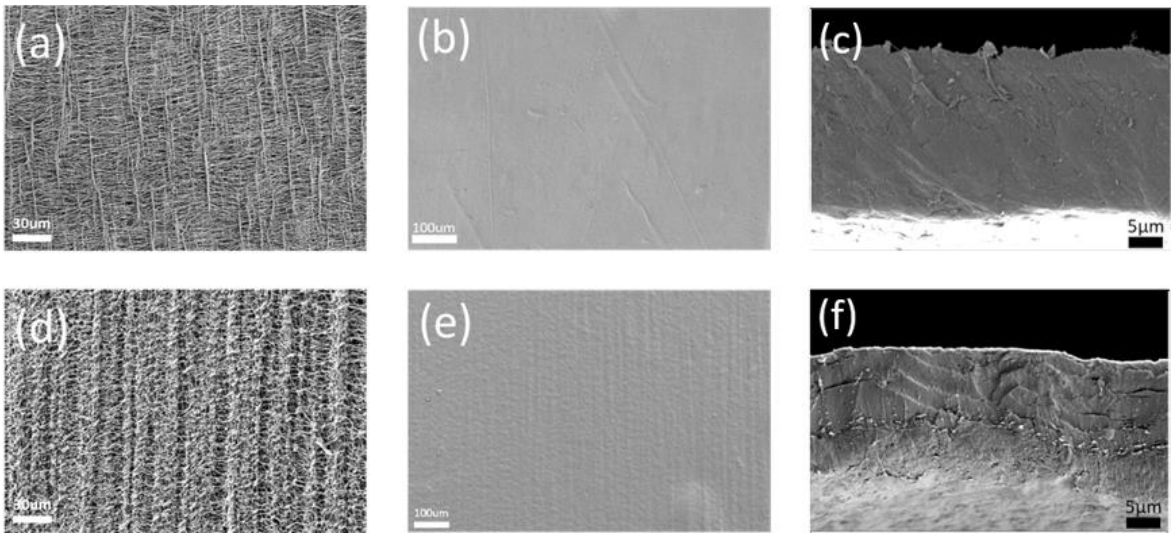


Figure 4.9: SEM images of: (a) top surface of the reinforcing ePTFE-L scaffold, (b) top surface of composite membrane cPPSA-ePTFE-A, (c) cross-section of cPPSA-ePTFE-A, (d) top surface of the reinforcing ePTFE-Z scaffold, (e) top surface of composite membrane cPPSA-ePTFE-B, (f) cross-section of cPPSA-ePTFE-B. Scale bars as shown on the images.

The major objective of the present study was the fabrication of a PEM with proton conductivity superior to that of Nafion PFSA across a wide range of air humidity, especially at low RH. For this benchmarking challenge, the in-plane proton conductivity was measured at 80 °C between 40 and 90 % RH, and the results for the two pore-filled membranes and Nafion XL are compared in Figure 4.10. Both composite membranes exhibited a very high conductivity over the tested relative humidity range. The highest conductivity was recorded for cPPSA-ePTFE-B (crosslinked at 210 °C for 1 h) and was over twice that of Nafion XL over 40 %RH (47 vs. 14 mS/cm) to 90 %RH (221 vs. 73 mS/cm). The conductivity of the cPPSA-ePTFE-A was also significantly greater than that of Nafion XL, although somewhat lower than cPPSA-ePTFE-B in the 60-90% RH range. The observed high conductivity of the both PFMs resulted from (i) the much higher ion-exchange capacity (IEC) of the pore-filled membranes, and (ii) the strong water retention of cPPSA even at low relative humidity, presumably due to the presence of the “frozen-in free volume” as proposed by Litt et al.

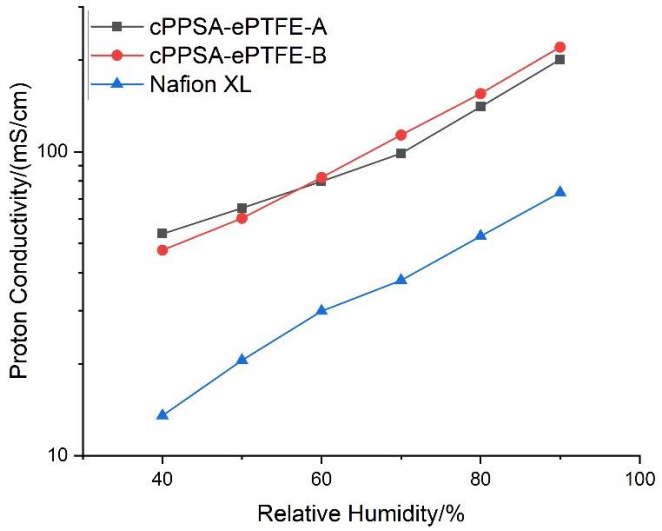


Figure 4.10: In-plane proton conductivity of two composite cPPSA-ePTFE pore-filled membranes and Nafion XL reference at 80 °C and 40-90% RH.

To further investigate the origin of the superior conductivity of the composite membrane, I performed water uptake and swelling experiments in a controlled humidity chamber at 80 °C. Figure 4.11 shows water uptake results that correlate qualitatively with the conductivity measurements in Figure 4.10. The water uptake of the two composite membranes increases from 23-26% at 40% RH to 91-101% at 90% RH. These values are much higher than the 6% at 40 %RH and 14% at 90 %RH for Nafion XL. The suggestion is that the high proton conductivity of the cPPSA-ePTFE pore-filled membrane is associated with the high water retention of cPPSA, even at low RH.

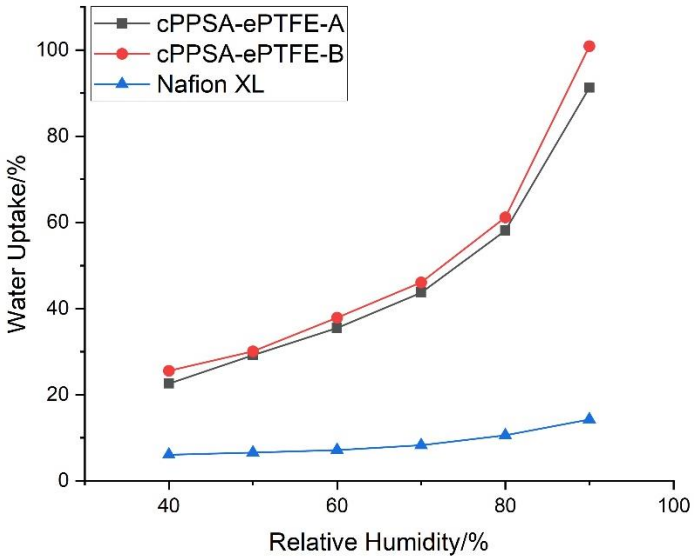


Figure 4.11: Water uptake of cPPSA-ePTFE pore-filled membranes and Nafion XL reference at 80 °C and 40 to 90 %RH.

The mechanical characteristics of cPPSA-ePTFE pore-filled membranes were acquired using a DMA analyzer. Figure 4.12 shows the results of stress-strain tensile tests at 25 °C and ambient (50 %RH) air in the machine (MD) and transverse (TD) directions. Data for a Nafion XL membrane are also shown. A moderate elongation at break was observed for the cPPSA-ePTFE pore-filled membranes, while for Nafion XL, the elongation at break was 199% in MD and 170% in TD, indicating the much greater ductility of Nafion. The composite membrane was very flexible in both the dry and wet states, thus overcoming the problem of brittleness in its dry state and softness in the wet state observed with solution-cast films from pristine cPPSA. The improvement in mechanical characteristics upon pore-filling is indicative of the absence of unfilled pores, which is consistent with the SEM imaging data. The ultimate stress of Nafion XL was higher in both directions (33 MPa), probably due to the presence of reinforcement material; however, the ultimate mechanical characteristics of the Nafion membrane were reached well beyond its elastic response limit of about 10–20% elongation.

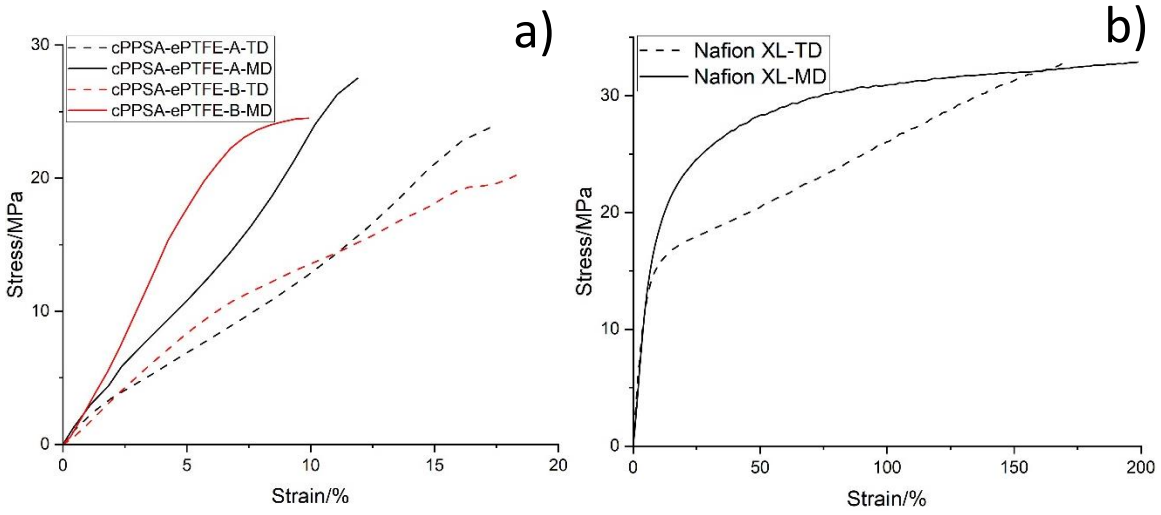


Figure 4.12: Tensile curves recorded for a) cPPSA-ePTFE pore-filled membranes and b) Nafion XL reference in the machine direction (MD) and transverse direction (TD). Samples were equilibrated in ambient air at 25 °C and 50 %RH.

The presence of the ePTFE scaffold was expected to not only stabilize the cPPSA mechanically but also to limit the lateral expansion of composite membranes. To verify this expectation, dimensional changes of the dry membranes were measured after exposure to 100 %RH air, at room temperature. The results obtained for composite membranes cPPSA-ePTFE-A and cPPSA-ePTFE-B, and for a reference film of unreinforced but crosslinked cPPSA were 10.9, 11.2, and 51.1%, respectively. It can be seen that embedding cPPSA in the ePTFE scaffolds reduced the in-plane swelling (lateral expansion) by 80%. Minimizing in-plane swelling is critical to extended membrane durability in PEM fuel cells and the significant reduction of in-plane swelling of highly charged cPPSA ionomer is an important characteristic of the composite membrane morphology. It

can also be concluded that varying the crosslinking conditions and the type of ePTFE scaffold had a negligible impact on membrane swelling.

### 4.3.3 Fuel Cell Performance

The most important evaluation of the composite proton exchange membranes was carried out in a $H_2$/air fuel cell. A cPPSA-ePTFE pore-filled membrane and a Nafion XL film were incorporated into MEAs with commercial Pt/C electrodes containing PFSA binder and tested at various relative humidity and backpressure at 80 °C, with $H_2$/air and $H_2/O_2$ feeds. The PFM-based MEAs were not hot-pressed, as no adhesion was observed between the Nafion-based GDEs and cPPSA-ePTFE pore-filled membrane surfaces. Nafion XL-based MEAs were made employing hot-pressing to improve interfacial compatibility.

Figure 4.13 shows fuel cell i-V and power density curves, for MEAs with the three membranes. Only cPPSA-ePTFE-B and Nafion XL were tested at 30 %RH. The MEA with PFM showed higher activation overpotentials, probably due to the mismatch of the ionomer in the membrane (cPPSA) and the catalyst layer (Nafion). cPPSA-ePTFE-B produced a higher power density when fully humidified (691 mW/cm$^2$ from Figure 4.13a), at 50 %RH (600 mW/cm$^2$ from Figure 4.13b), and at 30 %RH (452 mW/cm$^2$ from Figure 4.13c). These values were significantly greater than for Nafion XL, where the maximum power density was 632 mW/cm$^2$ at 100 %RH, and only 485 and 211 mW/cm$^2$ at 50 and 30 %RH, respectively. To summarize in relative terms, decreasing the cell humidification level from 100 to 50 %RH, led to a small (13%) reduction in the maximum power density with the cPPSA-ePTFE-B versus a 23% decrease with Nafion XL. Decreasing the cell humidification level from 100 to 30 %RH, led to only 35% reduction in the maximum power density with the cPPSA-ePTFE-B versus a 67% decrease with Nafion XL. The reduction in the maximum power density of Nafion XL was nearly twice that of cPPSA-ePTFE-B. The maximum power density of MEA with cPPSA-ePTFE-B at 30 %RH was similar to that of Nafion XL at 50 %RH, only around 7% difference, which proved the excellent water retention ability of cPPSA comparing with PFSA ionomer. Additionally, the MEA with a cPPSA-ePTFE-B showed higher power retention at 50 %RH, as compared to MEAs with alternative sulfonated polyphenylene membranes as reported in the literature, e.g., in Ref. [7].

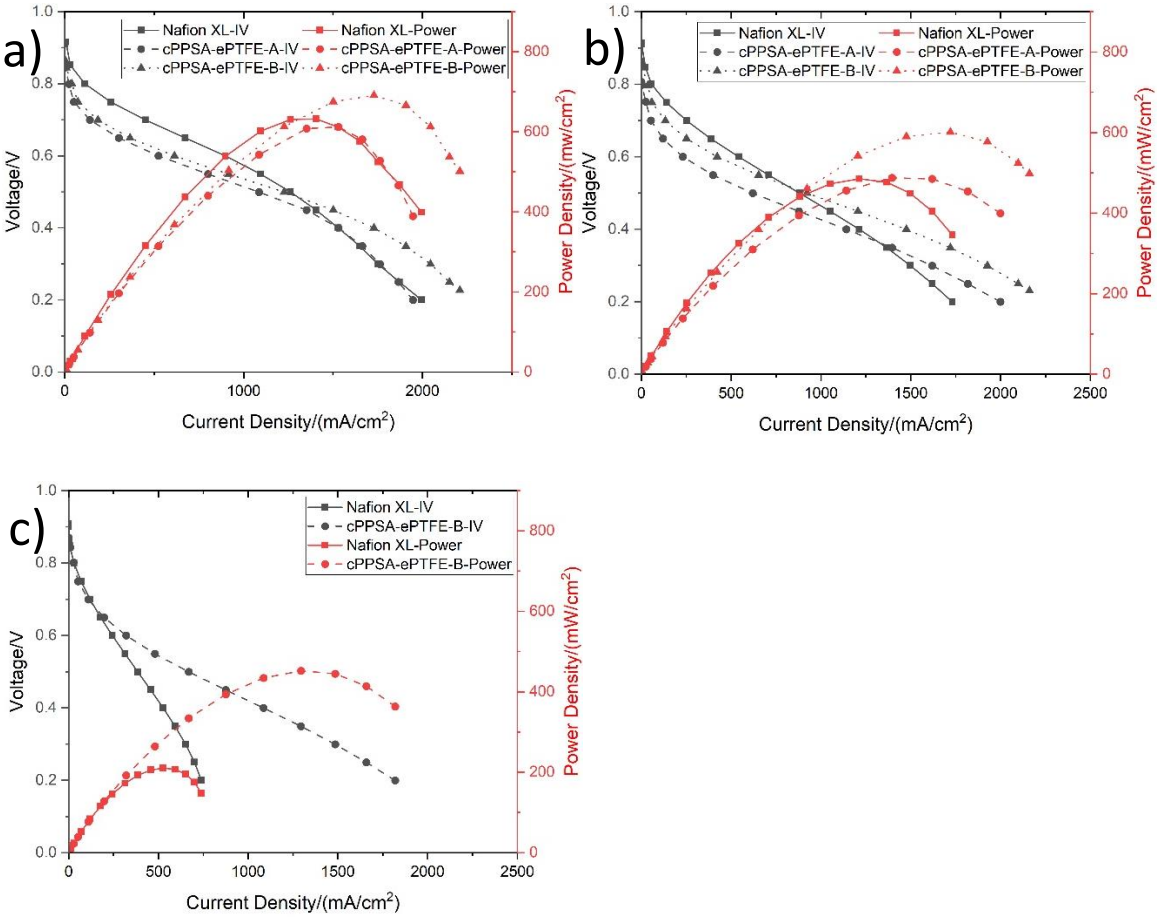


Figure 4.13: Fuel cell performance comparison of the MEAs with cPPSA-ePTFE pore-filled membranes (not hot-pressed) and Nafion XL membranes (hot-pressed) at 80 ℃ and (a) 100 %RH, (b) 50 %RH and (c) 30 %RH, without back pressure.

cPPSA-ePTFE-B was selected for an extended testing because of its better fuel cell performance. The superior power output at high current density of the PFM-based MEA, compared to that with Nafion XL, is not surprising in view of cPPSA-ePTFE's much higher proton conductivity. Figure 4.14 compares the area specific high frequency resistance (HFR) for the two MEAs. At 100 %RH, the cPPSA-ePTFE-based MEA had a HFR of 52 - 60 mΩ $cm^2$, as compared to 70 - 72 mΩ $cm^2$ for the Nafion XL-based MEA. Similarly, at 50 %RH, the resistance of the cPPSA-ePTFE-based MEAs was significantly lower (93 -109 mΩ $cm^2$) as compared to the Nafion XL-based MEA (180 - 189 mΩ $cm^2$). At 30 %RH, the resistance of cPPSA-ePTFE-based MEAs (127 -168 mΩ $cm^2$) was only one third the resistance of the Nafion XL-based MEA (389 - 450 mΩ $cm^2$). At 30 % RH, the resistances of cPPSA-ePTFE-based MEAs are even lower than the resistance of Nafion XL-based MEA at 50 %RH, proving the excellent water retention ability of cPPSA compared to Nafion XL. The HFR data (ratio of HFRs at different relative humidity conditions) roughly follow the in-plane proton conductivity ratios calculated based on Figure 4.10, which justifies the use of in-plane conductivity rather than through-

plane conductivity (very unreliable) for probing membrane proton conductivity.

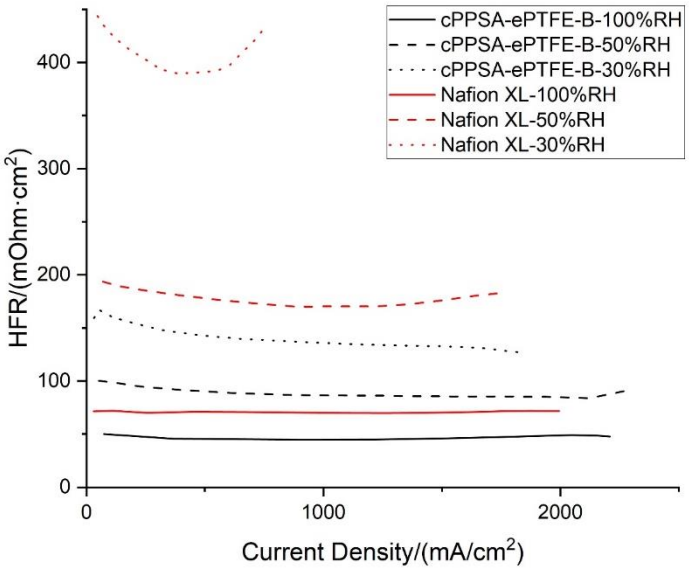


Figure 4.14: HFR dependence on current density for cPPSA-ePTFE-B MEA (black lines) and Nafion XL MEA (red lines) at 80 ℃ at 100 %RH (solid lines), 50 %RH (dashed lines), and 30 %RH (dotted lines).

To verify complete pore-filling of ePTFE scaffolds, $H_2$ crossover measurements were performed in a fuel cell at 80 ℃ with no backpressure. The results were compared to those collected with Nafion XL. Figure 4.15 contains the resultant linear sweep voltammetry curves for 100, 50, and 30 %RH. In the figure, the crossover current density at 100 %RH was very low at 0.90 mA/cm$^2$ for the cPPSA-ePTFE-B MEA vs. 1.60 mA/cm$^2$ for a Nafion XL MEA. The crossover current density at 50 %RH was lower, as the reduction of membrane swelling generally led to a lower hydrogen permeability, 0.57 and 1.25 mA/cm$^2$, for the cPPSA-ePTFE-B and Nafion XL MEAs, respectively. Relative humidity near 30%RH showed a more significant difference of 0.42 mA/cm$^2$ for cPPSA-ePTFE-B vs. 1.15 mA/cm$^2$ for Nafion XL. The lower limiting current for cPPSA-ePTFE was expected, due to the cPPSA pore-filler stiff chain structure (rigid rod chains) which limited both gas solubility and diffusion [8]. The crossover data also confirm that the ePTFE scaffold pores were effectively filled with no voids percolating through the membrane, as indicated previously in Figure 4.7b and c.

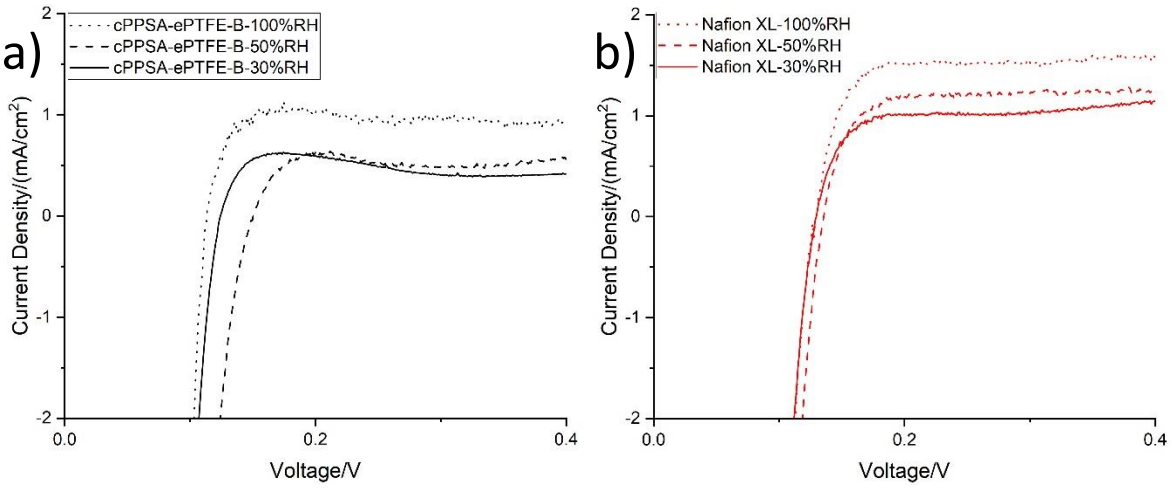


Figure 4.15: Linear sweep voltammetry $H_2$ limiting current density curves recorded at 80 ℃ for MEAs with (a) cPPSA-ePTFE-B, and with (b) Nafion XL, at 30 %RH (solid lines), 50 %RH (dashed lines) and 100 %RH (dotted lines).

To extend the range of cPPSA-ePTFE-B MEA testing, additional fuel cell experiments were performed at different backpressures with a cathode fed with either air or pure oxygen. Figure 4.16-4.17 are the results polarization curves. Based on these additional data, while the maximum power density of the MEA with cPPSA-ePTFE-B was always greater than that of an MEA with Nafion XL, at 80 ℃ and relative humidity over 30-100%, the most pronounced advantage of the cPPSA-ePTFE-based MEA was at low RH condition. The highest ratio of (maximum power with a cPPSA-ePTFE-B MEA)/(maximum power with a Nafion XL MEA) was 2.5, which was obtained with pure oxygen as the cathodic feed, without backpressure. The lowest ratio of 1.36 was obtained at 200 kPa backpressure, with air as the cathodic feed.

Fuel cell performance of cPPSA-ePTFE-based MEA was obviously higher than that of Nafion XL MEA at 100 %RH, with backpressure. The superiority of cPPSA-ePTFE-based MEA became more significant at 30 %RH conditions. Especially, the maximum power density of cPPSA-ePTFE-based MEA with 100 kPa backpressure at 30 %RH even higher than the maximum power density of Nafion XL MEA with 100 kPa backpressure at 100 %RH, which came from good proton conductivity of cPPSA even in low relative humidity condition. With 200 kPa backpressure, the maximum power densities at 100 and 30 %RH of cPPSA-ePTFE-based MEAs almost the same (less than 2% difference). In the same conditions, there was still a reduction between 100 and 30 %RH of Nafion XL MEA, which is 15%. One important observation was that at 100 %RH, the MEA with cPPSA-ePTFE-B showed higher overpotentials in the activation polarization region, probably due to the non-ideal attachment of the GDEs to cPPSA-ePTFE-B and the incompatibility of cPPSA and Nafion electrode binder.

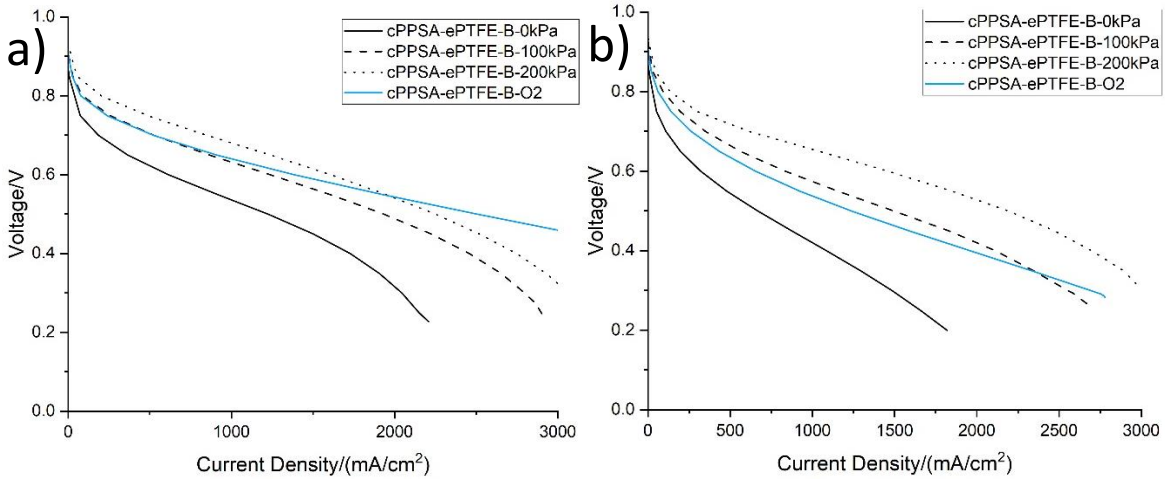


Figure 4.16: Comparison of the Fuel cell performance of the cPPSA-ePTFE-B MEA (not hot-pressed) at (a) 100 %RH and (b) 30 %RH, with air and with oxygen. Solid black line – air, no backpressure, long dashes – air, 100 kPa, short dashes – air, 200 kPa, solid blue line – oxygen, no backpressure.

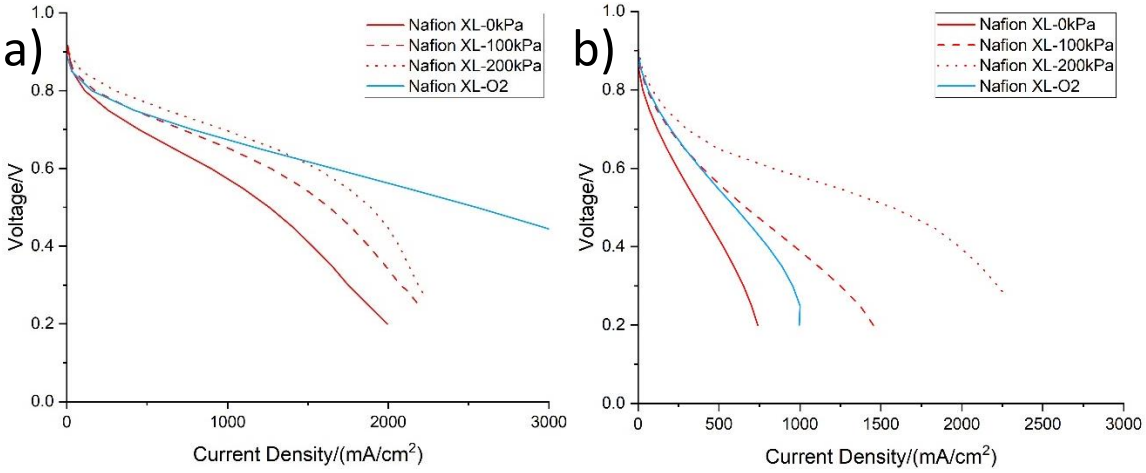


Figure 4.17: Comparison of fuel cell performance of the Nafion XL MEA (hot-pressed) at (a) 100 %RH and (b) 30 %RH, with air and with oxygen. Solid red line – air, no backpressure, long dashes – air, 100 kPa, short dashes – air, 200 kPa, solid blue line – oxygen, no backpressure.

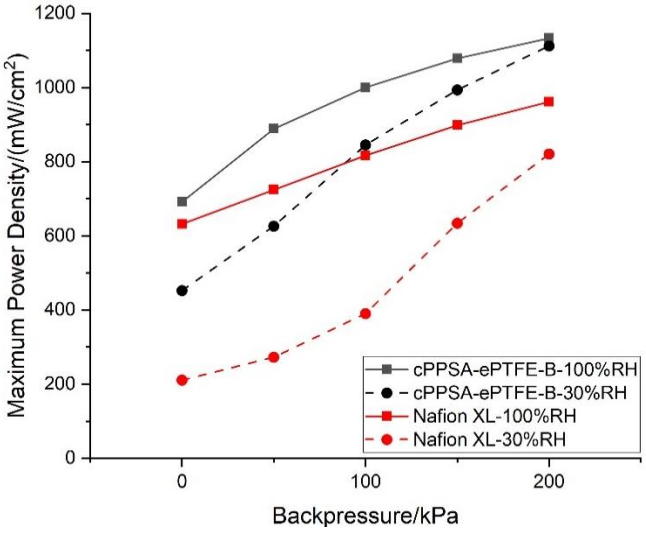


Figure 4.18: Comparison of maximum power densities of the cPPSA-ePTFE-B and Nafion XL MEAs at 100 %RH and 30 %RH with different backpressure. Solid lines – 100 %RH, dashed lines – 30 %RH.

Figure 4.19 is the fuel cell power output as a function of time for a cPPSA-ePTFE-B MEA operated at 80 ℃, 100 %RH and 30 %RH, with no backpressure. The cell was repeatedly kept at 0.4 V for 1 h, followed by idling for 1 min at open circuit. Over the period of 20 h, the power density was slowly increasing, at a rate of 2 mW/cm$^2$/h at 100 %RH. At 30 %RH, the power density was slowly increasing with rate of 3 mW/cm$^2$/h at first and then became stable. There was no indication of MEA degradation within 20 h testing in both 100 %RH and 30 %RH conditions.

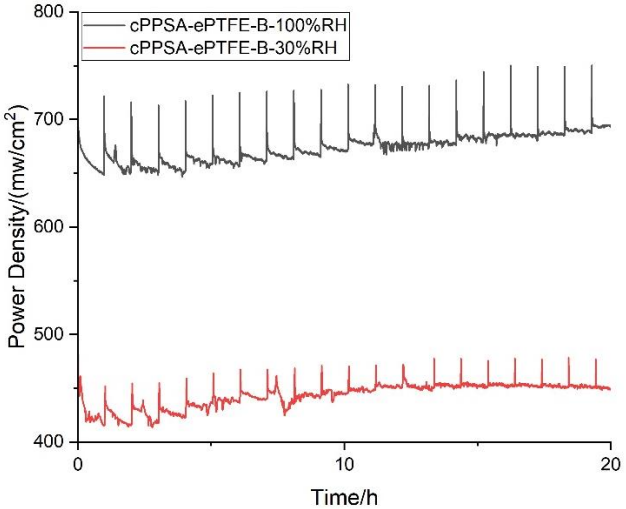


Figure 4.19: Fuel cell power output as the function of time for a cPPSA-ePTFE-B MEA operated at 80 ℃, 100 %RH and 30 %RH, with no backpressure. The testing protocol was 1 h at 0.4 V followed by 1 min at open circuit, repeated continuously. The spikes represent transitions between the 1 min open circuit periods and the 1 h power-on periods.

For a more intuitive comparison with other kind of hydrocarbon ionomer, a recently published paper from Steven Holdcroft group was selected, in which the authors claimed that their MEA with hydrocarbon membrane and binder had state-of-the-art performance [9]. I tested a cPPSA-ePTFE-based MEA under the same experimental conditions as Steven Holdcroft's group did. The experiment was executed at 50 %RH with 150 kPa backpressure. Figure 4.20 is the comparison of fuel cell performance between cPPSA-ePTFE-based MEA and their Pemion-based MEA. As can be seen, the maximum power density of Pemion-based MEA can only reach 1.1 W/cm$^2$ in this testing condition. But PFM-based MEA can get maximum power density higher than 1.2 W/cm$^2$.

Both cPPSA-ePTFE-based MEA and Pemion-based MEA showed higher activation loss comparing with PFSA-based MEA. But the activation loss of cPPSA-ePTFE-based MEA is less than that of Pemion-based MEA. For example, the current density of cPPSA-ePTFE-based MEA at 0.7 V was 671 mA/cm$^2$, which is obviously higher than that of Pemion-based MEA around 500 mA/cm$^2$. At the same time, the ohmic loss of cPPSA-ePTFE-based MEA, determined from the slope, was also less than that of Pemion-based MEA. Between 0.7 V and 0.5 V, the current density of Pemion-based MEA increased from 500 to 2000 mA/cm$^2$, while the current density of cPPSA-ePTFE-based MEA increased from 671 to 3074 mA/cm$^2$ in the same voltage region. cPPSA-ePTFE-based MEA could reach current density as high as 3263 mA/cm$^2$ indicating reduction in mass transport loss as compared to that with Pemion-based MEA, which could reach 2600 mA/cm$^2$ only.

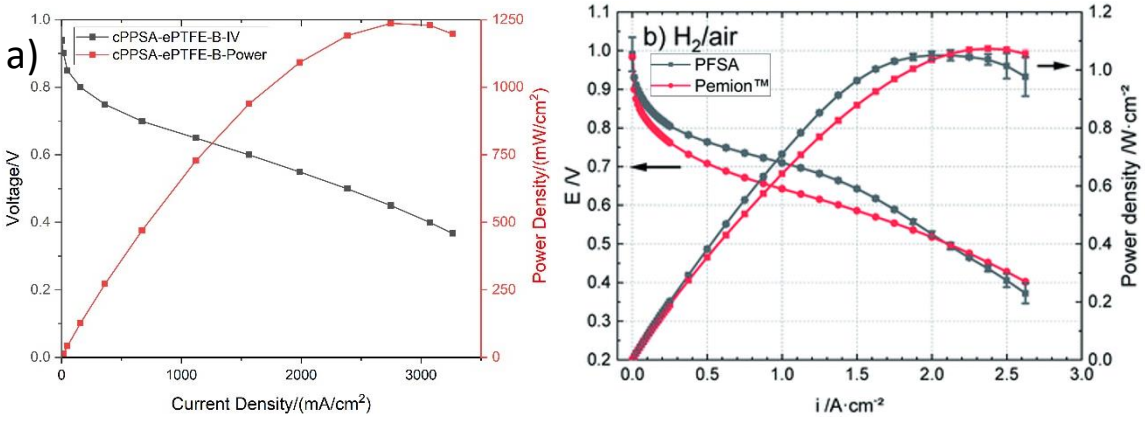


Figure 4.20: Comparison of fuel cell performance for cPPSA-ePTFE-B, Pemion and PFSA-based MEAs operated at 80 °C, 50 %RH, with 150 kPa backpressure.

Table 4.1 summarizes the differences between MEAs used in above-mentioned experiments and the Pemion-based MEA. The thickness of Pemion membrane was notably less than half the cPPSA-ePTFE-B thickness, and its cathode Pt loading of 0.4 mg/cm$^2$ was much higher than that of the cPPSA-ePTFE-based MEA (0.12 mg/cm$^2$). If all MEAs used the same Pt loading and if the Pemion membrane had the same thickness as cPPSA-

ePTFE-B, the difference of fuel cell performance between cPPSA-ePTFE-based MEA and Pemion-based MEA would likely become even more significant.

Table 4.1: Summary of characteristics of cPPSA-ePTFE-based MEA, Pemion-based MEA and PFSA-based MEA.

| Membrane | Thickness/μm | IEC/(mmol/g) | Pt loading/(mg/cm$^2$) |
|---|---|---|---|
| cPPSA-ePTFE-B | 15 | 2.7 | 0.12 for anode and cathode |
| Pemion | 7 | 2.9 | 0.1 for anode and 0.4 for cathode |
| PFSA | 15 | 1.4 | 0.1 for anode and 0.4 for cathode |

The in-plane proton conductivity was then measured at 60 °C between 30 and 90 %RH. Figure 4.21 shows the results for the cPPSA-ePTFE-B and Nafion XL. When the temperature decreased from 80 to 60 °C, the proton conductivity of both membranes also decreased. Due to its better water retention ability, the proton conductivity of cPPSA-ePTFE-B only decreased by 15%. In contrast, the proton conductivity of Nafion XL decreased more than 25%. The composite membrane exhibited a higher conductivity than Nafion XL over the tested relative humidity range at 60 °C. The highest conductivity for cPPSA-ePTFE-B was over two times greater than for Nafion XL of the full range of 30 %RH (23 vs. 6 mS/cm) to 90 %RH (189 vs. 55 mS/cm).

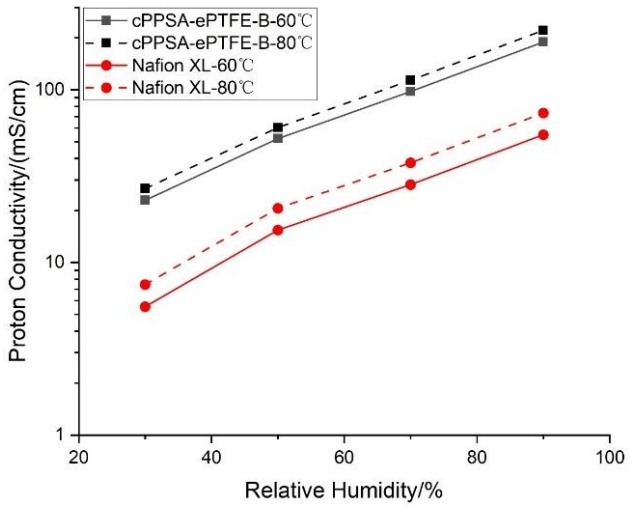


Figure 4.21: In-plane proton conductivity of the two composite cPPSA-ePTFE-B membranes and of Nafion XL reference at 60 and 80 °C and 30 - 90% RH.

Figure 4.22 shows the fuel cell i-V and power density curves, for MEAs with membranes tested at 60 °C. The MEA with cPPSA-ePTFE-B still showed higher activation overpotentials. But the activation overpotential difference was lower than that at 80 °C. cPPSA-ePTFE-B produced a higher power density when fully humidified (587 mW/cm$^2$ as per Figure 4.22a) and at 30 %RH (413 mW/cm$^2$ from Figure 4.22c). These values

were significantly greater than what was observed for Nafion XL, where the maximum power density was 476 mW/cm$^2$ at 100 %RH, only 177 mW/cm$^2$ at 30 %RH. To summarize in relative terms, decreasing the cell humidification level from 100 %RH to 30 %RH, led to a small (30%) reduction in the maximum power density with the cPPSA-ePTFE-B versus a 63% decrease with Nafion XL. The reduction in the maximum power density of Nafion XL was nearly twice as that of cPPSA-ePTFE-B. The high maximum power density of MEA with cPPSA-ePTFE-B at 30 %RH proved the excellent water retention ability of cPPSA compared to that with the PFSA ionomer.

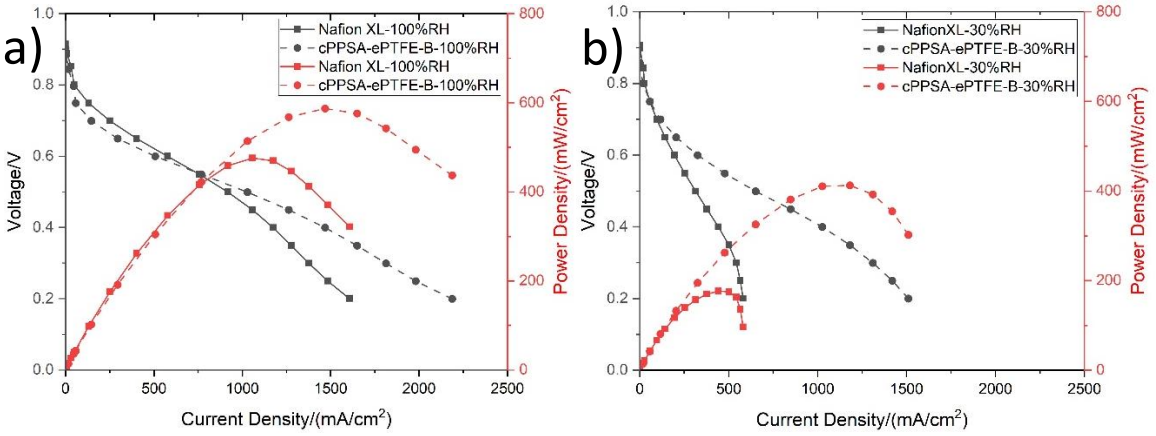


Figure 4.22: Fuel cell performance comparison of the MEAs with cPPSA-ePTFE-B (not hot-pressed) and Nafion XL membranes (hot-pressed) at 60 ℃ and: (a) 100 %RH and (b) 30 %RH no backpressures.

Figure 4.23 is the area specific high frequency resistance (HFR) for the two MEAs. It can be seen, that at 100 %RH, the PFM-based MEA had a HFR of about 52 mOhm cm$^2$ - 57 mOhm cm$^2$, as compared to 72 mOhm cm$^2$ -85 mOhm cm$^2$ for the Nafion XL-based MEA. Similarly, at 30 %RH, the resistance of the PFM-based MEAs is significantly lower (97 mOhm cm$^2$ -218 mOhm cm$^2$) as compared to the Nafion XL-based MEA (345 mOhm cm$^2$ – 500 mOhm cm$^2$). The resistance of PFM-based MEAs at 30 %RH proved the excellent water retention ability of cPPSA comparing with Nafion XL. The HFR ratios roughly follow the conductivity ratios calculated based on Figure 4.21.

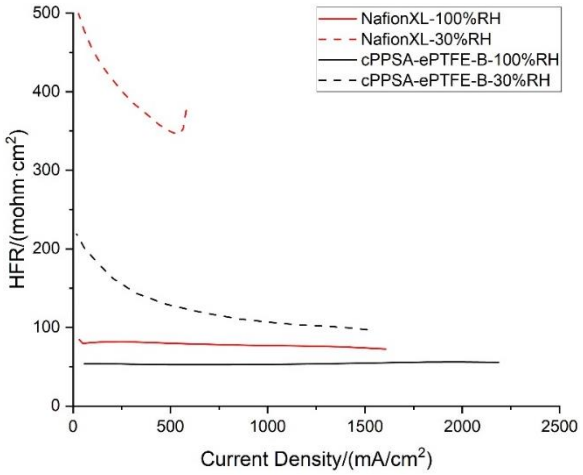


Figure 4.23: HFR dependence on current density for cPPSA-ePTFE-B MEA (black lines) and Nafion XL MEA (red lines) at 60 ℃ at 100 %RH (solid lines) and 30 %RH (dashed lines).

Figure 4.24 shows the resultant linear sweep voltammetry curves for 100 and 30 %RH. The crossover current density at 100 %RH was very low at 0.86 mA/cm$^2$ for the cPPSA-ePTFE-B MEA vs. 1.56 mA/cm$^2$ for a Nafion XL MEA. The crossover current density at 30 %RH was lower, as the reduction of membrane swelling generally led to a lower hydrogen permeability, 0.38 and 1.15 mA/cm$^2$ for the cPPSA-ePTFE-B and Nafion XL MEAs, respectively. The lower limiting current for cPPSA-ePTFE was expected, due to the cPPSA rigid rod chains which limited gas solubility and diffusion.

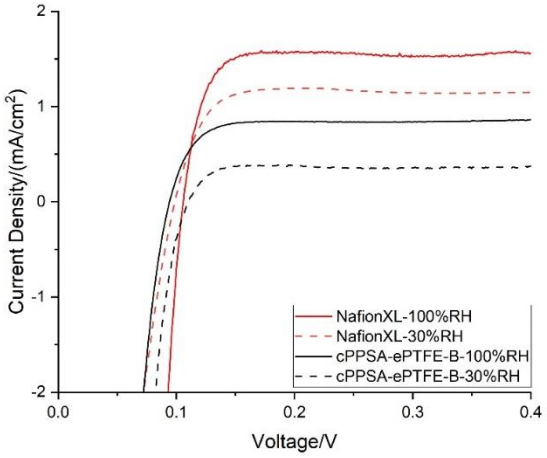


Figure 4.24: Linear sweep voltammetry $H_2$ limiting current density curves recorded at 60 ℃ for MEAs with cPPSA-ePTFE-B, and with Nafion XL, at 100 %RH (solid lines) and 30 %RH (dashed lines).

The fuel cell performance of the MEAs were also tested at an elevated temperature of 90 ℃ (Figure 4.25). Unfortunately, the power output decreased from that at 80 ℃, most likely due to the presence of PFSA binder in the GDEs. Even so, the decrease in power with the cPPSA-ePTFE-based MEA was still lower than with the

Nafion-based MEA.

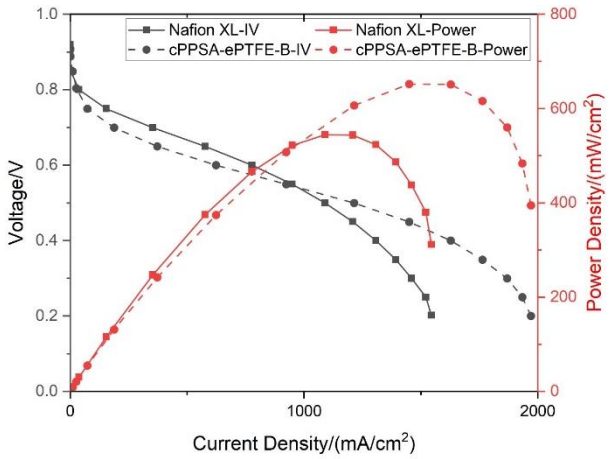


Figure 4.25: Comparison of fuel cell performance for cPPSA-ePTFE-B MEA and Nafion XL MEA operated at 90 ℃ and 100 %RH without backpressure.

### 4.3.4 PEM Fabrication Material Cost Analysis

Cost estimation should include (Material Cost + Processing Cost + Assembly Cost) x Markup Factor. In this section material cost estimation is described only. Material cost was estimated using available on internet quotations mostly from Chinese and Indian suppliers. Median prices for single kilograms and liters of the reagents were acquired. No formal inquiries were submitted to the suppliers identified during the online search. The estimated material cost for the three synthetic stages are as follows: (1) Sulfonation of the starting dibromoarylenes - $31.8/kg of the Li-form monomers (2) Copolymerization of the monomers - $136.7/kg of PPSA (3) Biphenyl grafting - $226.8/kg of cPPSA.

Membrane fabrication though pore-filling was assumed with the use of either commercial ePTFE or electrospun nanofiber mat. Assuming the final membrane to be 15 μm thick with 75 wt.% cPPSA ionomer, the unit price for a 1,000 $m^2$ membrane roll (materials only) was calculated to be as follows: (i) cPPSA-ePTFE membrane - \$9.8/$m^2$ (ii) cPPSA-PPSU membrane - \$17.8/$m^2$. In the above calculation, the ePTFE unit price was obtained from a Chinese manufacturer (\$6/$m^2$), which supplied samples for our experiments, and the electrospun PPSU mat unit price (\$14/$m^2$) was taken from the analysis performed in 2018 by Strategic Analysis, Inc for the DOE. About 60 $m^2$ of membrane area with thickness of 15 μm should ideally be possible to be fabricated, using pore-filling, from 1 kg of the cPPSA ionomer.

For comparing the cost of cPPSA-based membrane and PFSA-based membrane, a 2018 study by Strategic Analysis, Inc. was selected as reference [10]. Figure 4.26 is the estimation of the cost of manufacturing PFSA-based composite fuel cell membranes. As can be seen, even in 10,000 annual production rate the cheapest one was still around \$20/$m^2$. This price was still much higher than that of cPPSA-ePTFE with 15 μm thickness.

This demonstrates the economic feasibility of using hydrocarbon ionomer in proton exchange membrane.

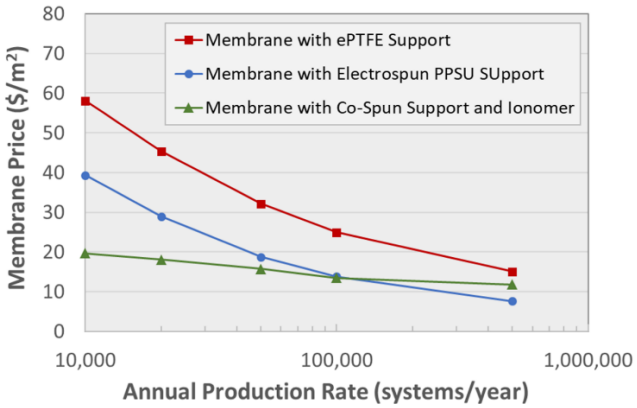


Figure 4.26: Relationship between composite membranes price and fuel cell stack (system) annual production rate, from an economic study carried out by strategic Analysis, Inc. All membranes are 14 μm in thickness with 95% Nafion PFSA ionomer.

### 4.4 Conclusion

Novel, composite fuel cell membranes (cPPSA-ePTFE) were fabricated by pore-filling of expanded polytetrafluoroethylene with proton-conducting sulfonated polyphenylene copolymer, followed by thermal crosslinking of the polyphenylene, to render the bulk of the membrane water insoluble, with a water-leaching fraction of less than 6%. The cPPSA-ePTFE-B, developed in this work, had a high proton conductivity at 80 °C of 47.5 mS/cm at 40 %RH and of 221 mS/cm at 90 %RH, with a tensile strength of 25 MPa and 21 MPa, in the machine and transverse directions, respectively, at room temperature.

The 15 μm-thick membrane performed well in a $H_2$/air fuel cell at 80 °C and 100 kPa backpressure with 0.12 mgPt/cm$^2$ GDEs as the anode and cathode. The maximum power density decreased by only 15%, from 1.00 to 0.85 W/cm$^2$, when the cell RH was reduced from 100 to 30%. In comparison, a MEA with Nafion XL showed a significant (52%) loss, from 0.82 to 0.39 W/cm$^2$, for similar reduction of the fuel cell humidification. The fuel cell performance of MEA was better than that of similar hydrocarbon ionomer membrane even with lower Pt loading.

After 20 h of fuel cell operation, the MEA with cPPSA-ePTFE-B continued to produce a steady power output at 100 and 30 %RH without loss. The fuel cell performance of MEA at 90 °C were lower than at 80 °C which was due to a performance (conductivity) decrease of PFSA binder in the gas diffusion electrode. Better binder is needed for improved fuel cell performance at elevated temperature. The composite cPPSA-ePTFE-B met the DOE 2020 technical targets for hydrogen crossover (<2 mA/cm$^2$) and area specific resistance at 80 °C and a water partial pressure, between 30 and 45 kPa (0.02 Ω cm$^2$). PEM fabrication materials cost analysis showed the cost of fabricating cPPSA-ePTFE was significantly lower than using PFSA due to the low price of cPPSA.

### 4.5 References

[1] Hossain, M., et al. "Pore-Filled PEMs from Poly (Phenylene Sulfonic Acid) S and Electrospun Poly (Phenylene Sulfone) Fiber Mats." *ECS Transactions* 98.9 (2020): 367.

[2] Shang, Zhihao, Ryszard Wycisk, and Peter Pintauro. "Electrospun Composite Proton-Exchange and Anion-Exchange Membranes for Fuel Cells." *Energies* 14.20 (2021): 6709.

[3] Si, Kun, et al. "Rigid-rod poly (phenylenesulfonic acid) proton exchange membranes with cross-linkable biphenyl groups for fuel cell applications." *Macromolecules* 46.2 (2013): 422-433.

[4] Graybill, Bruce M. "Synthesis of aryl sulfones." *The Journal of Organic Chemistry* 32.9 (1967): 2931-2933.

[5] K.R. Cooper, Situ PEMFC Fuel Crossover & Electrical Short Circuit Measurement, Fuel Cell Magazine (2008), Aug/Sep 1-2, https://www.scribner.com/files/tech-papers/Scribner-on-Crossover-Fuel-Cell-Magazine-2008.pdf.

[6] Shang, Zhihao, et al. "Poly (phenylene sulfonic acid)-expanded polytetrafluoroethylene composite membrane for low relative humidity operation in hydrogen fuel cells." *Journal of Power Sources* 535 (2022): 231375.

[7] Adamski, Michael, et al. "Molecular branching as a simple approach to improving polymer electrolyte membranes." *Journal of Membrane Science* 595 (2020): 117539.

[8] Litt, Morton, and Ryszard Wycisk. "Poly (arylenesulfonic acids) with frozen-in free volume as hydrogen fuel cell membrane materials." *Polymer Reviews* 55.2 (2015): 307-329.

[9] Nguyen, Hien, et al. "Hydrocarbon-based Pemion™ proton exchange membrane fuel cells with state-of-the-art performance." *Sustainable Energy & Fuels* 5.14 (2021): 3687-3699.

[10] James, B.; Huya-Kouadio, J.; Houchins, C. 2018 DOE Hydrogen and Fuel Cells Program Review Fuel Cell Systems Analysis Project ID# FC163. 2018. Available online: https://www.hydrogen.energy.gov/pdfs/review18/fc163_james_2018_o.pdf.

## CHAPTER 5 - POLY(PHENYLENE SULFONIC ACID)S-PFSA BLEND MEMBRANES

### 5.1 Introduction

Prior research has already proved the feasibility of combining PFSA and high IEC hydrocarbon ionomer to make blend membranes and improving the fuel cell power output of PFSA [1,2]. The preparation and characterization of a PFSA-hydrocarbon ionomer blend membrane are described in this chapter. Due to the high IEC of cPPSA, PFSA with IEC closer to that of cPPSA might be suitable for blending. Typically, increasing the IEC of a PFSA ionomer involves adding more side chains to the backbone or by altering the side chain structure. In either case, the equivalent weight (gram polymer/mole equivalent sulfonic acid) is reduced. One notable example of this is 3M's low equivalent weight PFSA (Figure 5.1) [3]. Due to the relatively high IEC comparing with Nafion 1100EW and good mechanical property, 3M ionomer was selected to use in the following experiments.

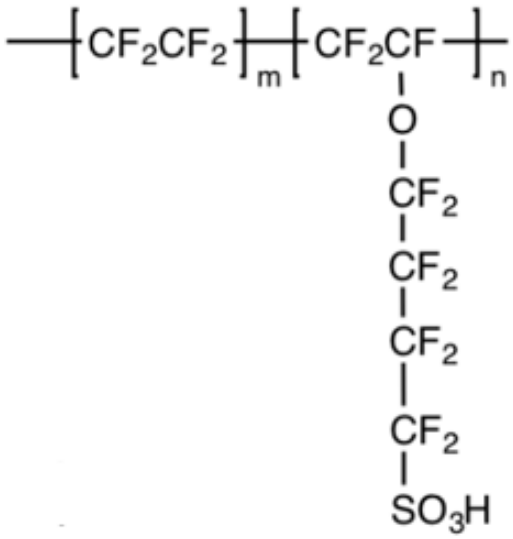


Figure 5.1: 3M PFSA, where m = 5, n = 1 for an 825 EW ionomer.

### 5.2 Experimental

#### 5.2.1 Membrane Fabrication

The blend 3M825-cPPSA membranes were fabricated by solution casting. A calculated volume of 3 wt.% 3M825-cPPSA solution in $H_2O$-EtOH was spread over on a Teflon-FEP sheet. After evaporation of the solvent at room temperature for 3h, the solution cast membrane was heated in a vacuum oven at 150 °C for 1 h, to crosslink cPPSA and to anneal 3M ionomer. The light brown color of the membrane slightly deepened indicating no significant desulfonation. Blend membranes with two compositions were fabricated, one with 10 wt.% cPPSA (Blend10) and the other one with 20 wt.% cPPSA (Blend20).

### 5.2.2 Characterization of Proton-Exchange Membranes

#### 5.2.2.1 Proton Conductivity

In-plane proton conductivity was determined by an AC impedance method, using a BekkTech four-electrode test cell. The BekkTech cell was placed in an ESPEC Corp. temperature/humidity controlled environmental chamber (Model: SH-241) and the impedance data was recorded in the frequency rage 1Hz – 1MHz, at 80 °C and 30 %RH - 90 %RH. In-plane conductivity was calculated using Equation 5.1

$$\sigma = \frac{1000L}{wtR} \qquad \text{(Equation 5.1)}$$

where σ (mS/cm) is in-plane proton conductivity, R (Ω) is the resistance (real axis intercept on Nyquist plot), L (cm) is the distance between the inner electrodes, w (cm) is the width of a membrane sample (typically 0.4 cm), and t (cm) is the thickness of the membrane sample. Vapor-equilibrated dimensions were used to calculate conductivity.

#### 5.2.2.2 Mechanical Properties

Stress and strain of composite membrane samples were measured with a TA Instruments Q800 dynamic mechanical analyzer (DMA, TA Instruments, New Castle, NY, USA). Stress-strain curves were obtained for membranes equilibrated in air at 25 °C. The DMA was operated in tension using the controlled strain mode, where the sample was strained at 10 %/min until failure.

#### 5.2.2.3 Gravimetric Water Uptake

Gravimetric water uptake of rectangular membrane samples was determined by measuring the relative change in sample weight and dimensions after equilibrating with water vapor at 30 - 90 %RH and 80 °C, and then drying at 80 °C in a vacuum oven. Gravimetric water uptake was calculated using Equation 5.2

$$Water\ Uptake\ (\%) = \frac{x_{wet} - x_{dry}}{x_{dry}} \qquad \text{(Equation 5.2)}$$

where $x_{wet}$ and $x_{dry}$ are the membrane masses in the wet or dry state, respectively.

#### 5.2.2.4 MEA Fabrication and Fuel Cell Testing

MEAs were prepared with a 3M825-cPPSA blend membranes and with AquivionE87-03S membrane. AquivionE87-03S membrane was selected since it is a commercial product with similar equivalent weight as 3M825. Commercial Pt/C GDEs with 5 $cm^2$ catalyzed area was used, purchased from the Fuel Cell Store. The anode and cathode Pt loading was 0.12 $mg/cm^2$. MEAs were evaluated using a Scribner 850e test station. Data were collected at 80 °C, 100 and 30 %RH, with and without backpressure, the same for the both feed streams. The $H_2$ and oxidant (air or oxygen) flow rates were 0.125 and 0.5 L/min, respectively.

$H_2$ crossover was measured via linear sweep voltammetry. The humidified hydrogen gas was fed to the anode

(reference electrode) while the cathode (working electrode) was purged with humidified nitrogen. The $H_2$ and $N_2$ flow rates were 0.125 and 0.5 L/min, respectively. An anodic sweep was applied between 0.01 and 0.4 V at a rate of 10 mV/s using a potentiostat (Reference 3000, Gamry Instruments), which resulted in oxidation of the $H_2$ permeating through the membrane. The cell current density at 0.4 V (plateau) represented the $H_2$ crossover rate.

## 5.3 Results and Discussion

### 5.3.1 Ex-situ Testing Results

The thickness of both dry 3M825-cPPSA blend membranes and AquivionE87-03S membrane are around 30 μm. Commercial AquivionE87-03S membrane was used as reference since it has similar equivalent weight (870) as 3M825. The cast 3M825-cPPSA blend membranes were nearly transparent with a light-brown color and appeared macroscopically homogeneous, no phase separation can be observed (Figure 5.2). Usually, the length and width of membranes are 4 cm.


Figure 5.2: Photograph of the 3M825-cPPSA Blend20 membrane sample.

Figure 5.3 is the surface and cross-sectional SEM images of the 3M825-cPPSA blend20 membrane. The images show no defect voids, consistent with no macroscopic phase separation of in the blend membrane.

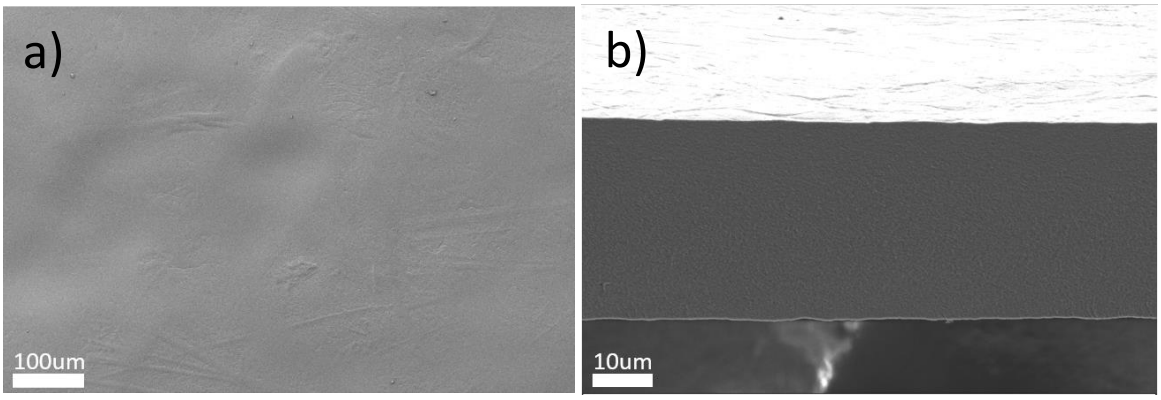


Figure 5.3: Surface and cross-sectional SEM images of the 3M825-cPPSA Blend20 membrane sample.

The major objective of the present study was to develop a new PEM with a proton conductivity superior to that of commercial Aquivion PFSA, particularly for fuel cell operation at low feed gas humidification. To verify that this objective was met, the proton conductivity of 3M825-cPPSA blend membranes and AquivionE87-03S film were tested at 80 °C, between 30 and 90 %RH. Figure 5.4 shows the results of conductivity. With larger amount of cPPSA in the blend membrane, higher proton conductivity was obtained. The blend membrane with 20 wt.% cPPSA had the highest proton conductivity, 135 and 19 mS/cm at 90 and 30 %RH, respectively. These values were significantly higher than those of a commercial AquivionE87-03S membrane (102 mS/cm and 11 mS/cm at 90 %RH and at 30 %RH, respectively). These experimental results of blend membranes were quite close to the expected conductivities based on data for pristine cPPSA and PFSA. For example, the expected conductivities were 16 and 20 mS/cm for Blend10 and Blend20, respectively, at 30 %RH. The actual conductivities were 16 and 19 mS/cm for Blend10 and Blend20, respectively. The improvement of proton conductivity at 90 %RH was not as significant as at low RH.

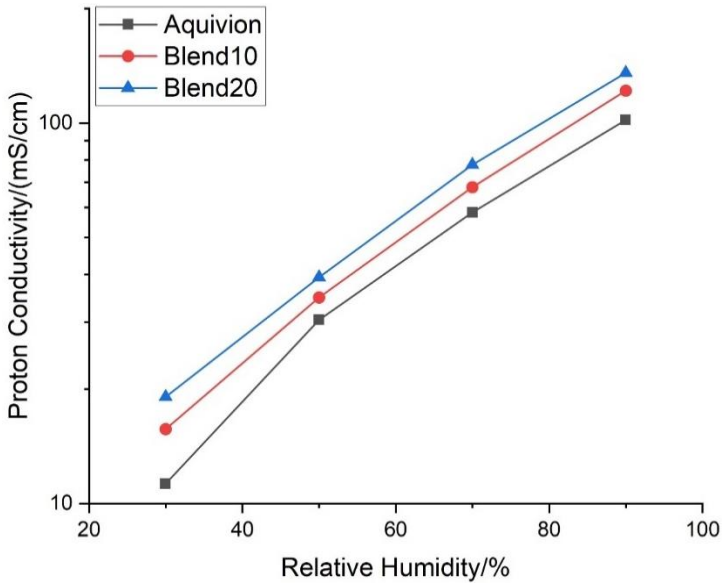


Figure 5.4: In-plane proton conductivity of the 3M825-cPPSA blend membrane and Aquivion reference, at 80 °C and 30 - 90 %RH.

The mechanical characteristics of 3M825-cPPSA blend membranes and AquivionE87-03S membrane were acquired using a DMA analyzer. Figure 5.5 shows the results of stress-strain tensile tests at 25 °C and ambient (50 %RH) air. The ultimate strain of commercial AquivionE87-03S membrane in ambient condition can reach to 199%, indicating the much greater ductility of AquivionE87-03S. Both of these two membranes had much lower ultimate strain (25% for Blend10 and 14% for Blend20) comparing with commercial AquivionE87-03S membrane, which proved cPPSA's mechanical property will significantly influence the blend membranes. The ultimate stresses of these 3M825-cPPSA blend membranes were higher than for commercial AquivionE87-

03S membrane by about 2-3 MPa; however, the tensile stress of Aquivion membrane at 14-25% strain was about 25% lower than that of the blend membranes. The blend membranes were very flexible in both the dry and wet states, thus overcoming the brittleness problem observed with solution cast films from cPPSA.

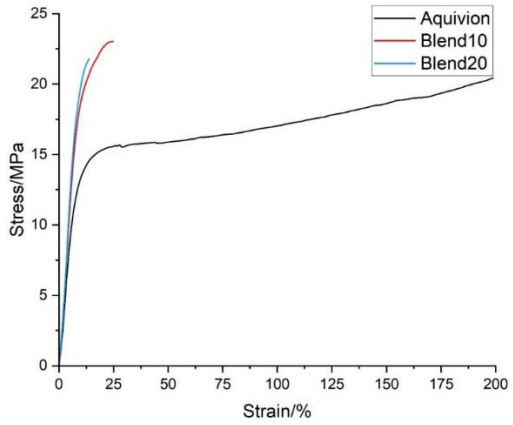


Figure 5.5: Tensile curves recorded for the 3M825-cPPSA blend membranes and for Aquivion reference, equilibrated in ambient air at 25 °C and 50 %RH.

Improved proton conductivity of 3M825-cPPSA blend membranes may be the result of both, decrease of the EW of the blends with respect to EW of pristine 3M825 as well as the increased water uptake of the blends. Figure 5.6 are the water uptake and through-plane swelling of the membranes tested at 80 °C and different relative humidity. With addition of 20 wt.% cPPSA to 3M ionomer (Blend20), water uptake reached 38 wt.% at 90 %RH. This is nearly twice as much as what was obtained for the commercial Aquivion membrane in the same condition. At 30%RH, the water uptake of 3M825-cPPSA Blend20 membrane reached 11 wt.%, which is still 57% higher than that of commercial Aquivion membrane.

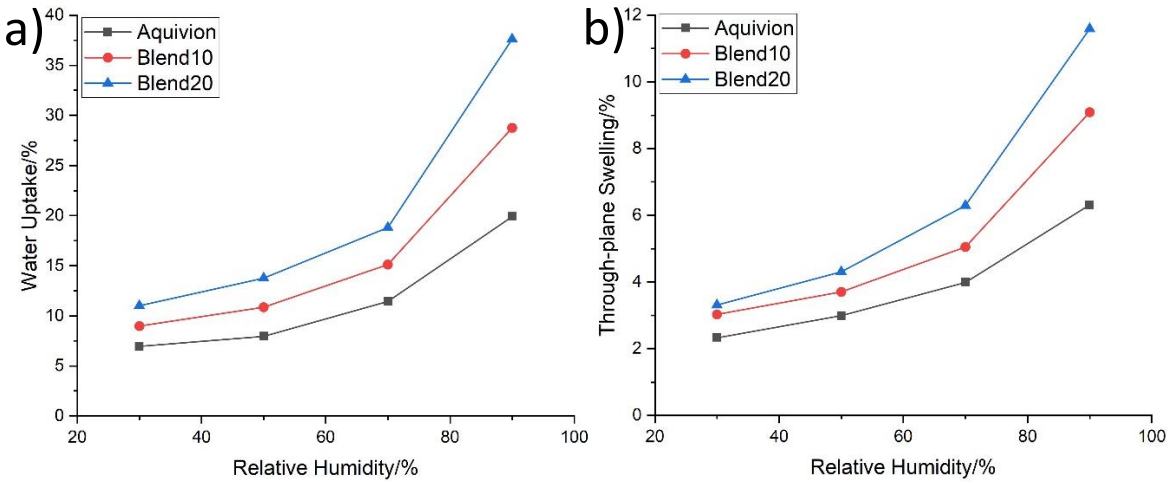


Figure 5.6: Comparison of a) water uptake and b) through-plane swelling of the 3M825-cPPSA blend membranes and Aquivion reference at 80 °C and 30 - 90 %RH.

### 5.3.2 Fuel Cell Performance

Fuel cell testing was performed in a hardware described earlier, at 80 °C and at two feed humidity values or 100 and 30 %RH. Figure 5.7 shows the i-V curves and the i-P curves obtained without backpressure. For both blend membranes, the activation polarization loss was higher for the blend than for the commercial AquivionE87-03S membrane at 100 %RH. The two i-V curves for 3M825-cPPSA blend membranes almost overlapped in that region. The mass transfer loss is slightly lower for the Blend10 and Blend20, compared to that for the commercial Aquivion membrane but there is not significant difference of maximum power density between these three membranes.

When the cell relative humidity was decreased to 30 %RH, the performance of MEAs with the three membranes dropped to significantly different degrees. However, with the Blend20 (20 wt.% cPPSA), the maximum power density reached 408 mW/cm$^2$, compared to only 247 mW/cm$^2$ with AquivionE87-03S membrane. This was the result of the cPPSA's excellent water retention ability which effectively helped the blend membrane to provide higher proton conductivity and thus improved fuel cell power output at low humidity. A blend membrane with 30 wt.% cPPSA content was also prepared but it fractured during the fuel cell break-in stage, reflecting the inability of PFSA to accommodate the increased swelling of the cPPSA component.

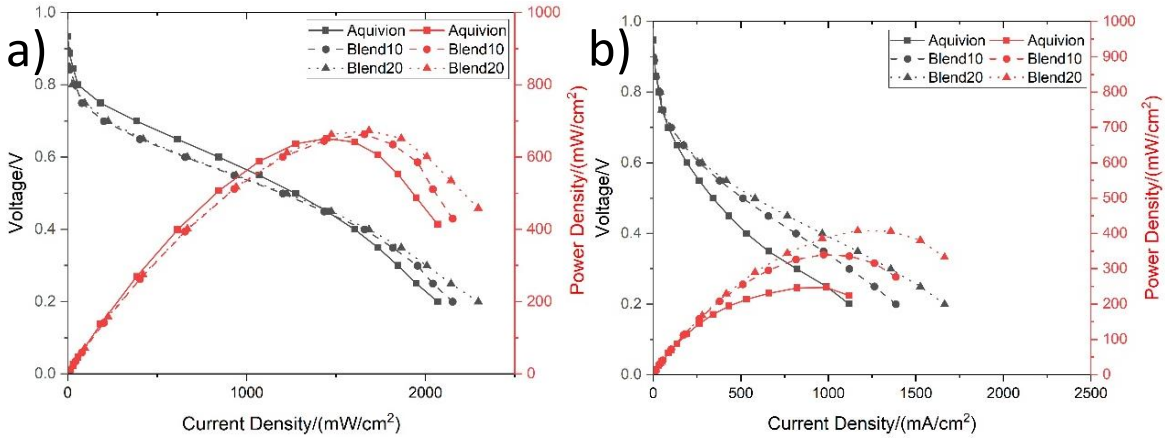


Figure 5.7: Fuel cell performance comparison of the MEAs with 3M825-cPPSA blend membranes and Aquivion membranes at 80 °C and: (a) 100 %RH and (b) 30 %RH no backpressures.

Figure 5.8 is the high frequency resistance of MEAs with these three kinds of proton exchange membranes at 100 %RH and 30 %RH. As can be seen the HFR values are lower for the both blend membranes as compared to HFR of the reference Aquivion membrane. While the differences are small at 100 %RH, they are significant at 30 %RH, 146-196 mΩ cm$^2$ with Blend10 and Blend20, and 318-436 mΩ cm$^2$ with the Aquivion reference membrane. These results proves that modification of PFSA materials by the addition of cPPSA might be a

useful strategy for obtaining the significant improvement in low RH performance.

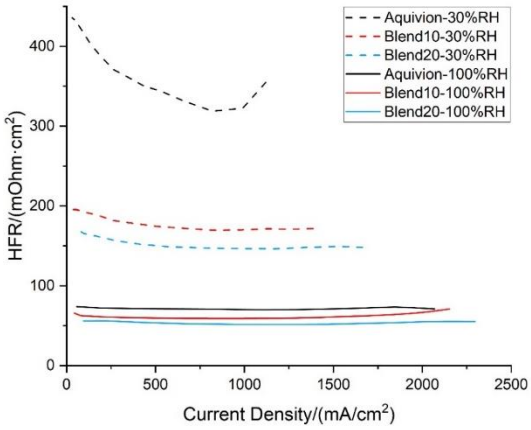


Figure 5.8: HFR dependence on current density for 3M825-cPPSA MEA and Aquivion MEA at 80 ℃ and RH of 100 % (solid lines) and 30 % (dashed lines).

Figure 5.9 is the linear sweep voltammetry curves for 100 %RH and 30 %RH. As can be seen, the crossover current density at 100 %RH was low at 1.06 mA/cm$^2$ for the MEA with Blend20 membrane vs. 1.47 mA/cm$^2$ for a MEA with AquivionE87-03S membrane. The crossover current density at 30 %RH was lower, as the reduction of membrane swelling generally led to a lower hydrogen permeability, 0.82 mA/cm$^2$ and 1.07 mA/cm$^2$, for the MEAs with Blend20 membrane and with AquivionE87-03S membrane, respectively. The lower limiting current for 3M825-cPPSA blend membranes was expected, due to the expected cPPSA co-crosslinked with PFSA and due to its stiff chain structure (rigid rod chains) which limited both, gas solubility and diffusion. The crossover data also confirm that there were no voids/defects percolating through the membrane.

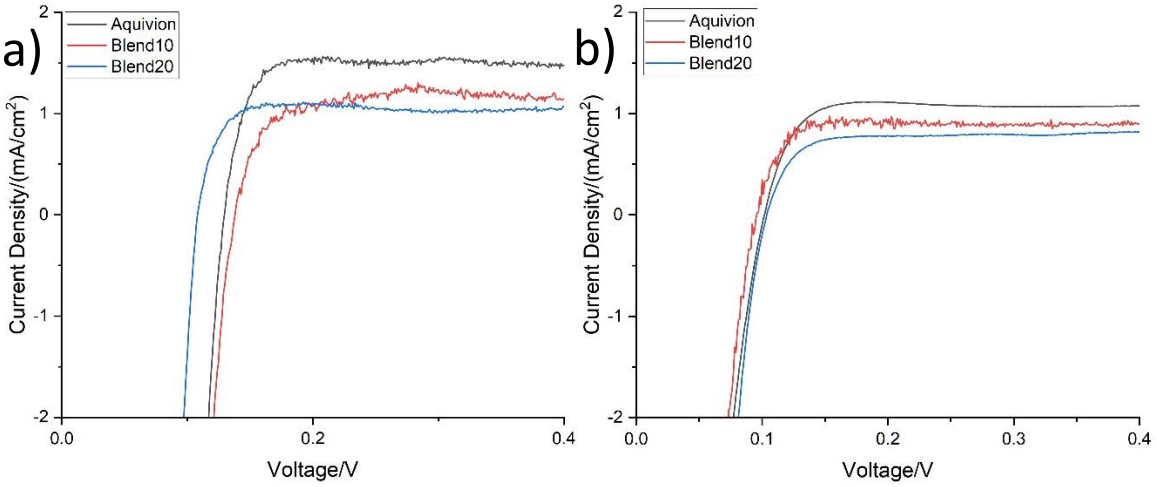


Figure 5.9: Linear sweep voltammetry $H_2$ limiting current density curves recorded at 80 ℃ for MEAs with the three membranes at a) 100 %RH and b) 30 %RH.

Figures 5.10 to 5.12 compare the fuel cell performance of MEAs with the three membranes at 80 ℃ and 100 %RH, and 30 %RH, with different backpressure (0 kPa, 100 kPa and 200 kPa). For commercial AquivionE87-03S membrane, the fuel cell power output increased with increasing backpressure at 100 %RH (Figure 5.10a), but when the backpressure reached to 200 kPa, increased mass transport loss was observed. This may be due to water flooding issue caused by the cathodic reaction. For the MEA with Blend10 (Figure 5.10a), the mass transport loss was still significant at 200 kPa backpressure but with Blend20, (20 wt.% cPPSA), the mass transport loss was greatly reduced.

With the increase of cPPSA content, the water retention ability of the blend membrane was improved, so that more water generated by the cathode could enter the blend membrane. It reduced the water flooding at cathode side and mass transport loss. With backpressure, blend membranes showed significantly higher power output than Aquivion at 30 %RH. The maximum power output of Blend20 was 813 mW/cm$^2$ with 100 kPa, which was 85% higher than that of Aquivion in the same condition, which was only 439 mW/cm$^2$. The higher proton conductivity of blend membranes also helped MEAs to get less ohmic drop during fuel cell test. It can be concluded blend membranes can have better performance in low RH than Aquivion.

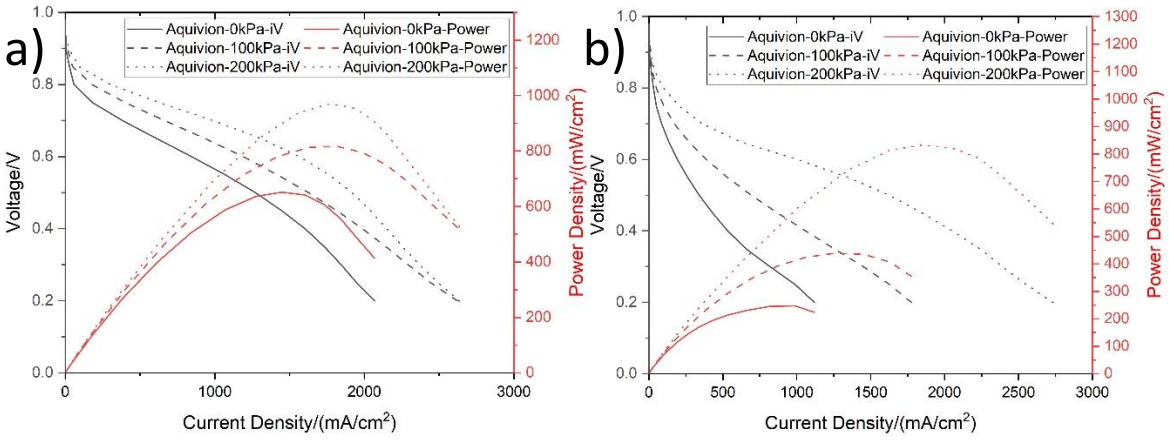


Figure 5.10: Fuel cell performance comparison of the Aquivion MEA at (a) 100 %RH and (b) 30 %RH, with air. Solid red line – air, no backpressure, long dashes – air, 100 kPa, short dashes – air, 200 kPa.

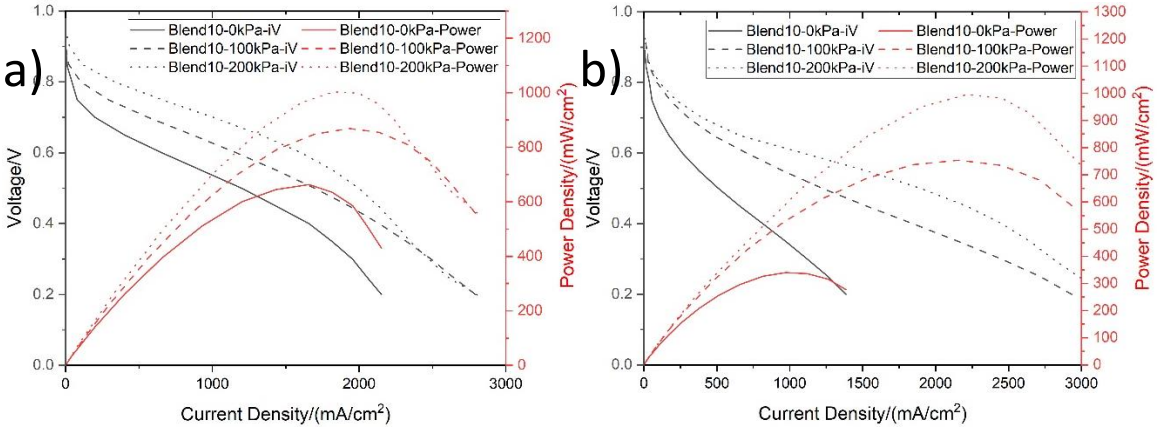


Figure 5.11: Fuel cell performance comparison of the Blend10 MEA at (a) 100 %RH and (b) 30 %RH, with air. Solid black line – air, no backpressure, long dashes – air, 100 kPa, short dashes – air, 200 kPa.

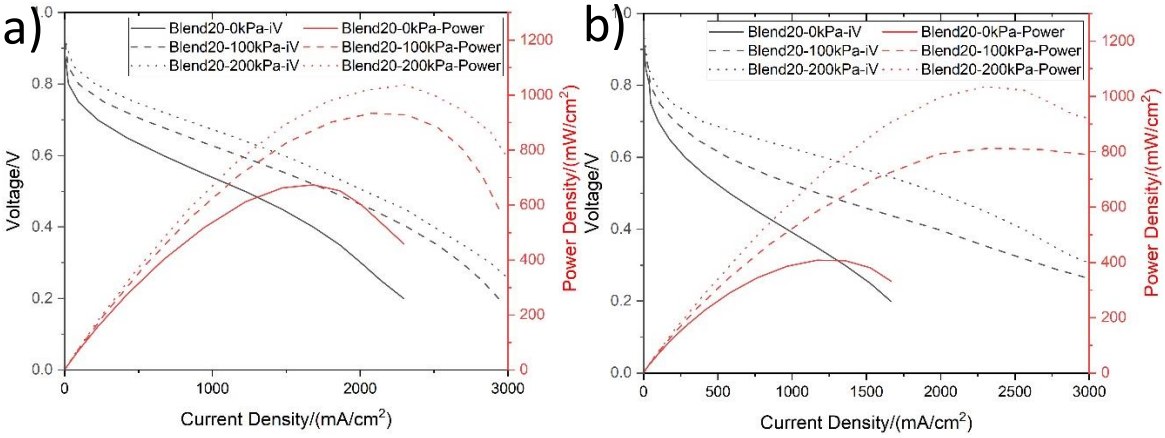


Figure 5.12: Fuel cell performance comparison of the Blend20 MEA at (a) 100 %RH and (b) 30 %RH, with air. Solid black line – air, no backpressure, long dashes – air, 100 kPa, short dashes – air, 200 kPa.

Figure 5.13 is the fuel cell maximum power output results obtained with these membranes. It can be seen that the maximum power density with the both blend membranes was always higher compared to that with the Aquivion reference, at a given RH value. Increasing backpressure led to minimization of the power output at 100 %RH and 30 %RH and for the EA with Blend20 the difference was negligibly small, compared to 135 mW/cm$^2$ with the Aquivion membrane. The MEA with Blend20 membrane (containing 20 wt.% cPPSA), showed comparable fuel cell performance to that with a cPPSA-ePTFE-B membrane described earlier [4].

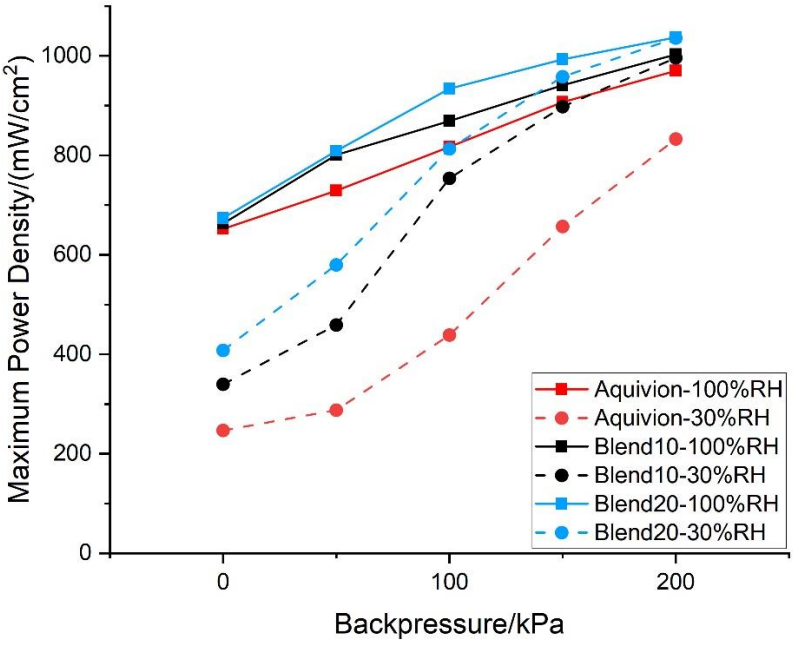


Figure 5.13: Maximum power density comparison of the MEAs with 3M825-cPPSA blend membranes and with Aquivion reference at 100 %RH and at 30 %RH, at different backpressure. Solid lines: 100 %RH, dashed lines: 30 %RH.

### 5.4 Conclusion

This work proved that the fuel cell performance of perfluorosulfonated ionomer (3M 825EW PFSA) membranes could be improved, particularly at low RH, by adding a very low EW crosslinkable sulfonated hydrocarbon ionomer (cPPSA [4]). The blend PFSA-cPPSA proton exchange membranes, containing 10 wt.% and 20 wt.% of cPPSA were transparent with no visible phase separation. Their proton conductivity and water uptake were greater than that of the pristine PFSA in the whole RH range tested. This led to improved fuel cell power output, particularly at low cell RH. The blend membrane with 20 wt.% cPPSA (Blend20) had similar power output as cPPSA-ePTFE-B.

## 5.5 References

[1] Guimet, Adrien, et al. "Strengthening of perfluorosulfonic acid ionomer with sulfonated hydrocarbon polyelectrolyte for application in medium-temperature fuel cell." *Journal of Membrane Science* 514 (2016): 358-365.

[2] Wang, Baolong, et al. "Property enhancement effects of side-chain-type naphthalene-based sulfonated poly (arylene ether ketone) on Nafion composite membranes for direct methanol fuel cells." *ACS applied materials & interfaces* 9.37 (2017): 32227-32236.

[3] Zhang, Wenjing, Daniel Lee Kish, and Peter Pintauro. "Morphology and performance of stretched PFSA for direct methanol fuel cells." *ECS Transactions* 33.1 (2010): 635.

## CHAPTER 6 - GAS DIFFUSION ELECTRODE WITH CPPSA BINDER

### 6.1 Introduction

Several papers reported the fabrication and use of AEMFC electrodes with grinded, insoluble crosslinked ionomers. Historically, one of the first reports on the use of crosslinked alkaline electrode binders came from the Varcoe group [1]. An anion exchange ionomer (AEI) was prepared from the radiation-grafting of vinylbenzyl chloride (VBC) onto poly(ethylene-co-tetrafluoroethylene) [ETFE] powders with powder particle sizes of less than 100 μm diameter. Quaternisation of the VBC grafted ETFE powders with trimethylamine resulted in AEIs that were chemically the same as the ETFE-based radiation-grafted alkaline anion exchange membranes that had been previously developed for use in low temperature alkaline polymer electrolyte fuel cells. The integration of the AEI powders into the catalyst layers (CL, Figure 6.1) of both electrodes resulted in a $H_2/O_2$ fuel cell peak power density of 240 mW/cm$^2$ at 50 °C.

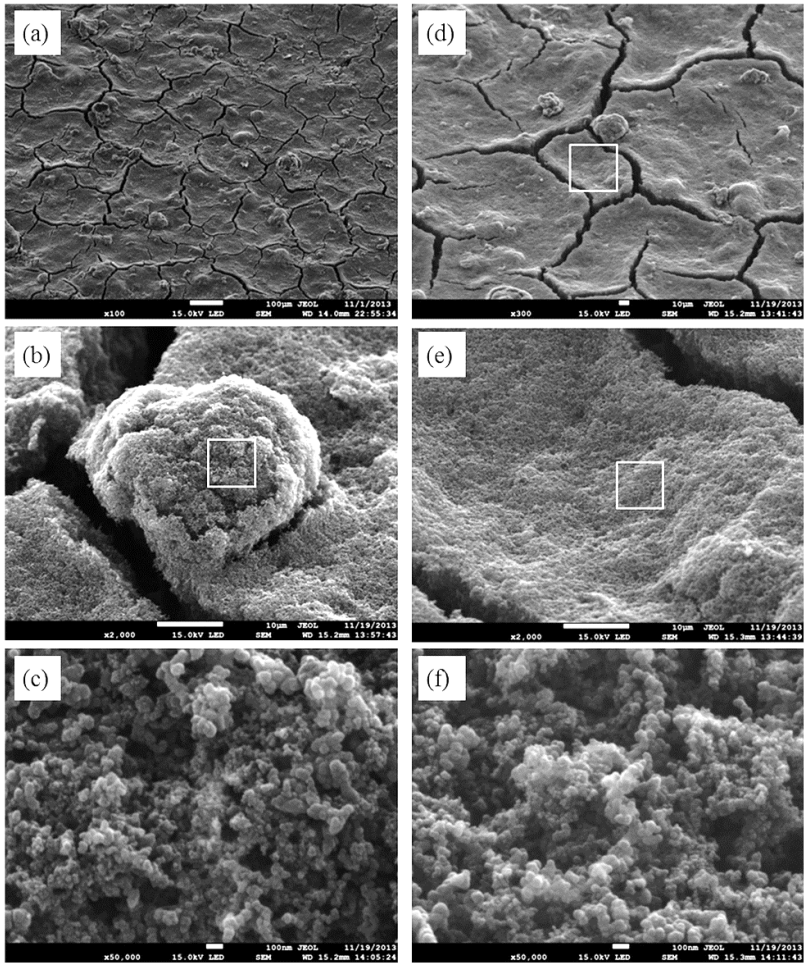


Figure 6.1: SEM images of the catalyst layer of a GDE sample with 15% mass AEI content (3 nm Au coating used for image clarification purposes). Distinct, isolated AEI particles are randomly distributed across the surface of the GDE.

Huang et al. [2] demonstrated an MEA employing a high-IEC norbornene-based tetrablock copolymer membrane and Varcoe's particulate electrode ionomer which in a $H_2/O_2$ AEMFC gave a peak power density of 3.5 W/cm$^2$ with a maximum current density of 9.7 A/cm$^2$ at 0.15 V and 80 °C. Hassan, et al. [3] utilized similar crosslinked norbornene based copolymer. They first soaked it in water, then added catalyst (40 wt.% Pt/C) and 2-propanol, and ground the mixture for 10+5 minutes using mortar and pestle. This ink was ultrasonicated in an ice bath and sprayed on Toray 60 GDL. For "Type 1" and "Type 2" GDE, Vulcan carbon was added to adjust composition so that the ionomer: carbon: Pt mass ratio = 1:2.5:1.5. For "Type 2" GDE, 8 wt.% (of catalyst mass) PTFE was added to the ink. Authors used a relatively high noble metal loading of 0.7 mg/cm$^2$ and 0.6 mg/cm$^2$ for anode and cathode, respectively, to obtain very stable performance with a high power output of 1.75 W/cm$^2$ in $H_2/CO_2$-free air AEMFC at 80 ℃ and optimized cathode/anode dew points.

Omasta, et al. [4] ground the crosslinked ETFE-g-poly(VBTMA+$Cl^-$) ionomer powder first, instead of soaking in water. Then they followed the procedure of Hassan et al. The I/C ratio was 20/80 and no additional carbon was admixed. The authors used high noble metal loading of 0.67 mg/cm$^2$ and 0.53 mg/cm$^2$ for anode and cathode, respectively with 5% PTFE, and obtained the power output as high as 1.4 W/cm$^2$ in $H_2/O_2$ AEMFC at 60 ℃ and ~75 %RH. Zheng, et al. [5] used similar fabrication procedure as Omasta et al. They kept the ionomer: carbon: noble metal ratio equal to 20:48:32. The authors also used high Pt loading of 0.6 mg/cm$^2$ for the anode and the cathode which resulted in power output above 2 W/cm$^2$ in $H_2/O_2$ AEMFC at 80 ℃ and ~100 %RH.

## 6.2 Experimental

### 6.2.1 Synthesis of cPPSA

1.0 g of P75B25 copolymer and 17.0 g of 85% $H_3PO_4$ (PA) were placed in a 100 mL round-bottom flask, heated to 80°C, and stirred at 175 rpm for 4h to dissolve the copolymer. Then, 1.35 g (0.009 mol) of biphenyl (BP) was added to the solution. After 10 minutes, 25 g of $P_2O_5$ was added in batches of ~2 g (~10 min.) to maintain the content at a temperature below 100 °C. Once all $P_2O_5$ was added, the temperature was raised to 125 °C over the period of about 30 minutes and the reaction was carried out for 64-72h. The reaction mixture was then cooled down and transferred into cold water (100 mL). The solution was neutralized with 20% alkali solution (~200 mL), and residual BP was removed by vacuum filtration. Final product cleaning was performed in an ultrafiltration cell. The graft polymer solution was then passed through an ion exchange column to obtain the $H^+$-form of cPPSA. After water evaporation, the polymer was dried at 80 °C for 24h. Typically ~0.7-0.8 g of cPPSA (BP grafted copolymer) was obtained with grafting degree 10-15% by $^1$H NMR (yield 70%).

Additionally, an over-grafting procedure was attempted, where reaction was carried out for 96 h, instead of the typical 64-72h. The purified soluble cPPSA fraction constituted about 0.1-0.2g. The insoluble fraction was treated with acetone, do extract BP and the was washed with 1M HCl to convert the remaining insoluble

cPPSA to the $H^+$-form, followed by extensive washing with DI water and drying at 80 ℃. About 0.9g of insoluble (over-grafted) cPPSA could be recovered. The insoluble PPSA will be used as the ionomer binder for the preparation of fuel cell electrodes.

### 6.2.2 Gas Diffusion Electrode Fabrication and Fuel Cell Testing

To prepare gas diffusion electrode with cPPSA, an insoluble cPPSA binder was prepared by the following ways. A solution-casted cPPSA film was crosslinked at temperatures 210 ℃. The crosslinked cPPSA film was then ground in a mortar and pestle to form a raw, particulate cPPSA binders. In the first ink preparation experiment, cPPSA powder obtained from the film crosslinked for 3 h at 210 ℃ was used. Prior to the use, the powder was extracted with methanol and hot water to remove the remaining soluble cPPSA fraction. The GDE preparation procedure is shown in Figure 6.2.

The ink preparation is similar to that described in Ref. [3]. The cPPSA powder was first soaked in water for half an hour to swell it. Then, the Pt/C catalyst (47.1% Pt) was added and the mixture was ground for 10 min. Next, methanol was added and the grinding was continued for another 5 minutes. The obtained ink was ultrasonicated in ice-water bath for one hour and then sprayed on carbon paper (Sigracet) with an airbrush to obtain a GDE. The ratio of catalyst to ionomer in electrodes was 52:48 and the Pt loading was 0.1 mg/cm$^2$ for both the anode and the cathode. The fuel cell was operated with no backpressure, and the performance was tested at 100 % RH and at 80 ℃. The flow rates of $H_2$ and air were 0.125 L/min and 0.5 L/min, respectively.

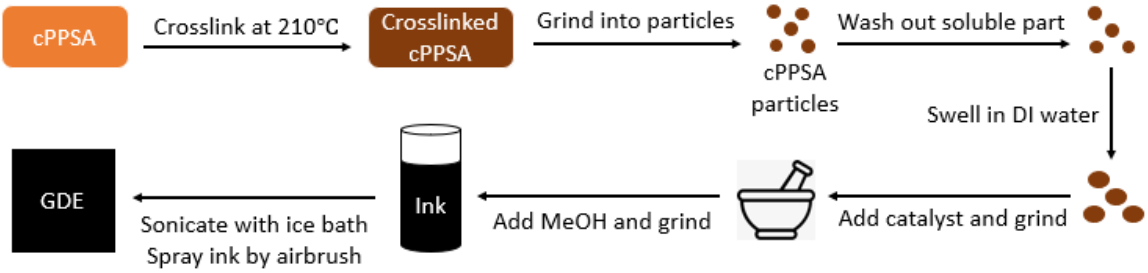


Figure 6.2: Procedure of preparation of the gas diffusion electrode (GDE) from the ink containing insoluble cPPSA particles.

## 6.3 Results and Discussion

### 6.3.1 NMR Spectrum

In Figure 6.3, a $^1$H NMR spectrum of one of the newly synthesized water-soluble cPPSA ionomers is shown. Based on the shown integrals, the BP grafting degree was estimated as 13%.

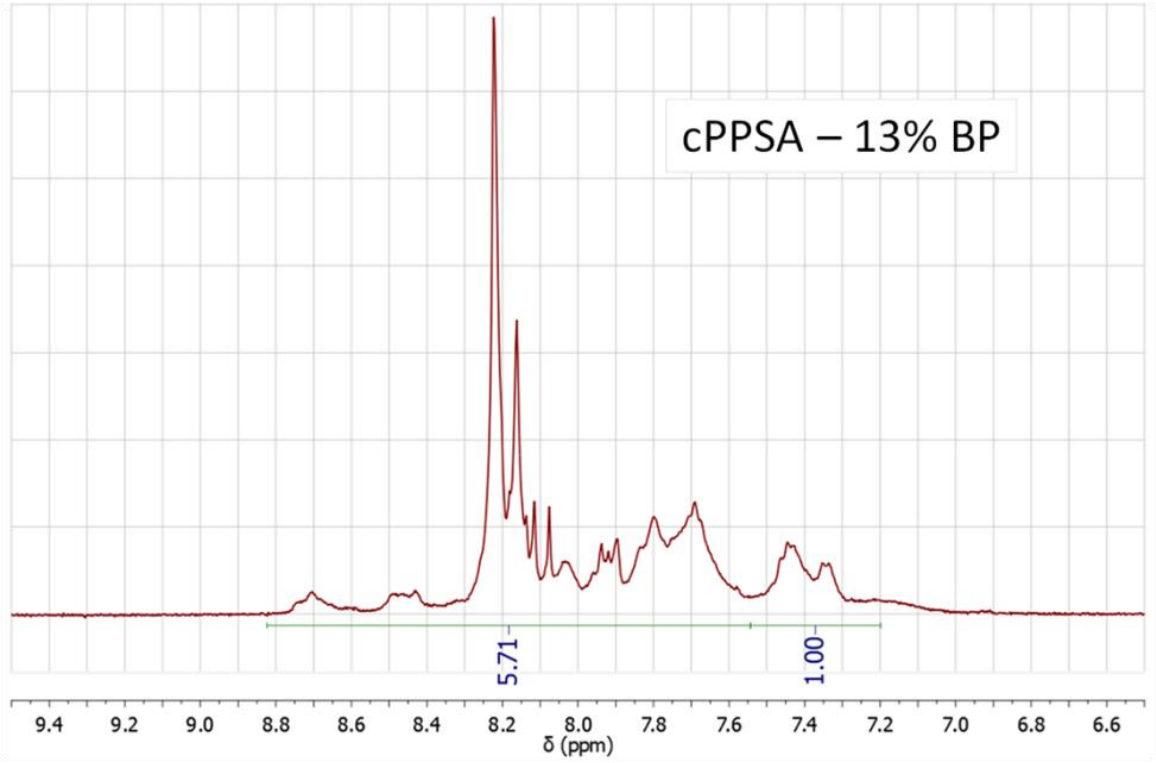


Figure 6.3: $^{1}H$ NMR spectrum of one of the newly synthesized water-soluble cPPSA ionomers dissolved in $CD_3OD$. The calculated degree of BP grafting is 13%.

### 6.3.2 Fuel Cell Performance and Morphology of GDEs

The resultant i-V curves obtained at 100 %RH and the power output curves are shown in Figure 6.4. When the weight ratio of catalyst to ionomer was 52:48, a very poor fuel cell performance with OCV of only 0.76 V and peak power density of 10 mW/cm$^2$ was associated with poor distribution and bulkiness of the cPPSA particles in the gas diffusion electrodes. In Figure 6.5, SEM images with different magnifications of the gas diffusion electrode (catalyst-ionomer-52-48) surface are shown, which reveal poor inclusion of the binder particles in the gas diffusion electrode and their macroscopic size, ranging from 5 µm to 60 µm. Beneath the catalyst coated cPPSA particles, a dense catalyst layer appears to form with such a poor ionomer-catalyst content and negligible catalyst-binder contact area, the observed very low fuel cell performance is not surprising. Also, the probability of membrane penetration by the bulky cPPSA chunks is very high. A better method for grinding and mixing is evidently needed.

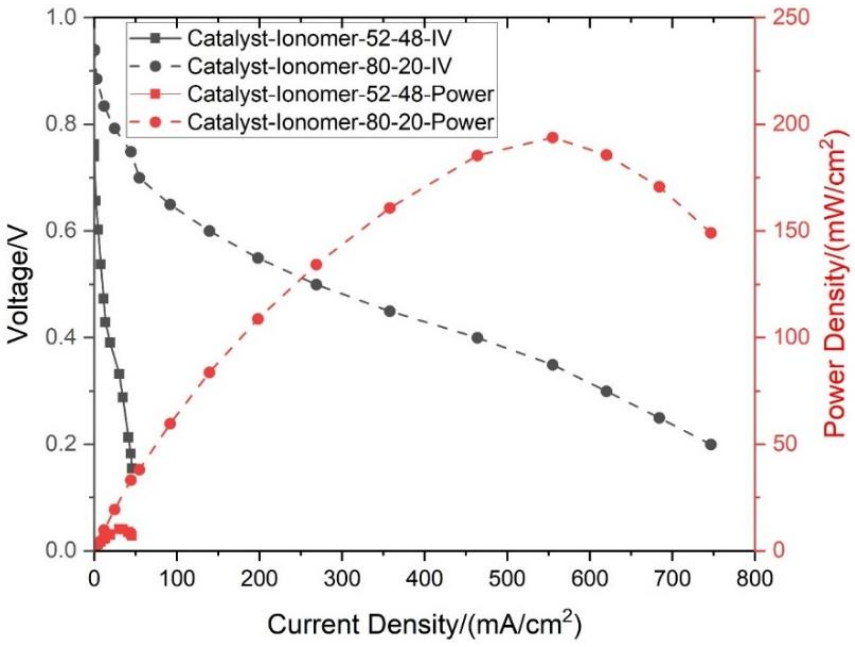


Figure 6.4: Fuel cell performance of the gas diffusion electrode (GDE) from the ink containing insoluble cPPSA particles.

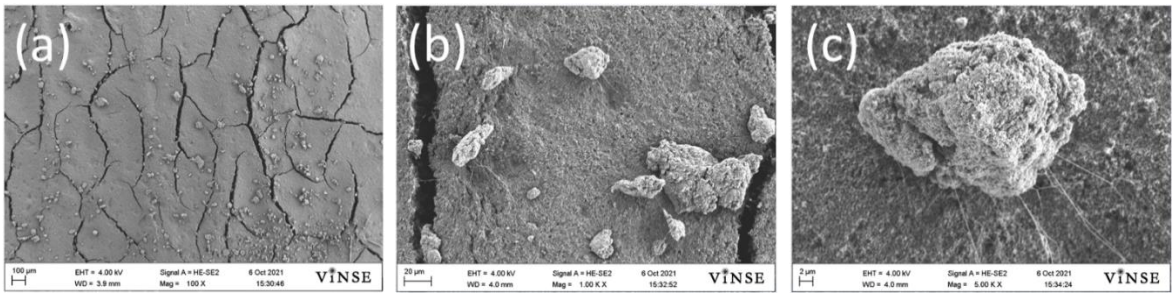


Figure 6.5: SEM images of the electrode (catalyst-ionomer-52-48) surface at different magnification: (a) 100x, (b) 1,000x, and (c) 5,000x.

In the next experiment, the amount of the catalyst was increased to obtain a 4:1 ratio of catalyst: cPPSA. The fuel cell test conditions were the same as in the previous experiment. The power density and the i-V curves are also shown in Figure 6.4. As can be seen, the fuel cell power output increased significantly, reaching a peak power density of 194 mW/cm$^2$, and the OCV was close to the normal level at 0.94V, but this performance was still unsatisfactory. Figure 6.6 shows the SEM images of the electrode surface at different magnifications. Particles of cPPSA ionomer 20-40 µm in size, coated with the catalyst can be still seen. The whole electrode structure appears to be an aggregate of these particles. It is evident, that in this case, the catalyst-binder contact is improved which translates to a better than the earlier demonstrated, fuel cell performance. Unfortunately, the binder content is relatively low and thus the proton transport is impeded, and the catalyst-binder interfacial area is still low, which does not allow achieving the desired performance characteristics.

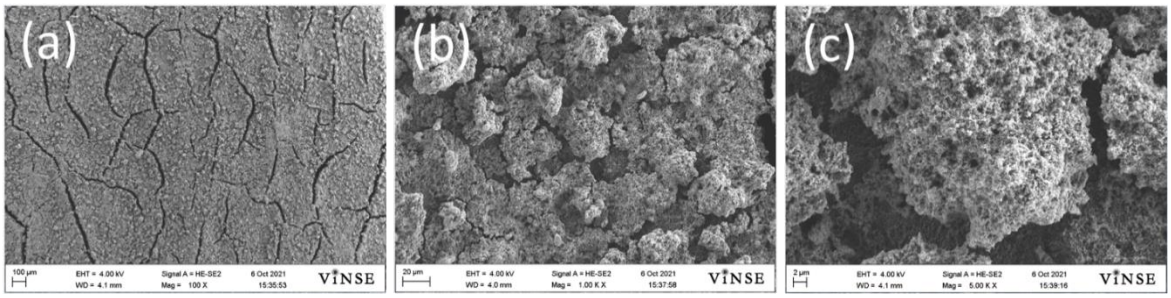


Figure 6.6: SEM images of the electrode (catalyst-ionomer-80-20) surface at different magnification: (a) 100x, (b) 1,000x, and (c) 5,000x.

The final ink was prepared with over-grafted cPPSA particles, obtained as described in the first section. Here no post-grafting heating was needed as the ionomer become insoluble due to an excessively long grafting time. SEM images of one of the over-grafted cPPSA particles obtained after brief grinding with mortar and pestle is shown in Figure 6.7. High magnification (30,000x) reveals that the particle was an agglomerate of smaller, primary particles of sub-micrometer size. This type of ionomer may be the most desirable if it will be possible to break the agglomerated down to the primary constituents.

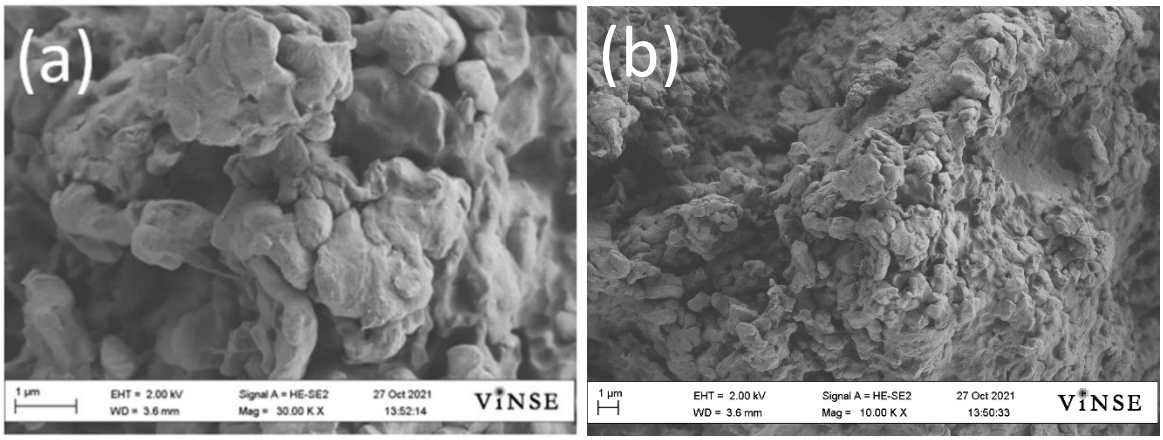


Figure 6.7: SEM image of a big chunk of ground over-grafted (crosslinked) cPPSA film. The presence of sub-micrometer primary particles is evident.

The electrode ink was made by further grinding the cPPSA in a mortar, then adding 1 mL DI water, waiting for 30 mins to swell the cPPSA, followed by additional grinding for 10 min. Then, the Pt/C catalyst and methanol were added, and the mixture was ground for 10 min followed by ultrasonication in a water-ice bath for 1h, followed by an additional ultrasonication using high power horn in ice for 1h. The ink was sprayed onto Sigracet 22B GDL with an airbrush. The ionomer: catalyst ratio was 1:4. The fuel cell experiment followed the same protocol as described earlier ($H_2$ flowrate - 0.125 L/min, air flowrate - 0.500 L/min, temperature 80 ℃ and 100% RH, 5 $cm^2$ cell).

The resultant i-V and power density curves are shown in Figure 6.8. An OCV of 0.94 V can be seen and the maximum power density reached 270 mW/cm$^2$, the best power output so far, with cPPSA particulate binder. The value of HFR was 26.3 mOhm, which was typical for standard MEAs with N212 membranes. Since the cPPSA particle size was reduced, thinner proton exchange membrane can be use without risk of puncture, Nafion 211 membrane was tried again and higher maximum power density can be obtained.

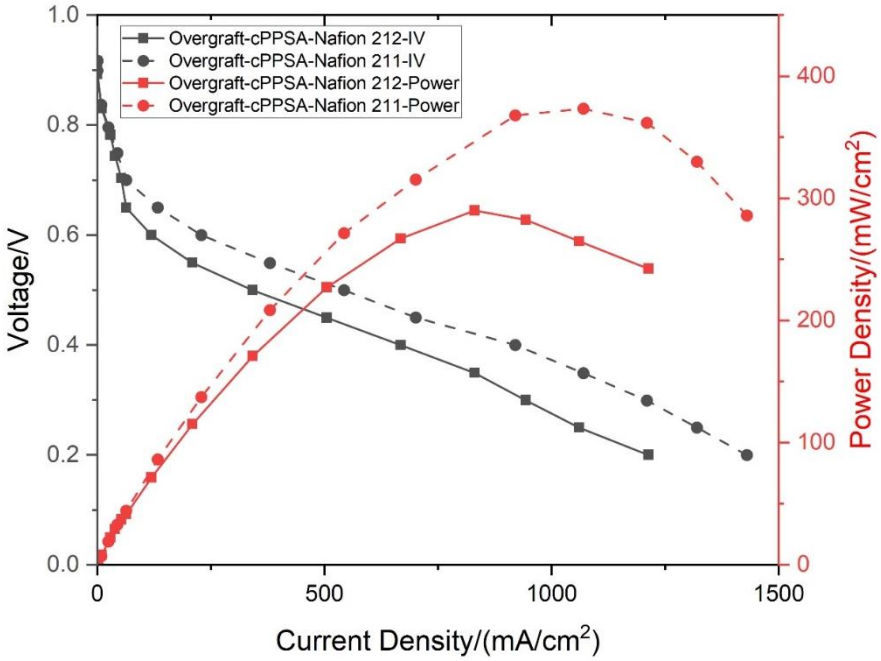


Figure 6.8: $H_2$/Air fuel cell performance of Nafion MEA with electrodes made with ground over-grafted cPPSA ionomer binder. catalyst: ionomer ratio was 4:1, and Pt loading was 0.1 mg/cm$^2$, for both the anode and the cathode.

### 6.4 Conclusion

Particulate binders were fabricated from crosslinked and over-grafted cPPSA, and tested in MEAs with Nafion membranes. Progressively improved fuel cell performance was observed when the binder content in the electrode and the particle size was decreased. When the catalyst: ionomer ratio increased from 52:48 to 80:20, the fuel cell power output was significantly increased. When the cPPSA particles size decreased from 20 μm to 1 μm, the fuel cell power output continued to increase and penetration was also avoided. Thinner proton exchange membrane could be combined with smaller cPPSA particles, but the $H_2$/air fuel cell power output was still not as good as with gas diffusion electrode using PFSA as binder.

## 6.5 References

[1] Poynton, Simon D., et al. "Preparation of radiation-grafted powders for use as anion exchange ionomers in alkaline polymer electrolyte fuel cells." *Journal of Materials Chemistry A* 2.14 (2014): 5124-5130.

[2] Huang, Garrett, et al. "Ionomer optimization for water uptake and swelling in anion exchange membrane electrolyzer: oxygen evolution electrode." *Journal of the Electrochemical Society* 167.16 (2020): 164514.

[3] Ul Hassan, Noor, et al. "Achieving high-performance and 2000 h stability in anion exchange membrane fuel cells by manipulating ionomer properties and electrode optimization." *Advanced Energy Materials* 10.40 (2020): 2001986.

[4] Omasta, T. J., et al. "Importance of balancing membrane and electrode water in anion exchange membrane fuel cells." *Journal of Power Sources* 375 (2018): 205-213.

[5] Zheng, Yiwei, et al. "Effect of reacting gas flowrates and hydration on the carbonation of anion exchange membrane fuel cells in the presence of CO2." *Journal of Power Sources* 467 (2020): 228350.

## CHAPTER 7 - SUMMARY AND CONCLUSION

1. PPSU and PBI fiber reinforced composite proton exchange membranes containing cPPSA ionomer were fabricated via dual-fiber electrospinning and via pore-filling, for the application in $H_2$/air fuel cells. Electrospun dual fiber mats were densified by solvent exposure to melt cPPSA, which filled the void volume between reinforcing PPSU fibers. This led to composite membranes with PPSU fibers embedded in cPPSA matrix. Solution cast cPPSA films were also prepared and evaluated as a reference. The best membranes, in terms of proton conductivity, were made by pore-filling technique and crosslinking at 210 ℃ for 1h, while the lowest conductivity was observed for dual-fiber membranes fabricated with PEO as the cPPSA electrospinning carrier. All pore-filled membranes containing 85 wt.% cPPSA and 15 wt.% reinforcing fibers were superior to Nafion XL PFSA membrane in terms of both the proton conductivity in the 40–90 %RH at 80 °C. The fuel cell performance of cPPSA-PPSU pore-filled membrane was lower than that of Nafion XL due to the poor adhesion between the membranes and the electrodes and additionally, the membranes were damaged during fuel cell test, where typically cracks developed along the edge of the carbon paper electrode.

2. A composite fuel cell membrane (cPPSA-ePTFE) was fabricated by pore-filling of expanded polytetrafluoroethylene with cPPSA, followed by thermal crosslinking of the polyphenylene, to render the bulk of the membrane water insoluble, with a water-leaching fraction of less than 5%. The cPPSA-ePTFE, developed in this work, had a very high proton conductivity at 80 ℃, 47.5 mS/cm at 40 %RH, and 221 mS/cm at 90 %RH, with a tensile strength of 25 MPa and 21 MPa, in the machine and transverse directions, respectively, at room temperature. The 15 μm-thick membrane performed well in a $H_2$/air fuel cell at 80 ℃, and 100 kPa backpressure, with 0.12 mgPt/cm$^2$ GDEs as the anode and cathode. The maximum power density decreased by only 15%, from 1.00 W/cm$^2$ to 0.85 W/cm$^2$, when the cell RH was reduced from 100% to 30%. In comparison, a MEA with Nafion XL showed a significant (52%) loss, from 0.82 W/cm$^2$ to 0.39 W/cm$^2$, for similar reduction of the fuel cell humidification. The composite cPPSA-ePTFE met the DOE 2020 technical targets for hydrogen crossover (<2 mA/cm$^2$) and area specific resistance at 80 ℃ and a water partial pressure, between 30 kPa and 45 kPa (0.02 Ohm cm$^2$).

3. Proton exchange membrane from perfluorosulfonated ionomer was enhanced by adding a certain amount of cPPSA ionomer. A series of hybrid membranes combining a low-equivalent-weight perfluorosulfonated ionomer, namely, 3M825, with an aromatic polyelectrolyte, cPPSA, with 10 wt.% and 20 wt.% content were fabricated and characterized. With cPPSA, the proton conductivity and water uptake of 3M825-cPPSA blend membranes were improved compared to those of commercial AquivionE87-03S membrane. Due to the improvement of water uptake, 3M825-cPPSA blend membranes had higher fuel cell power output than PFSA membrane at low relative humidity. There was no significant

performance difference at high RH. The blend membrane with 20 wt.% cPPSA had similar power output as cPPSA-ePTFE-B, even though the 3M825-cPPSA blend membrane was thicker than cPPSA-ePTFE-B.

4. To utilize the high proton conductivity of cPPSA, particulate binders were fabricated from crosslinked and from over-grafted cPPSA and tested in MEAs with Nafion membranes. Progressively improved fuel cell performance was observed when the binder content in the gas diffusion electrodes and the size of cPPSA particles were decreased. When the weight ratio of ionomer to catalyst in gas diffusion electrodes decreased from 52:48 to 80:20, the fuel cell power output was significantly increased. When the average cPPSA particles size decreased from 20 μm to 1 μm, the fuel cell power output continued increasing and the problem of membrane penetration caused by large cPPSA particles was also avoided. Thinner proton exchange membrane can be combined with smaller cPPSA particles to get better fuel cell performance without membrane penetration. The $H_2$/air fuel cell power output of gas diffusion electrodes with cPPSA as binder was still not as good as with gas diffusion electrodes employing PFSA as binder, indicating smaller particle size was needed to improve the utilization of catalyst.

# CHAPTER 8 - FUTURE WORK

## (I) BETTER ELECTRODE BINDER

### (a) PFSA Binder

To push further the performance of the cPPSA-ePTFE composite membranes, custom-designed electrodes, most probably with a commercial PFSA ionomer binder, should be employed. Low EW PFSA, such as 3M825 ionomer or Aquivion would most probably help in extending the operational range of the MEAs to above 100 $^{o}$C. The interfacial compatibility between gas diffusion electrodes and the composite membrane needs to be also addressed.

### (b) cPPSA Binder

The ideal situation would be to employ cPPSA as an electrode binder. The preliminary study, described in the present work, did not give expected outcomes. Further investigation is needed, particularly, if an all-hydrocarbon-based MEA is of interest. Both paths, one utilizing pre-crosslinked cPPSA and the other one, employing post-crosslinking, are worth exploring.

## (II) BETTER WATER MANAGEMENT

Proper water management in a $H_2$/air fuel cell is critical for achieving high power densities due to the tendency of the anode to dry-out during operation. Typically, water generation at the cathode and drying of the anode creates a concentration gradient that leads to back-diffusion of water. Thinner reinforced membrane could be made by using thinner scaffold. Such a membrane could promote the back-diffusion of water during fuel cell operation, allowing for further reduction of the cell humidification to be tolerated.

## (III) REDUCTION OF THE ANNEALING (CROSSLINKING) TEMPERATURE AND TIME

At present high temperature, long time and vacuum are needed for effective cPPSA crosslinking which would increase the production cost of cPPSA-based composite membranes. It is therefore necessary to reduce either the crosslinking time, or temperature, or both. Some approaches, for example, the use of 1,4-benzenedimethanol, showed some promise but more effective, rapid strategies need to be developed.

## (IV) BETTER SCAFFOLD FROM HYDROCARBON POLYMER

To avoid the use of fluoropolymers in the target composite PEM either further optimization of the electrospun PPSU scaffold is needed or another, suitable, hydrocarbon polymer should be identified and tested. Necessary wettability of the scaffold can be accomplished by adjusting the pore size in the electrospun mats or by plasma treatment. Proper interfiber welding is critical to maximize mechanical strength of the scaffold and to

accommodate the high swelling of cPPSA.